Poly(*p*-xylylene) Nanotubes Prepared via the Tubes by Fiber Templates Process as Catalytic Nanoreactors

DISSERTATION

zur Erlangung des akademischen Grades eines Doktors der Naturwissenschaften (Dr. rer. nat.) im Fach Chemie der Fakultät für Biologie, Chemie und Geowissenschaften der Universität Bayreuth

vorgelegt von

Fabian Mitschang

geboren in Neuwied

Bayreuth, 2014

Die vorliegende Arbeit wurde in der Zeit von November 2010 bis September 2012 in Marburg am Lehrstuhl Makromolekulare Chemie und in der Zeit von Oktober 2012 bis April 2014 in Bayreuth am Lehrstuhl Makromolekulare Chemie II unter Betreuung von Herrn Prof. Dr. Andreas Greiner angefertigt.

Vollständiger Abdruck der von der Fakultät für Biologie, Chemie und Geowissenschaften der Universität Bayreuth genehmigten Dissertation zur Erlangung des akademischen Grades eines Doktors der Naturwissenschaften (Dr. rer. nat.).

Dissertation eingereicht am: 24.04.2014

Zulassung durch die Promotionskommission: 30.04.2014

Wissenschaftliches Kolloquium: 06.08.2014

Amtierender Dekan: Prof. Dr. Rhett Kempe

Prüfungsausschuss:

Prof. Dr. Andreas Greiner (Erstgutachter)

Prof. Dr. Rhett Kempe (Zweitgutachter)

Prof. Dr. Matthias Breuning (Vorsitz)

Prof. Dr. Stephan Förster

Contents

Contents

Summary

The aim of this thesis was to develop and evaluate highly versatile methods for the preparation of continuous functional nanotubes for applications, such as catalysis and microelectronics. Hence, the suitability of the corresponding tubes as reusable tea bag-like catalyst systems as well as for the preparation of continuous conductive nanowires was studied.

The underlying concept for each method was the tubes by fiber templates (TUFT) process: First, continuous template nanofibers were prepared using the electrospinning process, which is generally suitable for a huge variety of materials. The resulting nonwovens were coated from the gas phase with poly(*p*-xylylene) (PPX), based on the chemical vapor deposition process. Subsequently, the inner template material of the corresponding core-shell fibers was removed using either solvent extraction or pyrolysis.

Accordingly, nanotubes with surface-immobilized catalysts were prepared by coating poly(ethylene oxide) nanofibers with an ethynyl-functionalized PPX. After removal of the template material, the tubes were suitable for "click" chemistry,[1] and were subsequently equipped with either a (2,2,6,6-tetramethylpiperidin-1-yl)oxy (TEMPO) catalyst or a bipyridine ligand. The bidentate chelating ligand was then used to immobilize copper. In order to test the tube catalysts, suitable model reactions were conducted: The TEMPO-functionalized tubes were used for the oxidation of benzyl alcohol, resulting in $> 98\,\%$ of benzaldehyde even after 20 catalytic cycles. In addition, the copper-carrying tubes were used for the click reaction of benzyl azide with phenyl propargyl ether. After 17 cycles, the yield was still above $90\,\%$.

In contrast to the surface-immobilization of catalysts onto PPX, the suitability of the tubes for encapsulation of transition metal-based catalysts was studied. Polyurethane template fibers featuring incorporated palladium- and copper-functionalized poly(amido amine) dendrimers were electrospun and subsequently coated with PPX. Extraction of the template material resulted in semipermeable PPX nanotubes carrying the dendritic catalysts. The prepared nanoreactors did not show catalyst leaching and were used for homogeneous catalysis inside the

---

[1]More precisely, the azide-alkyne Huisgen 1,3-dipolar cycloaddition.

tea bag-like PPX confinement: Whereas the palladium-based dendrimers catalyzed various Suzuki-Miyaura coupling reactions with yields around 88%, the copper catalyst was used for the click reaction of benzyl azide with different alkynes, resulting in quantitative conversions. Both catalyst systems were conveniently reused for at least 14 cycles, albeit the corresponding yields decreased slightly over time.

As an alternative to encapsulated dendrimers, gold nanoparticles were immobilized inside PPX tubes in order to compare the suitability and reusability for catalysis. First, poly(L-lactide)-stabilized gold nanoparticles were synthesized and subsequently used for the TUFT process. According to leaching studies based on UV-vis spectroscopy, the resulting PPX tubes successfully encapsulated the particles. Next, the suitability of the gold-carrying PPX nanoreactors for catalysis was evaluated: Both the hydrolytic oxidation of dimethylphenylsilane and the corresponding alcoholysis with n-butanol gave the corresponding product in quantitative yield at room temperature. After removal of the tea bag-like catalyst system, no product purification was necessary. Further, the catalyst was reused 20 times with no decrease in activity.

Based on the concept of gold-carrying PPX tubes, another application was developed: Composite nanofibers featuring circa $60\,\mathrm{wt}\%$ of gold were electrospun and subjected to the TUFT process. Thermal treatment up to $1050\,℃$ resulted in degradation of the PPX shell and simultaneous formation of continuous conductive gold nanowires featuring a smooth surface. The corresponding heat-induced transition was studied by scanning helium ion microscopy.

In conclusion, highly versatile methods for the preparation of continuous functional nanotubes were developed, suitable for a variety of materials and applications. In order to prove the concept, different catalysts were encapsulated inside PPX tubes and, respectively, immobilized on the surface of the tubes. The resulting nanoreactors were used as potent tea bag-like catalyst systems and showed high reusability. Further, gold-carrying PPX tubes were used for the preparation of continuous conductive nanowires.

Zusammenfassung

Ziel dieser Arbeit war die Entwicklung geeigneter Methoden zur Herstellung kontinuierlicher funktionaler Nanoröhrchen für Anwendungen in Katalyse und Mikroelektronik. Ergänzend wurde die Eignung dieser Röhrchen für wiederverwendbare Katalysatorsysteme sowie für kontinuierliche leitfähige Nanodrähte untersucht.

Das zugrundeliegende Konzept für die Herstellung der Nanoröhrchen basierte auf dem sehr flexibel einsetzbaren *tubes by fiber templates*- (TUFT-) Prozess: Zunächst wurden Vliese aus kontinuierlichen Nanofasern elektrogesponnen[1] und anschließend mittels chemischer Gasphasenabscheidung mit Poly(p-xylylen) (PPX) beschichtet. Die resultierenden Kern-Hülle-Nanofasern wurden von den innenliegenden Templatfasern befreit, woraufhin PPX-Röhrchen zurückblieben.

Analog dieser Vorgehensweise wurden Templat-Nanofasern aus Polyethylenoxid elektrogesponnen und mit einem PPX beschichtet, welches zuvor mit Ethin-Gruppen funktionalisiert wurde. Nach der Extraktion des Templats konnte die Oberfläche der PPX-Röhrchen mittels Klick-Chemie[2] mit einem 2,2,6,6-Tetramethylpiperidinyloxyl- (TEMPO-) Katalysator bzw. mit Bipyridin-Liganden ausgestattet werden. Anschließend wurde der oberflächenimmobilisierte Ligand mit Kupfer komplexiert. Um die hergestellten Systeme zu testen, wurde der TEMPO-Katalysator zur Oxidation von Benzylalkohol sowie der Kupfer-Katalysator für eine Klick-Reaktion mit Benzylazid verwendet. Auch nach 20 Katalysezyklen ergab die Oxidationsreaktion Ausbeuten von über 98 %, während die Cycloaddition nach 17 Wiederholungen noch eine Ausbeute von über 90 % aufwies.

Zusätzlich zur Oberflächenimmobilisierung mittels Klick-Chemie wurden sterisch anspruchsvolle Dendrimere funktionalisiert, mit Übergangsmetallen komplexiert und zur Katalyse in PPX-Nanoröhrchen eingeschlossen. Zunächst wurden Nanofasern aus Polyurethan mit eingebetteten dendritischen Palladium- und Kupferkatalysatoren elektrogesponnen und mit PPX beschichtet. Anschließend wurde das Polyurethan extrahiert, wobei die resultierenden PPX-Röhrchen die eingeschlossenen Dendrimere erfolgreich immobilisierten. Die palladiumbeladenen Nanoreak-

---

[1] Der Elektrospinn-Prozess ist eine geeignete Methode zur Herstellung von Nanofasern unterschiedlicher Materialien und Morphologien.

[2] Genauer: kupferkatalysierte 1,3-dipolare Cycloaddition von Aziden und Alkinen nach Huisgen.

toren katalysierten verschiedene Suzuki-Miyaura-Reaktionen mit Ausbeuten von über 88 %, während das Kupfer-System unterschiedliche Klick-Reaktionen in quantitativem Umsatz katalysierte. Die teebeutelähnlichen PPX-Reaktoren wurden für über 14 Katalysezyklen verwendet, wobei jedoch die Ausbeuten leicht abnahmen.

Als eine Alternative zu Dendrimeren wurde die Verwendung von katalytisch aktiven Nanopartikeln untersucht. Poly-L-laktid- (PLLA-) stabilisierte Goldnanopartikel wurden mit PLLA zu Kompositfasern elektrogesponnen und anschließend mit PPX beschichtet. Die Pyrolyse des PLLA-Templatmaterials bei 280 °C und vermindertem Druck resultierte in PPX-Röhrchen mit eingeschlossenem Gold. Diese Nanoreaktoren wurden für die Alkoholyse eines Silans mit *n*-Butanol sowie für die hydrolytische Oxidation des Silans verwendet. Beide Reaktionen konnten bei Raumtemperatur durchgeführt werden und führten zu einem quantitativen Umsatz. Die PPX-Röhrchen zeichneten sich durch eine hervorragende Wiederverwendbarkeit aus, da ihre katalytische Aktivität auch nach 20 Katalysezyklen nicht abnahm. Die Reaktionen konnten durch Herausnahme der PPX-Röhrchen vollständig unterbrochen werden. Es wurden keine Nebenprodukte bzw. Disiloxane gebildet.

Zusätzlich zur Katalyse mit goldbeladenen PPX-Röhrchen wurde deren Eignung zur Herstellung von kontinuierlichen leitfähigen Goldnanodrähten untersucht. Dazu wurden Goldnanopartikel mit 60 Gew.-% Gold synthetisiert und mit PLLA zu Komposit-Nanofasern elektrogesponnen. Nach der Beschichtung mit PPX wurde das PLLA entfernt und die goldgefüllten PPX-Röhrchen einer Temperatur von 1050 °C ausgesetzt. Zeitgleich mit der Pyrolyse des PPX sinterten die Goldnanopartikel zusammen und ergaben leitfähige Nanodrähte mit einer glatten Oberfläche. Der entsprechende Übergang wurde mittels Helium-Ionen-Mikroskopie untersucht.

Die entwickelten Methoden zur Herstellung kontinuierlicher funktionaler Nanoröhrchen bieten eine sehr flexible Grundlage für zahlreiche Materialien und Anwendungen. So wurden unterschiedliche Katalysatoren in PPX-Röhrchen eingeschlossen beziehungsweise auf der Oberfläche der Röhrchen immobilisiert. Die hergestellten PPX-Nanoreaktoren konnten analog eines Teebeutels verwendet werden, wodurch keine weitere Aufarbeitung der Katalyseprodukte notwendig war. Ferner eigneten sich die mit Gold beladenen Röhrchen zur Herstellung kontinuierlicher elektrisch leitfähiger Nanodrähte.

1 Introduction

Nanotechnology is a powerful tool which is used not only in scientific research and the chemical industry but also in manifold consumer goods and everyday life. In the following, the theory and the state of the art regarding nanomaterials and corresponding methods will be reviewed, in order to provide a foundation for the subsequent chapters. The addressed topics include nano-scale particles, fibers, and coatings followed by the respective combinations thereof that lead to nanotubes. Further, the use of nanoconfinements (in particular nanotubes) for the immobilization of catalysts will be discussed. With that in mind, the Thesis Objective will be presented with the goal to develop novel applications for catalysis and microelectronics. In addition, a detailed supplementary overview of the conducted research can be found in Section 2.

1.1 Gold Nanoparticles

In the far-reaching field of nanoparticles, gold has been shown to be one of the most prominent metals. In addition to the many versatile synthetic procedures for the preparation of colloidal gold,[1] the resulting nanoparticles can be highly stable against oxidation and further compounds. Moreover, gold nanoparticles feature outstanding optical[2] and electrical[3] properties and show pronounced catalytic activity for selected reactions (see below). The corresponding toxicity has been extensively studied, mostly indicating a very low health risk, if any.[4,5] Consequently, colloidal gold is of high importance for scientific research and numerous potential applications. Biomedical applications include biosensorics, laser phototherapy of tumors, targeted delivery of drugs, and optical bioimaging.[6–9] Further, the electrical properties of gold nanoparticles allow for novel nanoelectronics[3,9] and sensorics[10,11] and can be used to improve photovoltaic cells[12] and light-emitting diodes.[13] Despite the high chemical stability, nanoparticulate gold has been shown to catalyze a variety of reactions,[14–17] such as the oxidation or hydrogenation of alkenes or carbon-carbon coupling reactions.

As mentioned above, the synthesis of gold nanoparticles can be extremely convenient. For instance, even at room temperature and without the use of an inert

atmosphere, mixing the common precursor chloroauric acid[18,19] with water and cyclohexanone results in the formation of colloidal gold.[1] More complex procedures have been developed in order to prepare particles with a certain size, size distribution, shape, or functionalization. As a result, nearly monodisperse particles with average diameters from 1.2 nm up to and exceeding 100 nm can be prepared.[20–22] Depending on the reaction conditions and the use of selected ligands, for instance, the commonly used surfactant cetrimonium bromide (CTAB) which influences the growth of specific crystal facets,[23,24] shapes such as triangles, squares, stars, rods, and wires (see Section 1.2) can be prepared.[25,26]

Due to the high surface energy of nano-sized particles, colloidal gold tends to agglomerate in order to minimize the surface energy[27–29] of the system. Hence, a variety of methods have been developed for the essential stabilization of nanocolloids in both water and organic solvents. The two major techniques are based on electrostatic[30] or steric[7,31] interactions, and one of the most prominent ligands is sodium citrate.[18,25] It is a suitable ligand for many synthetic procedures and is mostly used in aqueous systems. If a different stabilizing agent is required for a specific system or application, respectively, a subsequent one- or two-phase ligand exchange can be performed after the formation of the colloid.[22,32] Alternatively, instead of sodium citrate, suitable ligands such as surfactants,[33] polymers,[34,35] dendrimers,[22] or gels[33] can be used for the stabilization and functionalization of the gold surface. Due to the pronounced affinity of gold for sulfur-based compounds, manifold potent ligands carrying thiol groups are known. Moreover, the strong gold-sulfur bond allows for the highly effective stabilization based on thiol end-capped polymers even for molecular weights above $200,000\,\mathrm{g\,mol^{-1}}$.[36] Figure 1.1 illustrates—true to scale—the proportions of the organic low molecular weight ligand dodecanethiol and a thiol end-capped polylactide in comparison to a gold nanoparticle.[1] Based on the diameter of a spherical, face-centered cubic gold particle, the number of contained atoms can be calculated using Equation 1 to 3. Whereas the volume V_{Atom} of a single gold atom can be expressed using its atomic radius r_{Atom}, the gold volume V_{NP} of a whole particle is given by its diameter d_{NP}

---

[1]The illustration was prepared using a combination of PyMOL (Schrödinger, Inc.) and Avogadro (open source project) based on face-centered cubic gold with an atomic radius of 144 pm.[37]
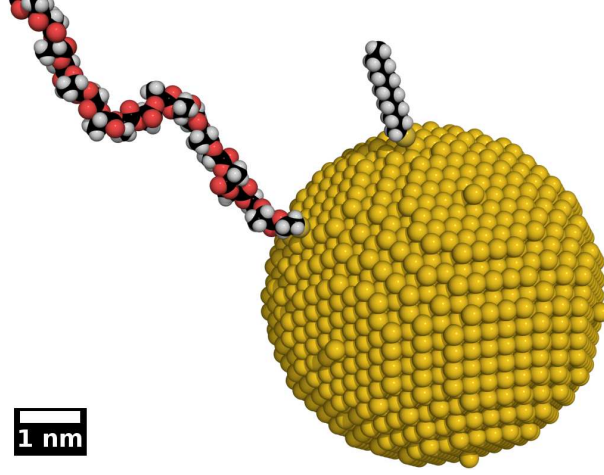
Figure 1.1. Illustration of a monocrystalline gold nanoparticle with two organic ligands true to scale. The attached compounds are a thiol end-capped polylactide (left) and dodecanethiol (top).

and the atomic packing factor ρ. Combining the two volumes reveals the number n of atoms.

$$V_{\text{Atom}} = \frac{4}{3}\pi r_{\text{Atom}}^3 \tag{1}$$

$$V_{\text{NP}} = C_{\text{Atom}} n = \frac{4}{3}\pi \left(\frac{d_{\text{NP}}}{2}\right)^3 \rho \tag{2}$$

$$n = \left(\frac{d_{\text{NP}}}{2}\right)^3 \rho \frac{1}{r_{\text{Atom}}^3} \tag{3}$$

Since the particle in Figure 1.1 has a diameter of $5.7\,\text{nm}$, the atomic packing factor of a face-centered cubic crystal is 0.74,[38] and the atomic radius of gold is $144\,\text{pm}$,[37] the number of contained atoms is about 5600. Figure 1.2 depicts the respective correlation between the number of gold atoms $n \approx 30.98\,d_{\text{NP}}^3\text{nm}^{-3}$ and the particle diameter d_{NP} (in nm).

It is well known that for nano-scale gold particles, the melting temperature is significantly reduced as opposed to the bulk metal. The dependence on the particle diameter is given in Equation 4.[39]

$$T_{\text{m,NP}} = T_{\text{m,}\infty} - \frac{4T_{\text{m,}\infty}}{d_{\text{NP}}\rho_{\text{s}}L}\left[\gamma_{\text{s}} - \gamma_{\text{l}}\left(\frac{\rho_{\text{s}}}{\rho_{\text{l}}}\right)^{\frac{2}{3}}\right] \tag{4}$$
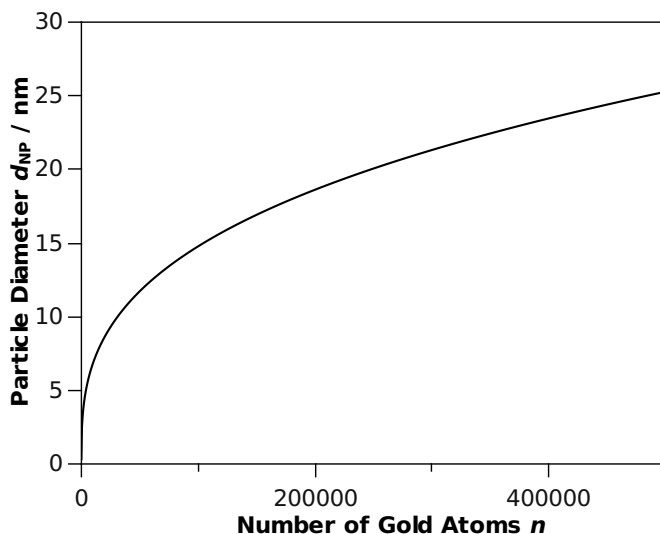
Figure 1.2. Correlation between the number *n* of gold atoms and the corresponding particle diameter d_{NP} of a spherical gold nanoparticle, according to Equation 3.

The associated parameters are the melting temperature $T_{\mathrm{m,NP}}$ of the gold nanoparticles, the melting temperature $T_{\mathrm{m},\infty}$ of the bulk, the latent heat L of fusion, the density ρ_{s} and ρ_{l} of the solid and the melt, respectively, and the respective surface tension γ_{s} and γ_{l}. Figure 1.3 compares the theoretical melting temperature of nano-sized gold to the bulk material. The graph depicts the pronounced decrease in T_{m} for particles below 5 nm. Above, the curve slowly approaches the melting temperature $T_{\mathrm{m},\infty}$ of bulk gold.

In order to characterize gold nanoparticles, a variety of supplementary techniques have been developed. Imaging methods, such as scanning electron microscopy (SEM),[26] transmission electron microscopy (TEM),[33] and atomic force microscopy (AFM)[40] provide information about the shape and the size distribution of nanoparticles and about the corresponding stability against agglomeration. Moreover, whereas both SEM and AFM represent the texture of the surface, TEM can display hollow confinements and characteristic lattice planes of crystalline particles. Additional tools for studying the size of nanocolloids can be dynamic light scattering,[41] size exclusion chromatography,[42,43] asymmetrical flow field-flow fractionation,[44] and ultraviolet-visible (UV-vis) spectroscopy.[26,45,46] The latter can be used to differentiate between spherical and anisotropic particles based on the surface plasmon
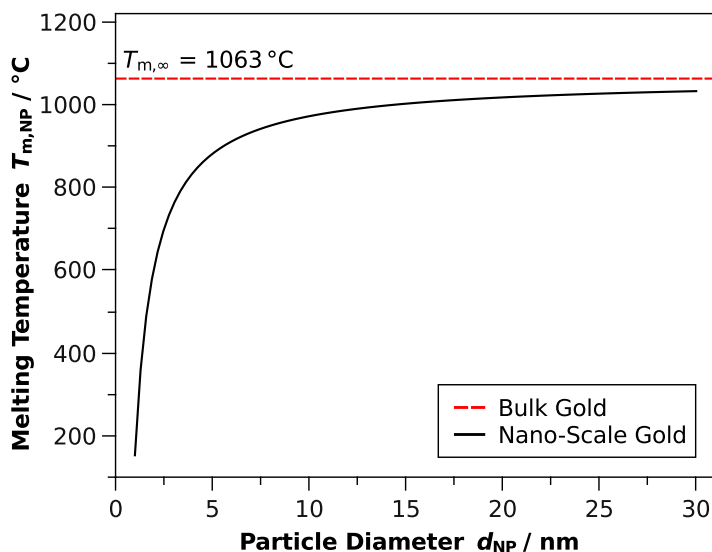
Figure 1.3. Calculated melting temperature of gold nanoparticles based on Equation 4 and comparison with the bulk metal.

resonance of colloidal gold. This characteristic absorption is the result of the correlation of the incoming electromagnetic light with the collective oscillation of the electron gas of the gold surface. Hence, at a wavelength of about 520 nm, the frequency of the corresponding photons matches the frequency of the surface electrons, establishing the resonance condition.[47] In addition to the characteristic diffraction pattern of gold, X-ray powder diffraction also provides information about the size of nano-scale crystals.[48] The resulting maxima of the diffraction pattern depict a dependent broadening by an amount inversely proportional to the crystallite size. Subsequent evaluation based on the Scherrer equation can reveal the average diameter of the measured particles.[49] An alternative X-ray-based technique, X-ray photoelectron spectroscopy, can be used for quantitative analysis of the elemental composition of the nanoparticles' surface.[33,50]

In order to quantify the amount of gold in the ligand-stabilized particles, thermogravimetric analysis (TGA) can be used to remove organic ligands, leaving behind the remaining metal.[33,51] Further, gel permeation chromatography equipped with a diode array detector provides information about the degree of functionalization and the force of the ligand-gold attraction.[52]

1.2 Nanowires

The term nanowire is used with highly varying meanings ranging from continuous insulating nanofibers[53] to conductive nanostructures featuring a very limited aspect ratio (e.g. 10).[1][54] Figure 1.4 illustrates different nano-scale objects, comparing their individual aspect ratios a. In the following, the focus will be on conductive
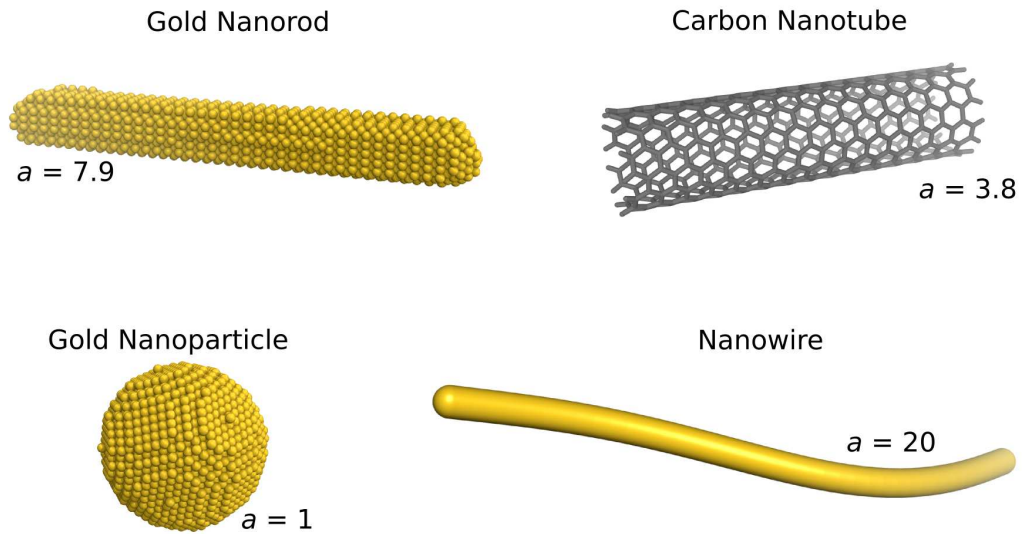
Gold Nanorod

Carbon Nanotube

$a = 7.9$

$a = 3.8$

Gold Nanoparticle

Nanowire

$a = 1$

$a = 20$

Figure 1.4. Illustration of different nano-sized objects, comparing their present aspect ratios. (Note that objects are not true to scale.)

nanowires with a high aspect ratio as opposed to insulating nanofibers and short nanorods. Depending on factors like size, aspect ratio, material, and morphology, there are highly diverse applications for nanowires. Prominent examples include microelectronics and sensorics,[55–57] as well as electrodes and catalysts featuring a very large surface area.[58,59] Further, since nanowires can be conductive yet are invisible to the naked eye, transparent electrodes can be prepared,[60,61] leading to improved LEDs[62] and photovoltaic cells.[63]

Despite the numerous potential applications, the preparation of conductive nanofibers remains a great challenge. As a result, only few top-down processes can be used to produce continuous nanowires, e.g. electrochemical size-reduction, mechanical reduction, and electron beam lithography.[57,64–66] In contrast, capable bottom-

---

[1]The aspect ratio of a shape is the ratio of the corresponding width to its height (with the width being larger than the height).

up techniques are mostly based on templates[67] or self-assembly effects,[68] such as the CTAB-assisted synthesis of gold nanorods (see Section 1.1) or the electrodeposition process.[69–71] Suitable templates can be porous membranes,[69,72] inorganic molecular chains,[73] micelles,[74] or polymer nanofibers.[75] However, despite the manifold preparative approaches, each technique has conceptual drawbacks: Most methods result in highly limited nanowire length, are only suitable for a few selected materials, or completely lack upscalability.

The characterization of nanowires mainly focuses on the analysis of the corresponding size, aspect ratio, conductivity, and magnetic properties. For the most part, the above mentioned methods for the characterization of gold nanoparticles can be used similarly for the analysis of gold nanowires. For instance, depending on the size and material of the nanowires, suitable techniques include SEM, TEM, and AFM, as well as X-ray crystallography, energy-dispersive X-ray spectroscopy, and UV-vis spectroscopy.[69,76] A very powerful tool for the characterization of nanowires has been developed recently: Scanning helium ion microscopy uses a helium ion beam—hence a very short De Broglie wavelength—featuring numerous advantages over conventional microscopy techniques based on photons or electrons.[77,78] As a result, scanning helium ion micrographs provide increased contrast, resolution, sharpness, and depth of focus. Detection of secondary electrons depicts the topology of a surface, whereas Rutherford backscattered ions highlight areas of high conductivity.[75,79,80] As opposed to this qualitative characterization of the conductivity of a nanowire, the exact measurement of the corresponding electrical properties remains a great challenge: Whereas SEM-based techniques require an installed nanomanipulation device[81] or the focused ion-beam deposition of Pt microleads onto the wires,[82] conducting-probe AFM can be an alternative using a home-made conducting probe extension.[83]

1.3 The Electrospinning Process

The electrospinning process is a highly versatile tool for the preparation of continuous nanofibers.[1][87–90] The essential parts of an electrospinning set-up are a voltage source, a reservoir—filled with the electrospinning formulation—and a collector electrode. Figure 1.5 shows a schematic illustration of a typical set-up based on a syringe as the reservoir connected to a nozzle (e.g. a cannula). Applying high
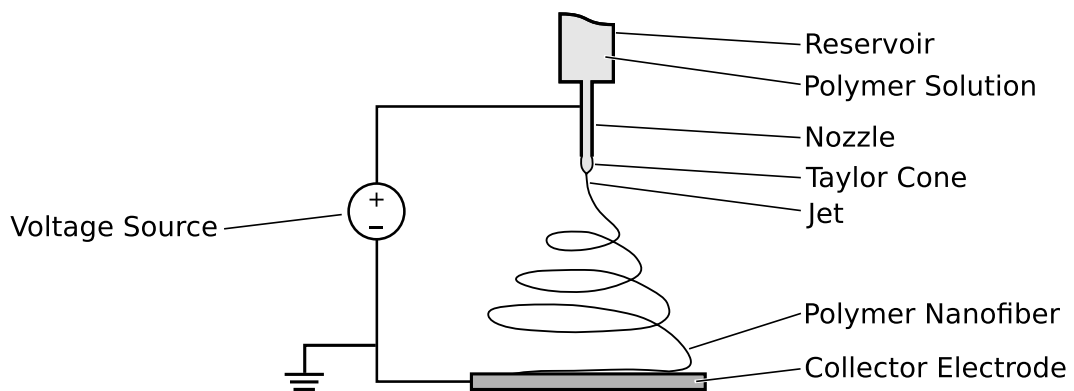

Figure 1.5. Illustration of a typical electrospinning set-up based on a syringe, an attached cannula, a collector electrode, and a voltage source.

voltage leads to the formation of the Taylor cone, resulting in a narrowing jet and eventually the deposition of the electrospun nanofiber.[91,92] The corresponding driving force is based on the repulsion of equal charges, guided by the induced electric field.

Whereas the traditional set-up requires a nozzle attached to the reservoir, nozzle-less electrospinning methods have been developed: A disk or a cylinder is connected to the power source and rotates through the reservoir, resulting in multiple jets along the electric field.[93,94] Alternatively, bubble electrospinning is based on aeration of a formulation, inducing an inhomogeneous surface of the liquid, hence generating multiple polymer jets and fibers, respectively.[95,96] An advantage of the nozzle-based system is its high flexibility that allows for easy modification: Specialized techniques have been developed, such as side-by-side electrospinning[97,98] and

---

[1]Whereas the electrospinning process is also compatible with low molecular weight compounds including gemini surfactants,[84] phospholipids,[85] and cyclodextrins,[86] this work focuses on polymer-based systems.

blowing-assisted electrospinning.[99] A very versatile method for the preparation of core-shell nanofibers is coaxial electrospinning,[90,100–102] which uses a coaxial nozzle which is connected to two separate reservoirs (Figure 1.6).[1] In addition to the ran-
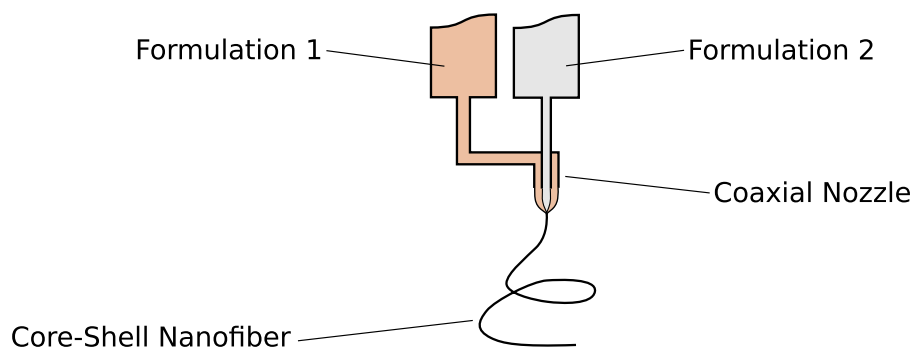

Figure 1.6. Schematic illustration of a coaxial nozzle for the preparation of electrospun core-shell nanofibers.

domly deposited nonwovens, highly oriented fibers can be prepared using near-field electrospinning,[103] a spinning disk as the collector electrode,[104] or an electrode featuring a narrow gap.[105] Depending on the parameters of both the electrospinning process and the formulation, manifold fiber morphologies can be produced. For instance, fibers featuring a high porosity can be electrospun,[89] as well as fibers shaped like ribbons,[106] barbed wires,[107] springs,[108] or pearl necklaces.[89,109] Important parameters of a formulation are its viscosity, conductivity, surface tension, and both the molecular weight and the concentration of the polymer. For the corresponding electrospinning process, crucial parameters are the electrode gap, the voltage, the present humidity, and the flow rate of the formulation.[87,88,110]

In addition to the highly versatile electrospinning process, it can easily be up-scaled and used for the continuous production of nonwovens.[111] Hence, it is a promising technique not only for research and the development of new materials, but also for the large-scale production of specialty nanofiber sheets. The various applications include filtration systems,[89,112] wound dressings,[88,113] superhydrophobic surfaces,[114] and tissue engineering.[87,115] Further, electrospinning nanofibers from water—rather than organic solvents—allows for environmental application, for instance in agriculture for plant protection.[116]

---

[1]Core-shell fibers can be used for the preparation of continuous nanotubes, as shown in Section 1.5.

Additives can be introduced to the formulation in order to equip the fibers with a desired compound or to improve the quality of the nanofibers. Composite nanofibers are necessary for many of the above-mentioned applications to tailor the mechanical properties or to incorporate functional compounds, such as pheromones,[116] bacteria,[117] catalysts,[88] or drugs.[113,115] Further, salts can be used to increase the conductivity of the mixture, whereas surfactants can decrease its surface tension. As a result, the formation of beads can be avoided and varying fiber diameters can be achieved.[110,118]

1.4 Chemical Vapor Deposition of Poly(*p*-xylylene)

Poly(*p*-xylylene) (PPX) is a high-performance polymer of importance for specialty coatings.[119,120] Whereas PPX can be synthesized using wet chemistry approaches,[121] the superior preparation technique is the solvent-free chemical vapor deposition (CVD) process that has many advantages (see below).[120,122] As shown in Figure 1.7, the CVD of PPX is based on different temperature zones at reduced pressure. First, the [2.2]paracyclophane precursor evaporates at 150 °C,[1] followed by
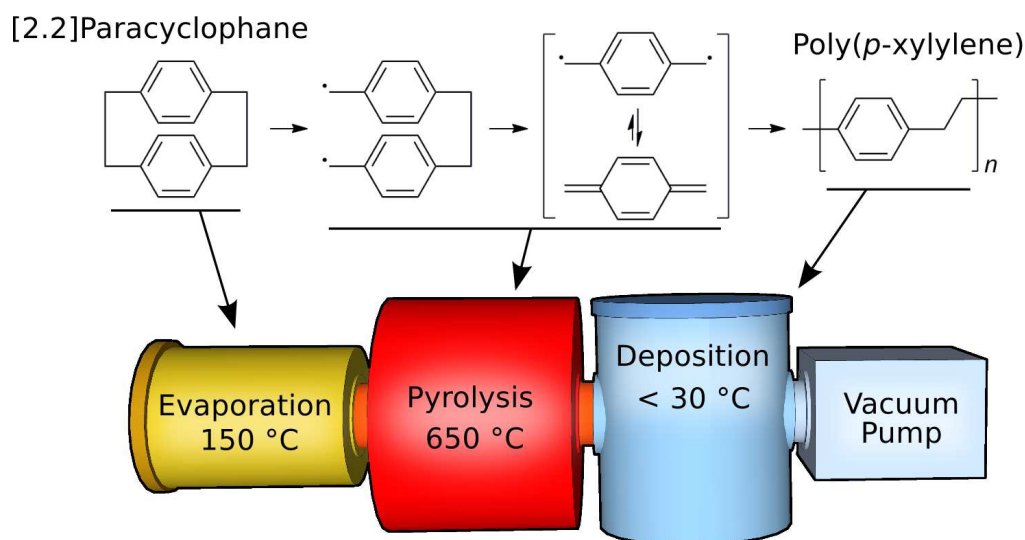

Figure 1.7. Illustration of the chemical vapor deposition process based on [2.2]paracyclophane (left). Pyrolysis at elevated temperatures and reduced pressure generates the *p*-quinodimethane monomer, polymerizing below 30 °C as poly(*p*-xylylene) (right).

---

[1]Corresponding pressure: 8.8 kPa.

cleavage of one of its ethylene bridges at elevated temperatures.[122–124] At a temperature greater than 600 °C, the corresponding diradical undergoes subsequent pyrolysis and splits into two equivalents of *p*-quinodimethane. Whereas the generated *p*-quinodimethane is predominantly in its singlet state, the excited triplet diradical acts as the actual monomer, polymerizing after adsorption by the substrate below 30 °C. The thickness of the resulting PPX layer can easily be controlled based on the amount of the provided precursor and allows for thin coatings down to a few tens of nanometers. Moreover, the deposited PPX forms a homogeneous, biocompatible, and transparent coating[125] featuring thermal stability[1] up to 400 °C[126] and insolubility below 250 °C.[119] Hence, PPX makes for an excellent barrier layer and is used for selected applications, such as sensoric devices, electronics, medical devices, and corrosion protection. Further, PPX coatings can reduce friction[127] and since the chemical vapor deposition of PPX shows a high gap penetration capability, it can be used for the reinforcement of micro-structures (see Section 1.5).[128]

Various derivatives of PPX have been developed in order to optimize the coatings' properties for specific applications.[119,120,129] For instance, chlorine-functionalized PPX shows improved barrier characteristics,[130] whereas fluorine moieties significantly reduce the coefficient of friction.[131] Further modifications include derivatives with increased thermal stability or improved mechanical properties.[132,133] Moreover, substitution with alkyl substituents can lead to improved solubility.[134] A versatile PPX derivative which is particularly important for the concept and research in this thesis is equipped with ethynyl moieties.[129,135–137] As a result, the present alkyne groups of the polymer can undergo subsequent reactions: Elevated temperature and UV light, respectively, can be used to cross-link the polymer, improving both the resistance to oxidation and thermal degradation.[136,137] Further, ethynyl-functionalized PPX is suitable for "click" reactions,[2] allowing for a convenient introduction of azide-based organic compounds.[129,135]

---

[1]Due to the polymorph character of PPX, there are two solid-to-solid transitions between 200 °C and 300 °C.[126]

[2]More precisely, the azide-alkyne Huisgen 1,3-dipolar cycloaddition.

1.5 The Tubes by Fiber Templates Process

The combination of both the electrospinning process and the chemical vapor deposition process provides a highly versatile basis for the preparation of continuous nanotubes.[90,138–140] As illustrated in Figure 1.8, the deposition of PPX onto electrospun nanofibers results in core-shell fibers. Subsequent removal of the in-
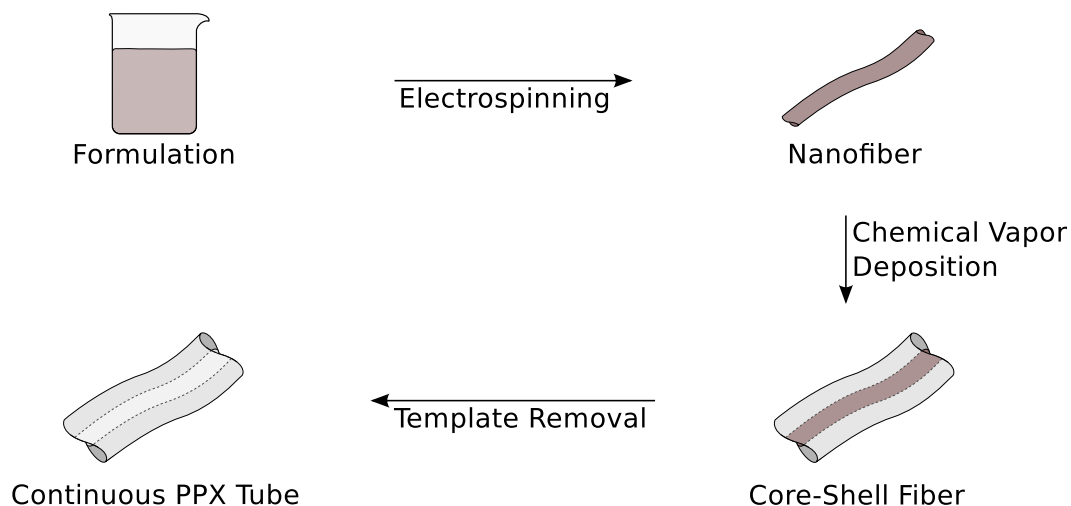
Formulation · Electrospinning · Nanofiber · Chemical Vapor Deposition · Continuous PPX Tube · Template Removal · Core-Shell Fiber

Figure 1.8. Illustration of the tubes by fiber templates process based on electrospun nanofibers, the chemical vapor deposition of PPX, and subsequent removal of the template core material.

ner fiber template yields hollow PPX tubes. Whereas different coating techniques such as dip coating or spray coating can also be used for the so-called tubes by fiber templates (TUFT) process, the chemical vapor deposition has the advantage of a very high gap penetration capability which is favorable for a homogeneous coating of nanofiber nonwovens. Depending on the material of the encapsulated core, several methods have been established to remove the template nanofibers. As opposed to sterically demanding, branched polymers or, respectively, cross-linked polymers, linear polymers have been shown to be able to permeate the PPX shell membrane,[125,141,142] allowing for a convenient solvent extraction of the template. Further, poly(L-lactide) (PLLA) is a suitable template polymer for the TUFT process since it undergoes thermal degradation to volatile products at elevated temperatures.[140] Hence, PLLA can be quantitatively removed from the PPX nanoconfinements using an vacuum oven resulting in continuous hollow PPX tubes.

The combination of composite nanofibers with the TUFT process allows for the preparation of PPX encapsulated systems. For instance, the incorporation of nanoparticles,[140,143] dendrimers,[142] and living bacteria[143] into tubular PPX confinements have been reported.

One of the very few alternatives for the preparation of continuous polymer nanotubes is the above-mentioned coaxial electrospinning process (see Section 1.3): After the electrospinning of core-shell nanofibers, the inner core template fiber can be removed, resulting in hollow polymer nanotubes.[90,101,102]

1.6 Catalysis in Confinements

Nowadays, the use of catalysts is ubiquitous not only for manifold large-scale production processes but also in many other fields, such as pollution control, food processing, medicine, and research.[144–146] The catalysts are necessary to accelerate a desired reaction or, respectively, to save energy. However, the catalytically active compounds can change the properties of the final product or can be highly expensive or toxic. Hence, as opposed to selected applications where the catalyst conceptionally cannot be removed from the product, such as dental implants or bone cement, it is favorable for the catalysts to be easily recoverable. As a result, various techniques have been developed to effectively immobilize catalysts while maintaining—or even promoting—their activity.[147,148] A convenient method is the immobilization of a catalyst onto a carrier's surface, such as alumina[149] or magnesium chloride.[150] Figure 1.9 illustrates a surface-immobilized heterogeneous catalyst and its typical application for a continuous large-scale production of a desired product. One drawback of this immobilization method can be its heterogeneous nature: As opposed to homogeneous catalysts, the corresponding catalytic activity can be significantly lower,[148] requiring a higher amount of the heterogeneous catalyst. Further, immobilizing a homogeneous catalyst onto an insoluble carrier can change its behavior (e.g. formation of side products or selectivity).

A promising approach in order to overcome some of these obstacles is the immobilization of catalysts using nano-sized confinements. Whereas catalyst supports like activated carbon,[151] zeolites,[147,148] metal-organic frameworks,[152,153] and highly porous aluminum oxide[147,149] are based on surface-immobilization, a variety of
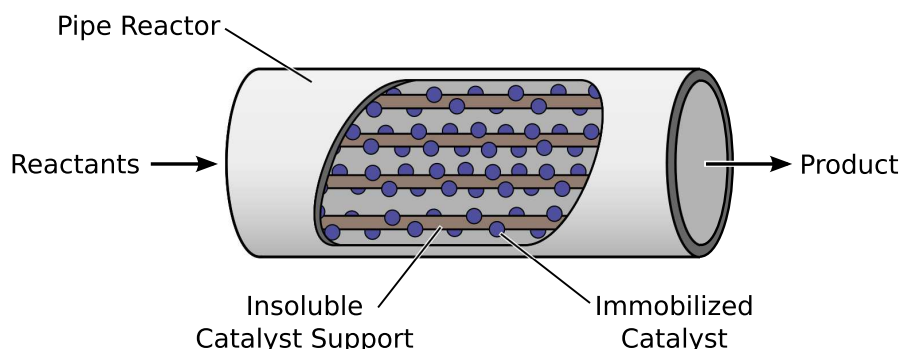
Figure 1.9. Schematic illustration of a pipe reactor for continuous production based on a surface-immobilized heterogeneous catalyst.

site-isolating, catalyst-confining alternatives have been developed, as illustrated in Figure 1.10. For instance, the immobilization of metal catalysts inside carbon nanotubes can result in modified redox properties[154] of the corresponding metals. Dendrimers can be used to encapsulate catalysts[155,156] and subsequently run a reaction in otherwise incompatible solvents (e.g. water).[157] Moreover, dendrimer encapsulated homogeneous catalysts can easily be isolated from the reaction mixture using dialysis.[158] Similarly, micelles[156,159,160] and polymer nanocapsules[156,160,161] can also be used to physically trap catalysts and make them compatible with a desired solvent. Further features of selected confinements include the prevention of poisoning of a catalyst and site-isolation from additional catalysts, allowing for one-pot tandem reactions.[1][162,163] Depending on the nature of the confinement, increased catalytic activities[164] can be achieved, as well as the promotion of asymmetric reactions or the selectivity for specific reactants (e.g. based on charge or shape).[161,165]

---

[1]A one-pot tandem reaction based on site-isolated incompatible catalysts is also referred to as "wolf and lamb" reaction.
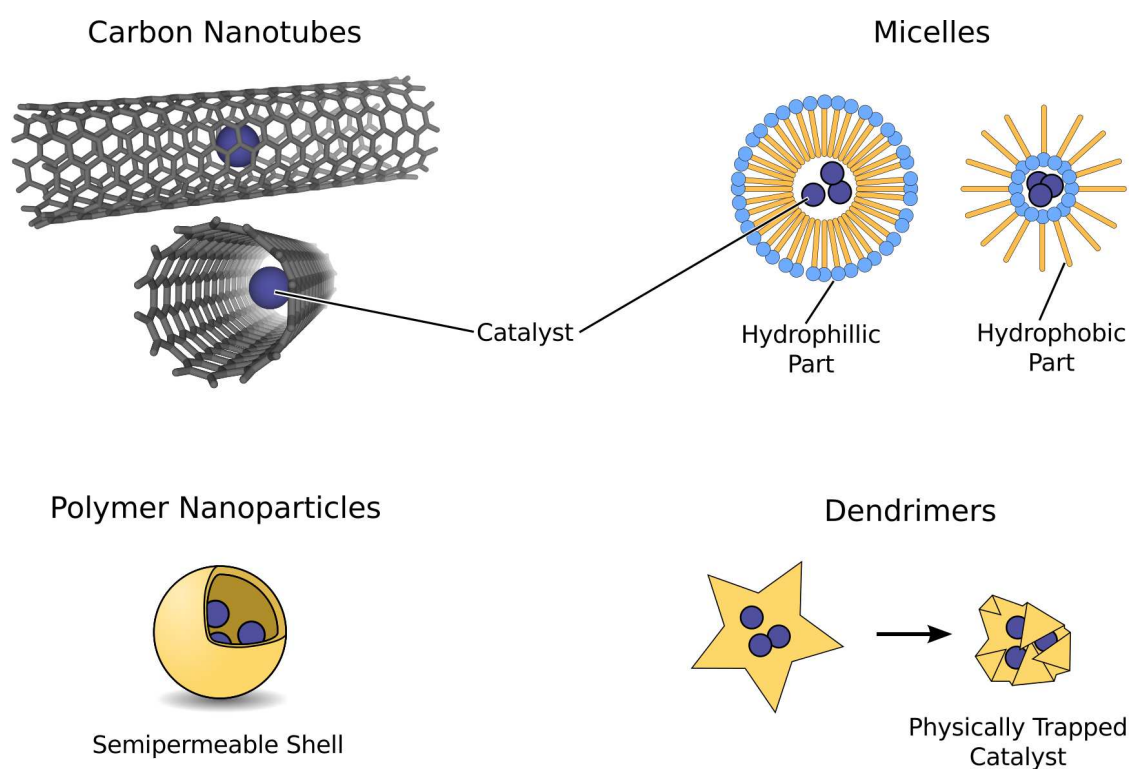
Figure 1.10. Schematic illustration of encapsulated catalysts based on nanoconfinements, such as single wall carbon nanotubes, micelles, hollow polymer nanoparticles, and wrapping dendrimers.

1.7 Thesis Objective

The aim of this thesis was the application of the TUFT process (see Section 1.5) for the development of novel functional tubes with inner diameters of less than $1\,\mu$m. As shown in Figure 1.11, the desired systems were continuous tubes featuring a clickable[166,167] surface and, respectively, hollow tubes loaded with catalysts such as gold nanoparticles or metal-functionalized dendrimers. Since the resulting nonwoven tube systems should be insoluble (see Section 1.4) and feature a high porosity and surface area, respectively, they could be promising tea bag-like catalysts: PPX tubes are easily recoverable from the reaction medium with no further product purification necessary.[142] Whereas the PPX-encapsulated gold nanoparticles could be used for heterogeneous catalysis, the confined dendritic catalysts should be suitable for homogeneous catalytic reactions. The clickable PPX tubes could be equipped with catalysts in order to obtain a catalytically active surface. In addition, thermal treatment of the gold-loaded PPX tubes could result in decomposition of the polymer material along with fusion of the metal nanoparticles. Hence, continuous conductive gold nanowires could be obtained for applications such as microelectronics and sensor devices,[55–57] photovoltaic cells,[63] and LEDs.[62]

Detailed information concerning the underlying motivation, related literature, the preparative strategy, suitable characterization methods, and both the application and evaluation of the prepared systems is given in the Thesis Overview (Chapter 2) and the subsequent chapters.
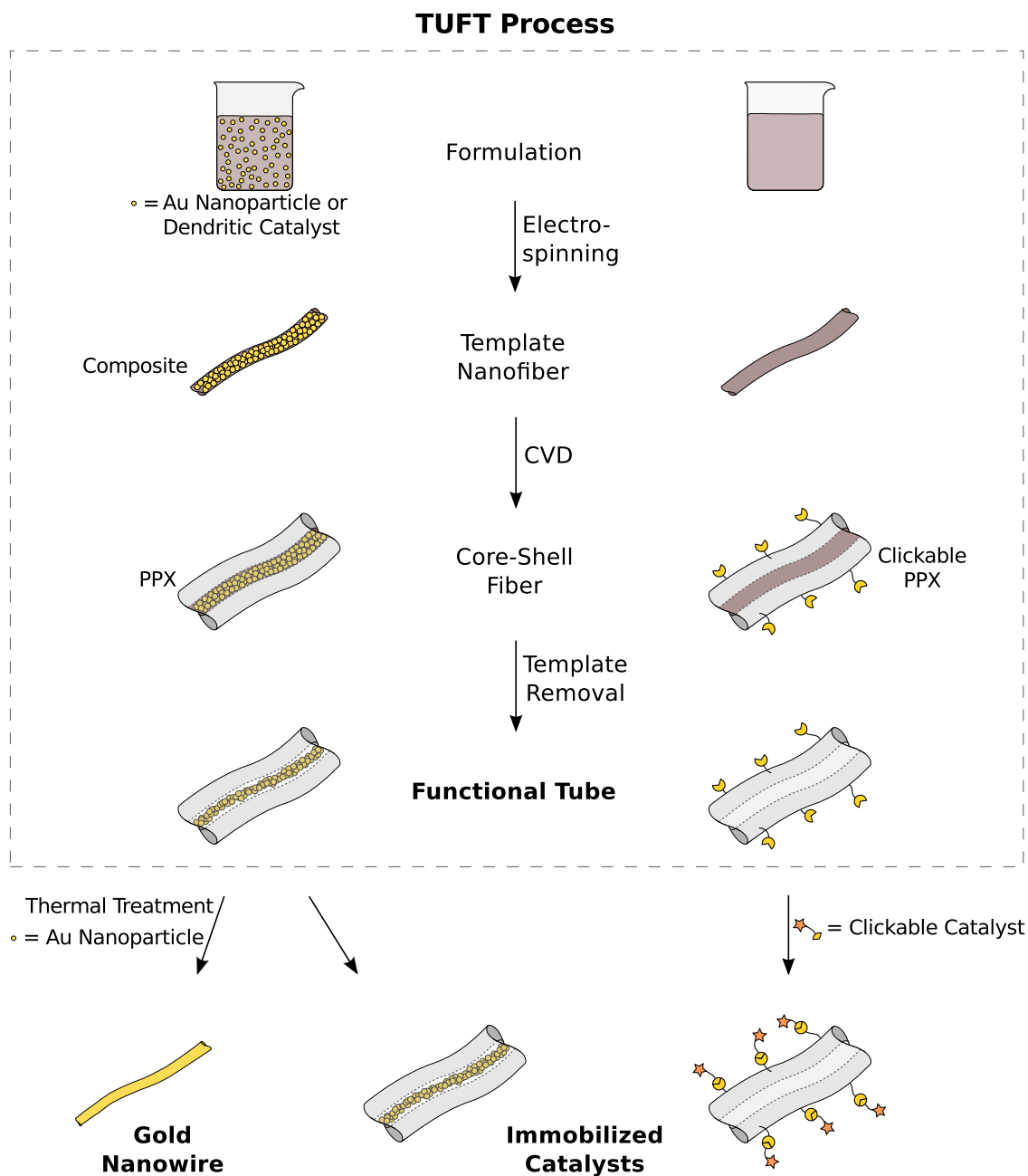
TUFT Process

∘ = Au Nanoparticle or
Dendritic Catalyst

Composite

PPX

Formulation

Electro-
spinning

Template
Nanofiber

CVD

Core-Shell
Fiber

Template
Removal

Functional Tube

Clickable
PPX

Thermal Treatment
∘ = Au Nanoparticle

⋆ = Clickable Catalyst

**Gold
Nanowire**

**Immobilized
Catalysts**

Figure 1.11. Overview of the preparative strategy in order to obtain novel functional tubes. After the TUFT process, the resulting tubes could be used for the preparation of continuous conductive nanowires, for catalysis, or for subsequent click reactions.

2 Thesis Overview

This thesis contains four scientific papers - three of which already have been published, whereas the fourth paper has been submitted to *Small* (Wiley-VCH). The corresponding content is presented in full detail in Chapter 4–7 and a conclusive overview of each paper is given in the following. The individual contribution to joint publications is denoted in Section 2.5. All papers are based on the TUFT process, combining a sequence of electrospinning, chemical vapor deposition of PPX, and the subsequent removal of the used template material. As a result, novel continuous functional PPX tubes for applications such as catalysis or microelectronics were successfully prepared.

2.1 Immobilization of Catalysts in Poly(*p*-xylylene) Nanotubes

In the chemical industry, the vast majority of large-scale production processes relies on the use of catalysts in order to maximize efficiency. However, in most cases it is necessary for the corresponding reaction products to be free of catalyst impurities since catalysts can be toxic, expensive, or affect the properties of the products. Whereas homogeneous catalysts show the highest activity, heterogeneous catalyst systems are generally easier to remove, for instance using filtration techniques (see Section 1.6). Normally, depending on the type of heterogeneous catalyst support, the surface area is either large, thus challenging purification (e.g. small porous particles such as activated carbon), or the surface area is very limited allowing for convenient recovery (e.g. large plates carrying the immobilized catalysts on the surface, see Figure 1.9 on page 18). In order to develop a highly versatile carrier for various catalysts, functional PPX tubes were prepared (based on the TUFT process, see Figure 1.11 on page 21) which featured a high surface area (see corresponding publication in Chapter 4). Subsequently, the tubes were equipped with either a TEMPO-based catalyst or bipyridine moieties, suitable for further complexation with transition metals (Figure 2.1). Studies were conducted to evaluate the surface-immobilization of the catalysts[1] and the resulting applicability for surface-catalysis. Further, the reusability of the heterogeneous catalyst systems was tested

---

[1]More precisely, the azide-alkyne Huisgen cycloaddition onto the solid PPX surface.
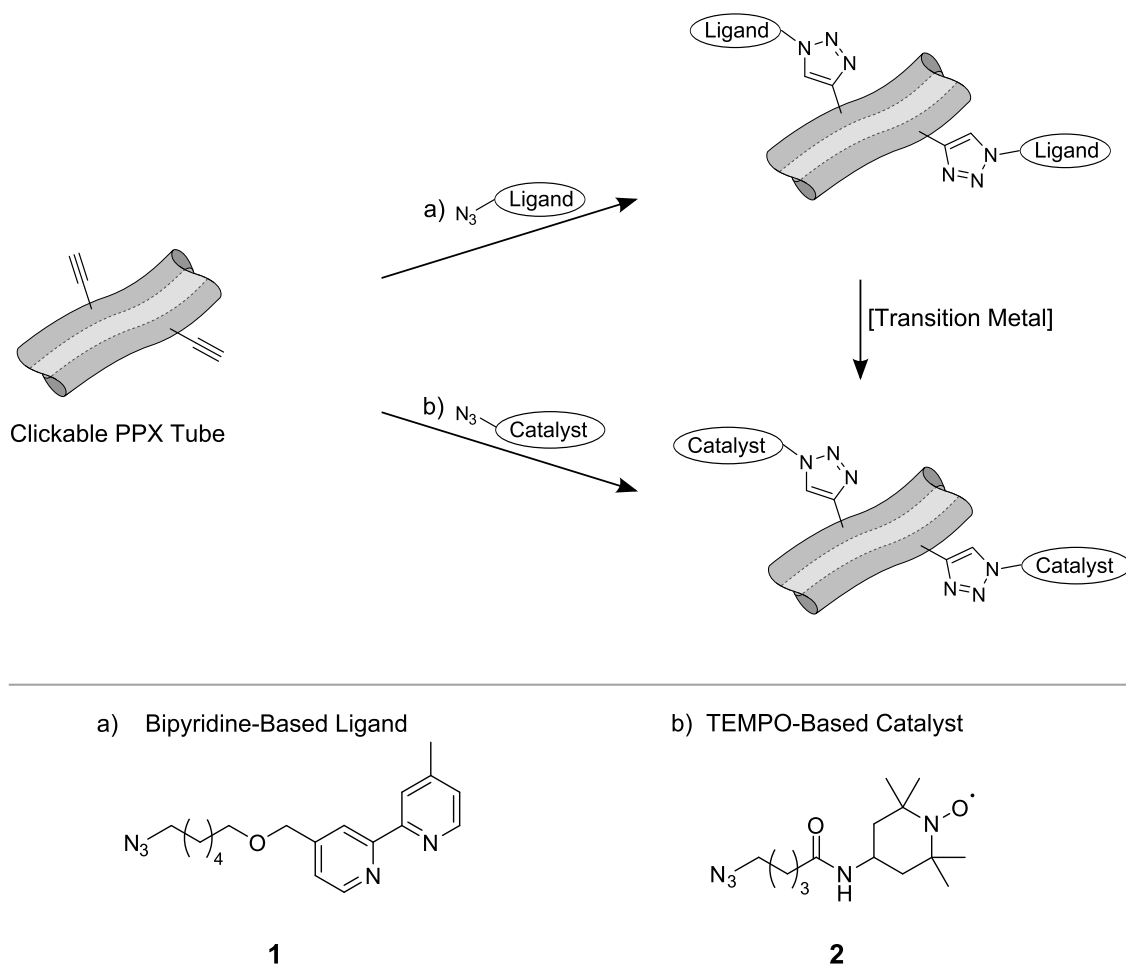
Figure 2.1. Concept for the surface-immobilization of a) a clickable bipyridine ligand or b) a TEMPO-based catalyst onto ethynyl-functionalized PPX tubes.

with regard to catalytic activity and stability of the carrier material.

First, poly(ethylene oxide) (PEO; 300,000 g mol⁻¹ molecular weight) template nanofibers were electrospun from an aqueous solution of 10 wt% PEO. The resulting fibers were free of beads and had an average diameter of 415 ± 59 nm. A clickable PPX precursor, 4-ethynyl-[2.2]paracyclophane, was prepared in three steps with a good yield and subsequently used for the CVD process. The deposited layer thickness on the nonwoven was about 115 nm, and no cracks or pores were visible. In agreement with previous studies,[141,142] the inner PEO template material could be extracted using water, whereas the PPX shell remained insoluble. The successful conversion to hollow PPX tubes was supported by gravimetric measurements and

scanning electron micrographs of the corresponding cross-sections. Next, in order to immobilize two different types of catalysts, a (2,2,6,6-tetramethylpiperidin-1-yl)oxy (TEMPO) derivative and a bipyridine ligand were synthesized. Each compound was prepared in three steps and was subsequently clicked onto the PPX surface of the ethynyl-functionalized tubes. After coupling the attached bipyridine ligand with copper, both catalyst systems were ready for use.

As shown in Scheme 2.1, the copper(I)-bipyridine catalyst **5** was used for the click reaction of phenyl propargyl ether (**3**) with benzyl azide (**4**), whereas the TEMPO-based catalyst system **8** was used for the oxidation of benzyl alcohol (**7**) to the corresponding aldehyde **9**. As a result, even after 17 cycles, the copper-based cata-
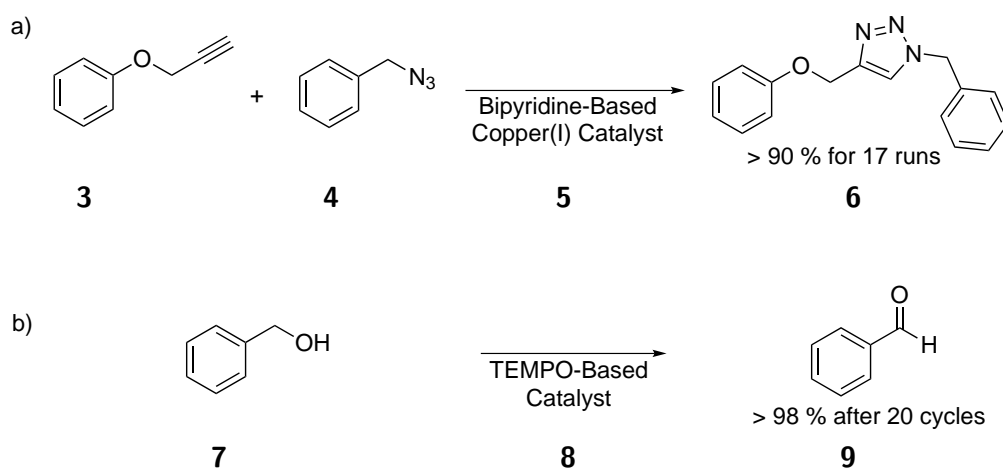
Scheme 2.1. Studied model reactions for both immobilized catalyst systems: a) Click reaction using the bipyridine-based copper(I) catalyst. b) TEMPO-catalyzed oxidation of benzyl alcohol (**7**).

lyst system **5** did not show abrasion. Further, the corresponding catalytic activity remained very high with yields of above 90 %, and there were signs of leaching of trace amounts of copper. In contrast, after 20 cycles the TEMPO catalyst **8** showed wearing[1] yet the catalytic activity remained excellent with yields of above 95 %.

The prepared functional PPX tubes are a promising basis for the surface-immobilization of various catalysts. Since the system is compatible with the highly versatile azide-alkyne click reaction, not only clickable catalysts can be attached but also clickable ligands for subsequent complexation with further catalysts.

---

[1]Most likely due to the harsh oxidizing reaction conditions, as stated in the paper (Chapter 4).

2.2 Transition Metal-Functionalized Dendrimers Encapsulated in PPX Tubes as Reusable Catalysts

In order to develop a powerful catalyst system, combining the activity of homogeneous catalysts with the advantages of immobilized heterogeneous catalysts (compare Section 1.6 and 2.1), continuous polymer tubes with encapsulated catalysts were prepared (see corresponding publication in Chapter 5). The underlying concept was based on preliminary studies concerning the physical encapsulation of sterically demanding dendrimers inside PPX tubes[142] with the focus on functionalized dendrimers and their suitability for transition metal catalysis. As illustrated in Figure 2.2, composite nanofibers were used for the TUFT process, resulting in PPX tubes with encapsulated dendrimer-based catalysts. As opposed to surface-
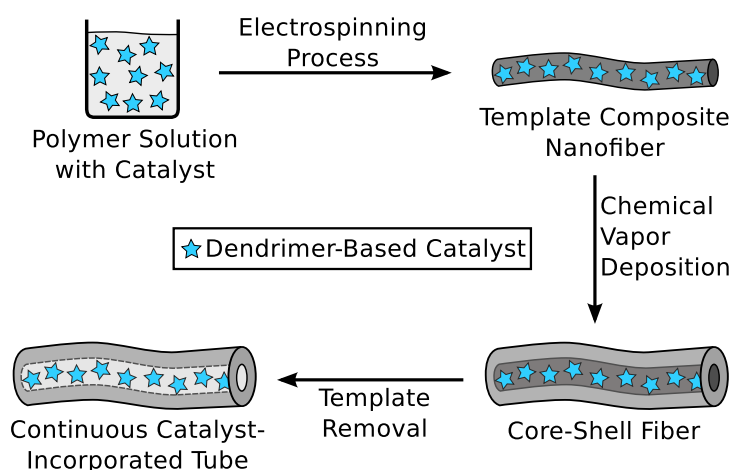

**Figure 2.2.** Concept for the preparation of PPX tube-encapsulated dendrimer catalysts.[1]

immobilized catalysts (Section 2.1), the tube-encapsulated catalysts could be used for homogeneous catalysis and also required no subsequent purification.

In order to prepare the dendrimer-based catalysts, commercially available poly-(amido amid) (PAMAM) dendrimers featuring NH_2–groups were used. Whereas generation 4 dendrimers have been shown to permeate the shell of PPX tubes, generation 5 dendrimers remain immobilized inside the confinement. Hence, the NH_2-moieties of a generation 5 PAMAM were first converted into diphenylphosphine-

---

groups, followed by complexation with either [PdCl(allyl)]$_2$ or Cu(I)Br. The corresponding dendritic catalysts were electrospun with a polyurethane template polymer, featuring excellent mechanical properties for further handling. The resulting composite nonwovens were then coated with PPX and subsequently immersed in tetrahydrofuran in order to extract the inner template polyurethane. Using inductively coupled plasma mass spectroscopy, the respective solvent was analyzed for leached catalysts confirming the successful immobilization of the encapsulated catalysts.

To study the suitability of the prepared PPX tubes for catalysis, various reactions based on the Pd-catalyzed Suzuki-Miyaura coupling and, respectively, the Cu-catalyzed azide-alkyne Huisgen cycloaddition were performed. As a result, yields of above 88 % were reached for the palladium catalyst, whereas the copper catalyst led to quantitative conversions. In particular, the two model reactions shown in Scheme 2.2 were tested in detail to evaluate the reusability of the PPX nanoreactors. In both cases, the respective catalyst system was reused at least 14 times,
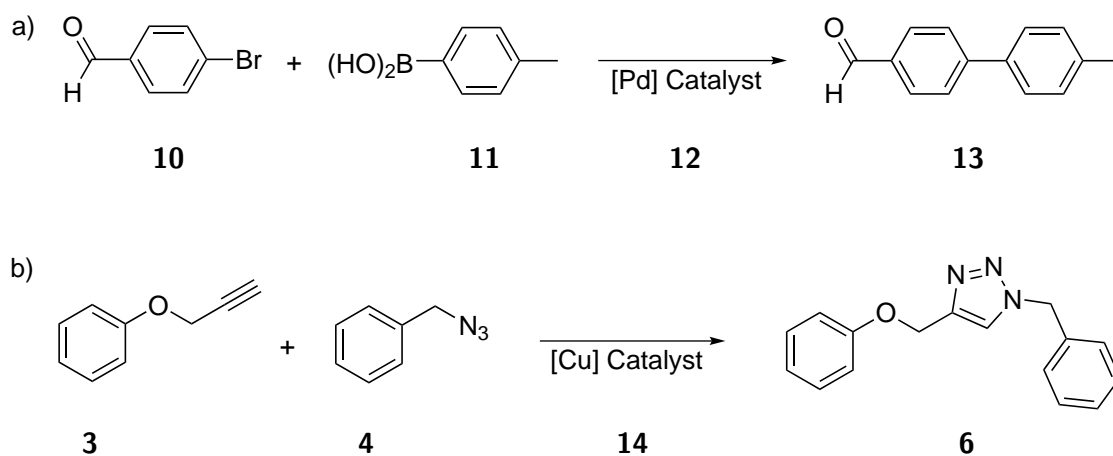
Scheme 2.2. Selected model reactions for the evaluation of the reusability of both catalyst systems: a) Suzuki-Miyaura coupling using Pd catalyst **12**. b) Cu catalyzed azide-alkyne Huisgen cycloaddition based on catalyst system **14**.

resulting in a slight decrease of the corresponding yields. However, the PPX surface remained intact and did not show signs of abrasion.

The successful combination of functionalization and encapsulation of dendrimers inside PPX nanoconfinements represents a highly versatile, promising proof-of-

concept: Sterically demanding catalysts based on dendrimers, nanoparticles, or enzymes could be immobilized, yet used for homogeneous catalysis. Further, a combination with surface-immobilized catalysts could allow for site-isolated tandem catalysis.[168]

2.3 Tea Bag-Like Polymer Nanoreactors Filled with Gold Nanoparticles

Similar to the encapsulation of dendrimers inside PPX tubes, the TUFT process was used for the immobilization of gold nanoparticles (see corresponding publication in Chapter 6). In comparison to the dendrimer-based system, the leaching behavior was studied as well as the suitability for catalysis.

Since PLLA can be quantitatively removed from PPX tubes (see Section 1.5), it was used for both the stabilization of the gold particles and the template material for the electrospun fibers. Hence, thiol-functionalized PLLA was first synthesized and subsequently used for the preparation of the gold nanoparticles. The resulting average diameter of the particles was 9.5 ± 2.8 nm, and the corresponding amount of gold was 18–20 wt%. GPC coupled with a diode array detector[52] proved the successful addition of the polymer onto the gold surface. A true to scale illustration of such a particle, as well as a TEM picture showing the respective lattice planes of the spherical gold crystals, is shown in Figure 2.3 a) and b), respectively.

Next, a solution of 10 wt% of the particles was electrospun from dichloromethane. In order to avoid the formation of beads, 0.25 wt% of the organosoluble salt tetraoctylammonium bromide was added as well as 0.5 wt% of free PLLA to improve the mechanical properties of the resulting nonwovens. The composite fibers had an average diameter of 322 ± 72 nm and were coated with about 195 nm of PPX. Thermal treatment at reduced pressure led to quantitative decomposition of the encapsulated PLLA template material. The obtained PPX tubes are shown in Figure 2.3 c) and were characterized using SEM and TEM. According to performed leaching studies, the particles were successfully immobilized despite the thin PPX layer of less than 200 nm. The suitability for catalysis was tested based on the two model reactions in Figure 2.3: At room temperature, the silane alcoholysis d) of silane **15**
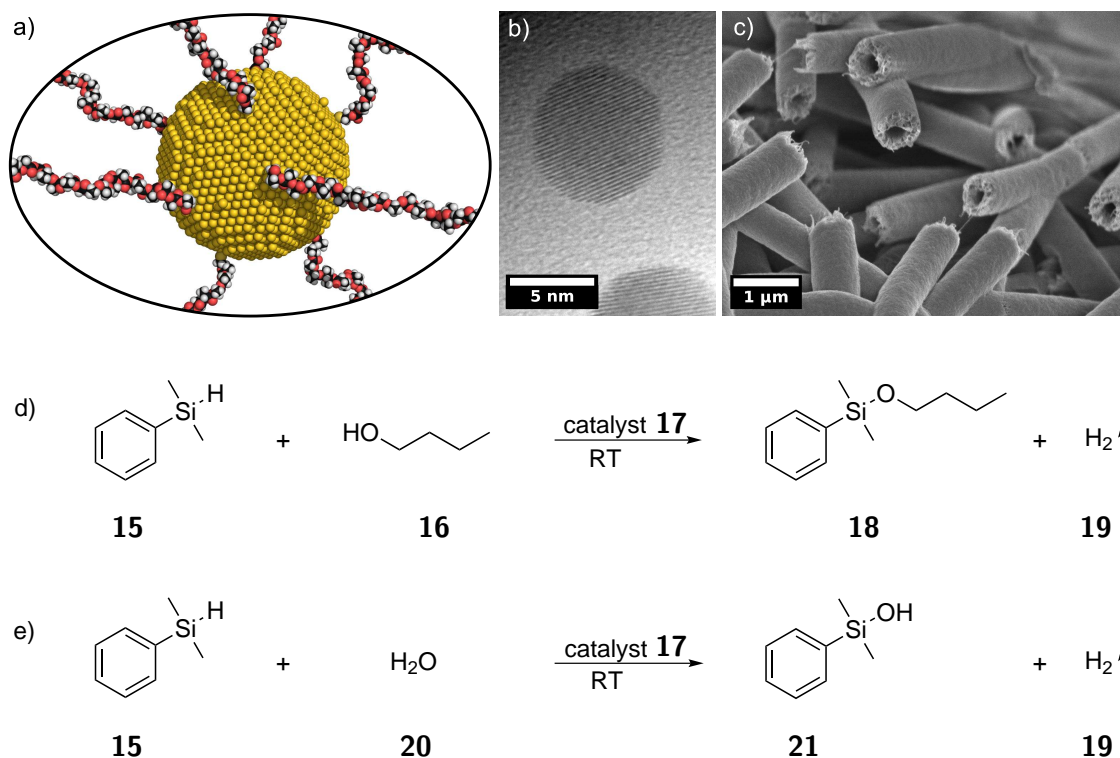
Figure 2.3. a) Illustration of a PLLA-stabilized gold nanoparticle with a 5.7 nm core diameter (atoms are true to scale). b) Corresponding TEM picture showing the characteristic lattice planes of monocrystalline gold. c) SEM picture of the resulting PPX tubes with encapsulated gold nanoparticles after the TUFT process. d) Performed silane alcoholysis of silane **15** and *n*-butanol in order to study the gold-based PPX nanoreactors **17**. e) Hydrolytic oxidation of the corresponding silane using the same catalyst.[1]

and *n*-butanol yielded 100% of the corresponding siloxane **18** in 26 h, whereas the hydrolytic oxidation e) resulted in a quantitative conversion to silanol **21** after 3.5 h. Removing the tea bag-like catalyst system during the reaction resulted in a dormant state until reintroduction, confirming the successful encapsulation of the gold nanoparticles. The catalyst system was used 18 times with no decrease in activity and no signs of abrasion, according to SEM measurements.

The encapsulation of catalytically active nanoparticles inside continuous PPX tubes could be used to prepare very robust, tea bag-like catalyst systems. There was no sign of leaching or wearing of the material. As for the PPX-encapsulated dendrimers, a combination with surface-immobilized catalysts could allow for site-

---

isolated tandem catalysis.

2.4 Conductive Gold Nanofibers Based on Gold-Filled Polymer Tubes

As mentioned in the previous section, the gold-carrying PPX tubes were an excellent basis for catalysis applications. Yet since the polymer-stabilized gold nanoparticles showed an outstanding redispersibility in organic solvents, another promising application was developed: Increasing the amount of confined gold inside the PPX tubes allowed for the preparation of continuous conductive gold nanowires (see corresponding paper in Chapter 7).

First, PLLA-stabilized gold nanoparticles with 61 wt% gold were synthesized and subsequently used for the TUFT process (Figure 2.4): Composite nanofibers of
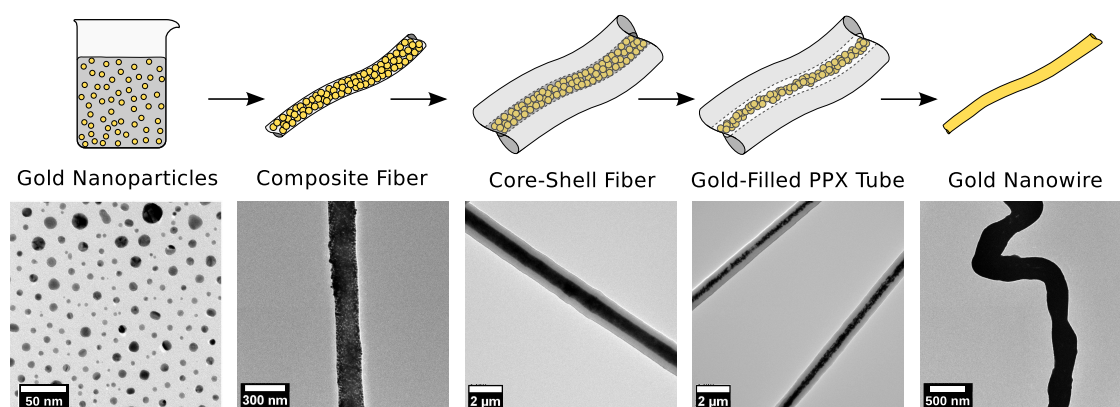

| Gold Nanoparticles | Composite Fiber | Core-Shell Fiber | Gold-Filled PPX Tube | Gold Nanowire |

Figure 2.4. Preparation of continuous conductive gold nanowires based on the TUFT process. Top: Illustration of the underlying concept. Bottom: Transmission electron micrographs of the corresponding nanoparticles, composite fibers, core-shell fibers, PPX tubes, and final gold nanowires.

118 ± 38 nm diameter were electrospun and coated via CVD with 345 ± 36 nm of PPX. Subsequent removal of the confined PLLA template material resulted in gold-filled PPX tubes. Thermal treatment up to 1050 °C led to the decomposition of the PPX shell along with fusion of the encapsulated gold aggregates. As a result, gold nanofibers featuring a smooth surface were obtained.

Using a combination of TEM and scanning helium ion microscopy, the heat-induced transition towards conductive gold nanowires was studied. Further, trans-

mission high energy electron diffraction confirmed the presence of polycrystalline gold.

2.5 Individual Contributions to Joint Publications

In the following, the individual contribution of each author and, respectively, co-author to each paper is specified in detail.

Immobilization of Catalysts in Poly(*p*-xylylene) Nanotubes

Published in *RSC Advances* **2013**, *3*, 25976.
By Johannes A. M. Hepperle, Fabian Mitschang, Anna K. Bier, Barbara K. Dettlaff, Andreas Greiner, and Armido Studer.

I prepared the functionalized PPX tubes combining the TUFT process and the ethynyl-functionalized [2.2]paracyclophane precursor based on preliminary studies by Anna K. Bier. This included the electrospinning process, the CVD process, the template removal, and the accompanying characterization using SEM and TEM. Further, I wrote the corresponding sections for the manuscript and the Supporting Information. Johannes A. M. Hepperle and Barbara K. Dettlaff equipped the tubes with the catalysts and performed the catalytic studies. The manuscript was completed by J. Hepperle. Prof. Andreas Greiner and Prof. Armido Studer supervised the project, providing help in developing the concept and giving scientific feedback, and also proofread the manuscript.

Transition Metal-Functionalized Dendrimers Encapsulated in PPX Tubes as Reusable Catalysts

Published in *Macromolecules* **2013**, *46*, 8784.
By Fabian Mitschang, Barbara K. Dettlaff, Jean-Pierre Lindner, Armido Studer, and Andreas Greiner.

I developed, prepared, and characterized the PPX tubes with encapsulated transition metal-functionalized dendrimers. The modification of the dendrimers and the catalytic studies were performed by Barbara K. Dettlaff and Jean-Pierre Lind-

ner. The manuscript and the Supporting Information were written by me. Prof. Andreas Greiner and Prof. Armido Studer supervised the project, contributing scientific feedback and shaping the concept. Together with Barbara K. Dettlaff, they proofread the publication.

Tea Bag-Like Polymer Nanoreactors Filled with Gold Nanoparticles

Published in *Angewandte Chemie, International Edition* **2014**, *in press.*
By Fabian Mitschang, Holger Schmalz, Seema Agarwal, and Andreas Greiner.

I developed and performed all experiments. Both the manuscript and the Supporting Information were written by me. Prof. Andreas Greiner helped develop the project's concept, supervised it, and continually motivated towards a successful outcome. Prof. Seema Agarwal and Holger Schmalz, Ph.D., provided scientific input along with new insights and helped shape the project as it progressed. Together with Prof. Greiner, they proofread the publication.

Conductive Gold Nanofibers Based on Gold-Filled Polymer Tubes

Submitted to *Small.*
By Fabian Mitschang, Markus Langner, Henning Vieker, Armin Gölzhäuser, and Andreas Greiner.

With the help of my intern Markus Langner, I prepared the gold nanoparticles and the corresponding gold nanowires. The TUFT process was performed by me including the electrospinning process, the CVD process, and the pyrolysis of the template material. All analysis was done by me except for the scanning helium ion microscopy, which was conducted by Henning Vieker under supervision of Prof. Armin Gölzhäuser (Bielefeld University). The manuscript was written by me. Prof. Andreas Greiner supervised the project, provided scientific feedback, and guided the direction of the research. Further, Prof. Greiner proofread the manuscript.

3 References

[1] M. A. Uppal, A. Kafizas, M. B. Ewing, I. P. Parkin, *J. Mater. Chem. A* **2013**, *1*, 7351.

[2] N. N. Long, L. V. Vu, C. D. Kiem, S. C. Doanh, C. T. Nguyet, P. T. Hang, N. D. Thien, L. M. Quynh, *J. Phys. Conf. Ser.* **2009**, *187*, 012026.

[3] G. Schmid, U. Simon, *Chem. Commun.* **2005**, *6*, 697.

[4] Y. Pan, S. Neuss, A. Leifert, M. Fischler, F. Wen, U. Simon, G. Schmid, W. Brandau, W. Jahnen-Dechent, *Small* **2007**, *3*, 1941.

[5] E. E. Connor, J. Mwamuka, A. Gole, C. J. Murphy, M. D. Wyatt, *Small* **2005**, *1*, 325.

[6] L. A. Dykman, N. G. Khlebtsov, *Acta Naturae* **2011**, *3*, 34.

[7] D. A. Giljohann, D. S. Seferos, W. L. Daniel, M. D. Massich, P. C. Patel, C. A. Mirkin, *Angew. Chem. Int. Ed.* **2010**, *49*, 3280.

[8] W. Cai, T. Gao, H. Hong, J. Sun, *Nanotechnol. Sci. Appl.* **2008**, *1*, 17.

[9] M. Homberger, U. Simon, *Phil. Trans. R. Soc. A* **2010**, *368*, 1405.

[10] M. E. Franke, T. J. Koplin, U. Simon, *Small* **2006**, *2*, 36.

[11] X. Zhang, Q. Guo, D. Cui, *Sensors* **2009**, *9*, 1033.

[12] C. C. D. Wang, W. C. H. Choy, C. Duan, D. D. S. Fung, W. E. I. Sha, F.-X. Xie, F. Huang, Y. Cao, *J. Mater. Chem.* **2012**, *22*, 1206.

[13] J. H. Park, Y. T. Lim, O. O. Park, J. K. Kim, J.-W. Yu, Y. C. Kim, *Chem. Mater.* **2004**, *16*, 688.

[14] C. D. Pina, E. Falletta, L. Prati, M. Rossi, *Chem. Soc. Rev.* **2008**, *37*, 2077.

[15] A. Corma, H. Garcia, *Chem. Soc. Rev.* **2008**, *37*, 2096.

[16] G. C. Bond, *Catal. Rev. Sci. Eng.* **1999**, *41*, 319.

[17] D. T. Thompson, *Nano Today* **2007**, *2*, 40.

[18] J. Turkevich, P. C. Stevenson, J. Hillier, *Discuss. Faraday Soc.* **1951**, *11*, 55.

[19] M. Brust, M. Walker, D. Bethell, D. J. Schiffrin, R. Whyman, *J. Chem. Soc., Chem. Commun.* **1994**, 801.

[20] T. H. Tran, S. Y. Park, H. Lee, S. Park, B. Kim, O.-H. Kim, B. Oh, D. Lee, H. Lee, *Analyst* **2012**, *137*, 991.

[21] L. Polavarapu, Q.-H. Xu, *Nanotechnology* **2009**, *20*, 185606.

[22] R. Sardar, A. M. Funston, P. Mulvaney, R. W. Murray, *Langmuir* **2009**, *25*, 13840.

[23] L. Vigderman, B. P. Khanal, E. R. Zubarev, *Adv. Mater.* **2012**, *24*, 4811.

[24] B. Goris, S. Bals, W. van den Broek, E. Carbó-Argibay, S. Gómez-Graña, L. M. Liz-Marzán, G. van Tendeloo, *Nat. Mater.* **2012**, *11*, 930.

[25] S. K. Das, A. R. Das, A. K. Guha, *Small* **2010**, *6*, 1012.

[26] K. Sohn, F. Kim, K. C. Pradel, J. Wu, Y. Peng, F. Zhou, J. Huang, *ACS Nano* **2009**, *3*, 2191.

[27] H. Goesmann, C. Feldmann, *Angew. Chem. Int. Ed.* **2010**, *49*, 1362.

[28] W. Caseri, *Macromol. Rapid Commun.* **2000**, *21*, 705.

[29] J. Li, Y. Lin, B. Zhao, *J. Nanopart. Res.* **2002**, *4*, 345.

[30] J. Hang, L. Shi, X. Feng, L. Xiao, *Powder Technol.* **2009**, *192*, 166.

[31] C. Lourenco, M. Teixeira, S. Simões, R. Gaspar, *Int. J. Pharm.* **1996**, *138*, 1.

[32] P. Kalimuthu, S. A. John, *Mater. Chem. Phys.* **2010**, *122*, 380.

[33] M.-C. Daniel, D. Astruc, *Chem. Rev.* **2004**, *104*, 293.

[34] M. K. Corbierre, N. S. Cameron, M. Sutton, S. G. J. Mochrie, L. B. Lurio, A. Rühm, R. B. Lennox, *J. Am. Chem. Soc.* **2001**, *123*, 10411.

[35] D.-H. Han, C.-Y. Pan, *J. Polym. Sci., Part A: Polym. Chem.* **2007**, *46*, 341.

[36] H. Pletsch, L. Peng, F. Mitschang, A. Schaper, M. Hellwig, D. Nette, A. Seubert, A. Greiner, S. Agarwal, *Small* **2014**, *10*, 201.

[37] Y. Negishi, W. Kurashige, Y. Niihoria, K. Nobusada, *Phys. Chem. Chem. Phys.* **2013**, *15*, 18736.

[38] T. C. Hales, *Ann. Math.* **2005**, *162*, 1065.

[39] P. Buffat, J.-P. Borel, *Phys. Rev. A* **1976**, *13*, 2287.

[40] P. Georgiev, A. Bojinova, B. Kostova, D. Momekova, T. Bjornholm, K. Balashev, *Colloids Surf., A* **2013**, *434*, 154.

[41] B. N. Khlebtsov, N. G. Khlebtsov, *Colloid J.* **2011**, *73*, 118.

[42] G.-T. Wei, F.-K. Liu, C. R. C. Wang, *Anal. Chem.* **1999**, *71*, 2085.

[43] G.-T. Wei, F.-K. Liu, *J. Chromatogr. A* **1999**, *836*, 253.

[44] E. Bolea, J. Jiménez-Lamana, F. Laborda, J. R. Castillo, *Anal. Bioanal. Chem.* **2011**, *401*, 2723.

[45] G. A. Rance, D. H. Marsh, A. N. Khlobystov, *Chem. Phys. Lett.* **2008**, *460*, 230.

[46] S. Zeng, K.-T. Young, I. Roy, X.-Q. Dinh, X. Yu, F. Luan, *Plasmonics* **2011**, *6*, 491.

[47] A. Yadav, Y. K. Prajapati, V. Singh, J. P. Saini, *KIET Int. J. Commun. Electron.* **2013**, *1*, 17.

[48] O. Prymak, S. Ristig, V. Meyer-Zaika, A. Rostek, L. Ruiz, J. González-Calbet, M. Vallet-Regi, M. Epple, *Russ. Phys. J.* **2014**, *56*, 1111.

[49] J. I. Langford, A. J. C. Wilson, *J. Appl. Cryst.* **1978**, *11*, 102.

[50] S. D. Techane, L. J. Gamble, D. G. Castner, *Biointerphases* **2011**, *6*, 98.

[51] E. Mansfield, K. M. Tyner, C. M. Poling, J. L. Blacklock, *Anal. Chem.* **2014**, *86*, 1478.

[52] S. Bokern, K. Gries, H.-H. Görtz, V. Warzelhan, S. Agarwal, A. Greiner, *Adv. Funct. Mater.* **2011**, *21*, 3753.

[53] B. Ding, C. Li, Y. Maiyauchi, O. Kuwaki, S. Shiratori, *Nanotechnology* **2006**, *17*, 3685.

[54] S. Xu, Z. L. Wang, *Pure Appl. Chem.* **2011**, *83*, 2171.

[55] Y. Wu, J. Xiang, C. Yang, W. Lu, C. M. Lieber, *Nature* **2004**, *430*, 61.

[56] Y. Engel, R. Elnathan, A. Pevzner, G. Davidi, E. Flaxer, F. Patolsky, *Chem. Int. Ed.* **2010**, *49*, 6830.

[57] P. Arora, A. Sindhu, N. Dilbaghi, A. Chaudhury, *Appl. Nanosci.* **2013**, *3*, 363.

[58] C. K. Chan, H. Peng, G. Liu, K. McIlwrath, X. F. Zhang, R. A. Huggins, Y. Cui, *Nat. Nanotechnol.* **2008**, *3*, 31.

[59] H.-H. Li, S. Zhao, M. Gong, C.-H. Cui, D. He, H.-W. Liang, L. Wu, S.-H. Yu, *Angew. Chem. Int. Ed.* **2013**, *52*, 7472.

[60] H. Wu, L. Hu, M. W. Rowell, D. Kong, J. J. Cha, J. R. McDonough, J. Thu, Y. Yang, M. D. McGhee, Y. Cui, *Nano Lett.* **2010**, *10*, 4242.

[61] J. van de Groep, P. Spinelli, A. Polman, *Nano Lett.* **2012**, *12*, 3138.

[62] Z. Li, J. Kang, Z. Liu, C. Du, X. Lee, X. Li, L. Wang, X. Yi, H. Zhu, G. Wang, *AIP Adv.* **2013**, *3*, 042134.

[63] M. T. Borgström, J. Wallentin, M. Heurlin, S. Fält, P. Wickert, J. Leene, M. H. Magnusson, K. Deppert, L. Samuelson, *IEEE J. Sel. Top. Quant.* **2011**, *17*, 1050.

[64] A. M. Leach, M. McDowell, K. Gall, *Adv. Funct. Mater.* **2007**, *17*, 43.

[65] I. Park, Z. Li, A. P. Pisano, R. S. Williams, *Nanotechnology* **2010**, *21*, 015501.

[66] R. Juhasz, N. Elfström, J. Linnros, *Nano Lett.* **2005**, *5*, 275.

[67] L. Dupré, T. Gorisse, A. L. Lebranchu, T. Bernardin, P. Gentile, H. Renevier, D. Buttard, *Nanoscale Res. Lett.* **2013**, *8*, 123.

[68] H. Feng, Y. Yang, Y. You, G. Li, J. Guo, T. Yu, Z. Shen, T. Wub, B. Xing, *Chem. Commun.* **2009**, *15*, 1984.

[69] M. E. Toimil-Molares, *Beilstein J. Nanotechnol.* **2012**, *3*, 860.

[70] J. E. Hujdic, A. P. Sargisian, J. Shao, T. Yea, E. J. Menke, *Nanoscale* **2011**, *3*, 2697.

[71] E. C. Walter, M. P. Zach, F. Favier, B. J. Murray, K. Inazu, J. C. Hemminger, R. M. Penner, *ChemPhysChem* **2003**, *4*, 131.

[72]   C. Schönenberger, B. M. I. van der Zande, L. G. J. Fokkink, M. Henny, C. Schmid, M. Krüger, A. Bachtold, R. Huber, H. Birk, U. Staufer, *J. Phys. Chem.* **1997**, *101*, 5497.

[73]   J. H. Song, Y. Wu, B. Messer, H. Kind, P. Yang, *J. Am. Chem. Soc.* **2001**, *123*, 10397.

[74]   H. Wang, A. J. Patil, K. Liu, S. Petrov, S. Mann, M. A. Winnik, I. Manners, *Adv. Mater.* **2009**, *21*, 1805.

[75]   K. Gries, H. Vieker, A. Gölzhäuser, S. Agarwal, A. Greiner, *Small* **2012**, *8*, 1436.

[76]   Y. Ding, P. Zhang, Y. Qu, Y. Jiang, J. Huang, W. Yan, G. Liu, *J. Alloy. Compd.* **2008**, *466*, 479.

[77]   B. W. Ward, J. A. Notte, N. P. Economou, *J. Vac. Sci. Technol. B* **2006**, *24*, 2871.

[78]   M. S. Joens, C. Huynh, J. M. Kasuboski, D. Ferranti, Y. J. Sigal, F. Zeitvogel, M. Obst, C. J. Burkhardt, K. P. Curran, S. H. Chalani, L. A. Stern, B. Goetze, J. A. J. Filzpatrick, *Sci. Rep.* **2013**, *3*, 3514.

[79]   J. Morgan, J. Notte, R. Hill, B. Ward, *Micros. Today* **2006**, *14*, 24.

[80]   D. C. Bell, *Micros. Microanal.* **2009**, *15*, 147.

[81]   M. Wilms, J. Conrad, K. Casilev, M. Kreiter, G. Wegner, *Appl. Surf. Sci.* **2004**, *238*, 490.

[82]   Y. Long, Z. Chen, W. Wang, F. Bai, A. Jin, C. Gu, *Appl. Phys. Lett.* **2005**, *86*, 153102.

[83]   J. Alvarez, I. Ngo, M.-E. Gueunier-Farret, J.-P. Kleider, L. Yu, P. R. Cabarrocas, S. Perraud, E. Rouvière, C. Celle, C. Mouchet, J.-P. Simonato, *Nanoscale Res. Lett.* **2011**, *6*, 110.

[84]   M. P. Cashion, X. Li, Y. Geng, M. T. Hunley, T. E. Long, *Langmuir* **2009**, *26*, 678.

[85]   M. G. McKee, J. M. Layman, M. P. Cashion, T. E. Long, *Science* **2006**, *311*, 353.

[86] A. Celebioglu, T. Uyar, *Nanoscale* **2012**, *4*, 621.

[87] A. Greiner, J. H. Wendorff, *Angew. Chem. Int. Ed.* **2007**, *46*, 5670.

[88] D. Li, Y. Xia, *Adv. Mater.* **2004**, *16*, 1151.

[89] Z.-M. Huang, Y.-Z. Zhang, M. Kotaki, S. Ramakrishna, *Compos. Sci. Technol.* **2003**, *63*, 2223.

[90] R. Dersch, M. Steinhart, U. Boudriot, A. Greiner, J. H. Wendorff, *Polym. Adv. Technol.* **2005**, *16*, 276.

[91] Y. M. Shin, M. M. Hohman, M. P. Brenner, G. C. Rutledge, *Polymer* **2001**, *42*, 9955.

[92] D. H. Reneker, A. L. Yarin, H. Fong, S. Koombhongse, *J. Appl. Phys.* **2000**, *87*, 4531.

[93] H. Niu, T. Lin, X. Wang, *J. Appl. Polym. Sci.* **2009**, *114*, 3524.

[94] H. Niu, X. Wang, T. Lin, *J. Eng. Fiber. Fabr.* **2012**, *7*, 17.

[95] R. Yang, J. He, L. Xu, J. Yu, *Polymer* **2009**, *50*, 5846.

[96] Y. Liu, J.-H. He, J.-Y. Yu, *J. Phys. Conf. Ser.* **2008**, *96*, 12001.

[97] P. Gupta, G. L. Wilkes, *Polymer* **2003**, *44*, 6353.

[98] S. Chen, H. Hou, P. Hu, J. H. Wendorff, A. Greiner, *Macromol. Mater. Eng.* **2009**, *294*, 781.

[99] I. C. Um, D. Fang, B. S. Hsiao, A. Okamoto, B. Chu, *Biomacromolecules* **2004**, *5*, 1428.

[100] H. Qu, S. Wei, Z. Guo, *J. Mater. Chem. A* **2013**, *1*, 11513.

[101] I. G. Loscertales, A. Barrero, M. Márquez, R. Spretz, R. Valarde-Ortiz, G. Larsen, *J. Am. Chem. Soc.* **2004**, *126*, 5376.

[102] Z. Sun, E. Zussman, A. L. Yarin, J. H. Wendorff, A. Greiner, *Adv. Mater.* **2003**, *15*, 1929.

[103] D. Sun, C. Chang, S. Li, L. Lin, *Nano Lett.* **2006**, *6*, 839.

[104] H. Pan, L. Li, L. Hu, X. Cui, *Polymer* **2006**, *47*, 4901.

[105] D. Li, Y. Wang, Y. Xia, *Adv. Mater.* **2004**, *16*, 361.

[106] S. Koombhongse, W. Liu, D. H. Reneker, *J. Polym. Sci., Part B: Polym. Phys.* **2001**, *39*, 2598.

[107] A. Holzmeister, A. Greiner, J. H. Wendorff, *Polym. Eng. Sci.* **2009**, *49*, 148.

[108] S. L. Chen, H. Q. Hou, P. Hu, J. H. Wendorff, A. Greiner, S. Agarwal, *Macromol. Mater. Eng.* **2009**, *294*, 265.

[109] J.-M. Lim, J. H. Moon, G.-R. Yi, C.-J. Heo, S.-M. Yang, *Langmuir* **2006**, *22*, 3445.

[110] Q. P. Pham, U. Sharma, A. G. Mikos, *Tissue Eng.* **2006**, *12*, 1197.

[111] C. Herrmann, A. Turshatov, D. Crespy, *ACS Macro Lett.* **2012**, *1*, 907.

[112] H.-S. Park, Y. O. Park, *Korean J. Chem. Eng.* **2005**, *22*, 165.

[113] P. Zahedi, I. Retaeian, S.-O. Ranaei-Siadat, S.-H. Jafari, P. Supaphol, *Polym. Adv. Technol.* **2010**, *21*, 77.

[114] Z. Guo, W. Liu, B.-L. Su, *J. Colloid Interf. Sci.* **2011**, *353*, 335.

[115] T. J. Sill, H. A. von Recum, *Biomaterials* **2008**, *29*, 1989.

[116] P. Bansal, K. Bubel, S. Agarwal, A. Greiner, *Biomacromolecules* **2012**, *13*, 439.

[117] M. Gensheimer, A. Brandis-Heep, S. Agarwal, R. K. Thauer, A. Greiner, *Macromol. Biosci.* **2011**, *11*, 333.

[118] J. Shui, J. C. M. Li, *Nano Lett.* **2009**, *9*, 1307.

[119] A. Greiner, S. Mang, O. Schäfer, P. Simon, *Acta Polym.* **1997**, *48*, 1.

[120] P. Simon, S. Mang, A. Hasenhindl, W. Gronski, A. Greiner, *Macromolecules* **1998**, *31*, 8775.

[121] H. G. Gilch, W. L. Wheelwright, *J. Polym. Sci. A1* **1966**, *4*, 1337.

[122] W. F. Gorham, *J. Polym. Sci. A1* **1966**, *4*, 3027.

[123] W. R. Roth, H. Hopf, A. de Meijere, F. Hunold, S. Bornera, M. Neumann, T. Wassera, J. Szurowski, C. Mlynek, *Liebigs Ann.* **1996**, *12*, 2141.

[124] K. Smalara, A. Giełdoń, M. Bobrowski, J. Rybicki, C. Czaplewski, *J. Phys. Chem. A* **2010**, *114*, 4296.

[125] P. Hanefeld, F. Sittner, W. Ensinger, A. Greiner, *e-Polymers* **2006**, *26*, 1.

[126] N. T. Tung, Y. J. Yu, K. Kim, S.-H. Joo, J.-I. Jin, *Bull. Korean Chem. Soc.* **2004**, *25*, 31.

[127] M. Cetinkaya, S. Boduroglu, M. C. Demirel, *Polymer* **2007**, *48*, 4130.

[128] K. Y. Suh, R. Langer, *Appl. Phys. Lett.* **2003**, *83*, 4250.

[129] C. P. Tan, H. G. Craighead, *Materials* **2010**, *3*, 1803.

[130] A. Khabari, F. K. Urban III, *Polym. Prepr.* **2005**, *351*, 3536.

[131] R. Kumar, L. Young, D. Molin, F. Ke, A. Summers, *Polym. Prepr.* **2008**, *49*, 935.

[132] K. R. Williams, *J. Therm. Anal.* **1997**, *49*, 589.

[133] S. Tawfick, X. Deng, A. J. Hart, J. Lahann, *Phys. Chem. Chem. Phys.* **2010**, *12*, 4446.

[134] J. J. Senkevich, C. J. Mitchell, A. Vijayaraghavan, E. V. Barnat, J. F. McDonald, T.-M. Lu, *J. Vac. Sci. Technol. A* **2002**, *20*, 1445.

[135] H. Nandivada, H.-Y. Chen, L. Bondarenko, J. Lahann, *Angew. Chem. Int. Ed.* **2006**, *45*, 3360.

[136] J. J. Senkevich, *Chem. Vap. Deposition* **2011**, *17*, 204.

[137] J. J. Senkevich, B. W. Woods, J. J. McMahon, P.-I. Wang, *Chem. Vap. Deposition* **2007**, *13*, 55.

[138] M. Bognitzki, H. Hou, M. Ishaque, T. Frese, M. Hellwig, C. Schwarte, A. Scharper, J. H. Wendorff, A. Greiner, *Adv. Mater.* **2000**, *12*, 637.

[139] H. Hou, Z. Jun, A. Reuning, A. Scharper, J. H. Wendorff, A. Greiner, *Macromolecules* **2002**, *35*, 2429.

[140] Z. Sun, J. Zeng, H. Hou, H. Wickel, J. H. Wendorff, A. Greiner, *Prog. Colloid Polym. Sci.* **2005**, *130*, 15.

[141] A. Greiner, J. H. Wendorff, A. L. Yarin, E. Zussman, *Appl. Biomicrobiol. Biotechnol.* **2006**, *71*, 387.

[142] J.-P. Lindner, C. Röben, A. Studer, M. Stasiak, R. Ronge, A. Greiner, J. H. Wendorff, *Angew. Chem. Int. Ed.* **2009**, *48*, 8874.

[143] H. Hou, Z. Jun, Z. Sun, P. Hanefeld, M. Gensheimer, J. H. Wendorff, R. Kumar, A. Greiner, *Polym. Prepr.* **2008**, *49*, 952.

[144] S. F. Tahir, C. A. Koh, *Environ. Sci. Pollut. Res.* **1996**, *3*, 20.

[145] P. Fernandes, *Enzyme Res.* **2010**, *2010*, 1.

[146] C. T. Walsh, *J. Biol. Chem.* **2010**, *285*, 29681.

[147] S. M. George, *Chem. Rev.* **1995**, *95*, 475.

[148] X. S. Zhao, X. Y. Bao, W. Guo, F. Y. Lee, *Mater. Today* **2006**, *9*, 32.

[149] D. L. Trimm, A. Stanislaus, *Appl. Catal.* **1986**, *21*, 215.

[150] J. C. Chadwick, J. R. Severn, *Kinet. Catal.* **2006**, *47*, 186.

[151] H. Jüntgen, *Fuel* **1986**, *65*, 1436.

[152] G. Chen, S. Wu, H. Liu, H. Jiang, Y. Li, *Green Chem.* **2013**, *15*, 230.

[153] H. Liu, Y. Liu, Y. Li, Z. Tang, H. Jiang, *J. Phys. Chem. C* **2010**, *114*, 13362.

[154] X. Pan, X. Bao, *Chem. Commun.* **2008**, *47*, 6271.

[155] R. van Heerbeek, P. C. J. Kamer, P. W. N. M. van Leeuwen, J. N. H. Reek, *Chem. Rev.* **2002**, *102*, 3717.

[156] D. M. Vriezema, M. C. Aragonès, J. A. A. W. Elemans, J. J. L. M. Cornelissen, A. E. Rowan, R. J. M. Nolte, *Chem. Rev.* **2005**, *105*, 1445.

[157] L. J. Twyman, A. S. H. King, I. K. Martin, *Chem. Soc. Rev.* **2002**, *31*, 69.

[158] M. Gaab, S. Bellemin-Laponnaz, L. H. Gade, *Chem. Eur. J.* **2009**, *15*, 5450.

[159] J. W. Shield, H. D. Ferguson, A. S. Bommarlus, T. A. Hatton, *Ind. Eng. Chem. Fundam.* **1986**, *25*, 603.

[160] P. Cotanda, N. Petzetakis, R. K. O'Reilly, *MRS Commun.* **2012**, *2*, 119.

[161] K. Renggli, P. Baumann, K. Langowska, O. Onaca, N. Bruns, W. Meier, *Adv. Funct. Mater.* **2011**, *21*, 1241.

[162] B. Voit, *Angew. Chem. Int. Ed.* **2006**, *45*, 4238.

[163] B. J. Cohen, M. A. Kraus, A. Patchornik, *J. Am. Chem. Soc.* **1981**, *103*, 7620.

[164] S. Pariente, P. Trens, F. Fajula, F. D. Renzo, N. Tanchoux, *Appl. Catal., A* **2006**, *307*, 51.

[165] C. P. Canlas, J. Lu, N. A. Ray, N. A. Grosso-Giordano, S. Lee, J. W. Elam, R. E. Winans, R. P. van Dyne, P. C. Stair, J. M. Notestein, *Nat. Chem.* **2012**, *4*, 1030.

[166] J. E. Moses, A. D. Moorhouse, *Chem. Soc. Rev.* **2007**, *36*, 1249.

[167] W. H. Binder, R. Sachsenhofer, *Macromol. Rapid. Commun.* **2007**, *28*, 15.

[168] S. L. Poe, M. Kobašlija, D. T. McQuade, *J. Am. Chem. Soc.* **2006**, *128*, 15586.

4 Immobilization of Catalysts in Poly(*p*-xylylene) Nanotubes

Johannes A. M. Hepperle,[a] Fabian Mitschang,[b] Anna K. Bier,[b] Barbara K. Dettlaff,[a] Andreas Greiner,[b,] Armido Studer[a,*]*

[a]Organisch-Chemisches Institut, Westfälische Wilhelms-Universität Münster, Corrensstraße 40, 48149 Münster, Germany.

[b]Makromolekulare Chemie II, Universität Bayreuth, Universitätsstraße 30, 95440 Bayreuth, Germany.
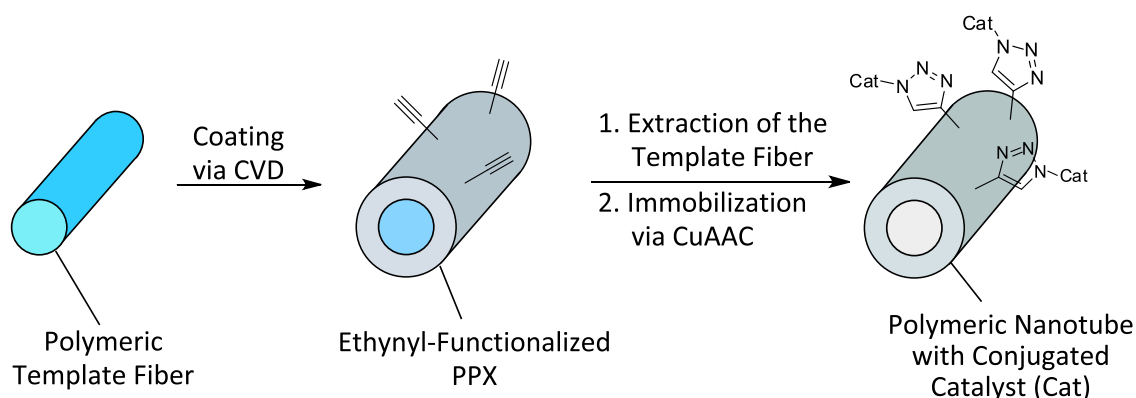
*Corresponding Authors:
A. Studer: E-mail: studer@uni-muenster.de; Fax: +49-251-8336523.
A. Greiner: E-mail: greiner@uni-bayreuth.de; Fax: +49-921-553393.

4.1 Abstract

This paper describes the immobilization of a TEMPO-derivative and a copper catalyst in ethynyl-functionalized poly(*p*-xylylene) nanotubes which are readily prepared by the Tubes by Fiber Templates (TUFT) process. Catalyst conjuga-

tion to the nanotubes is achieved via the Cu-catalyzed azide alkyne cycloaddition (CuAAC). The TEMPO-functionalized nanotubes are successfully used as recyclable catalysts for oxidation of benzyl alcohol. Recycling studies show that the TEMPO-modified nanotubes can be reused 20 times without loss of catalytic activity. Conjugation of the nanotubes with a bipyridine moiety provides a material that allows for immobilization of metal catalysts. Treatment with a Cu(I)-salt leads to a hybrid material, which shows high activity as a recyclable catalyst in the CuAAC. Recycling experiments reveal that these Cu-nanotubes can be reused for 18 runs.

4.2 Introduction

Immobilization of catalysts is currently a heavily investigated field of research which attracts great attention. It is well known that separation of homogeneous catalysts from the product can be problematic and it is therefore not surprising that various methods allowing for simple catalyst separation and recovery have been developed.[1,2] In particular if expensive catalysts are used at high loading recycling becomes an important issue. Despite the great achievements in this field development of new concepts and new approaches for catalyst immobilization is still important. [2.2]-*p*-Cyclophanes are known for more than 60 years.[3] During the last decade the interest in these compounds which can be readily polymerized to provide poly(*p*-xylylenes) (PPX) that are robust and highly stable polymers has been steadily increasing.[4,5] By chemical vapor deposition (CVD) of [2.2]-*p*-cyclophanes various surfaces can be coated and thereby modified with very good conformity and uniform thickness. The resulting surfaces covered with poly(*p*-xylylenes) are very stable and resistant towards bases, acids and most solvents. By introducing a functional group to the [2.2]-*p*-cyclophane shell, for example an ethynyl substituent, it is possible to prepare via CVD coatings bearing the corresponding functionalities.[6] These functionalized coatings can then be further chemically modified to provide highly valuable materials.[7]

Recently, we showed that it is possible to immobilize catalysts into electrospun polymer fibers.[8,9] Such electrospun nanofibers are also suitable templates for the TUFT process which is the basis for the preparation of polymeric nanotubes.[10] In this process the template nanofiber is first covered with a PPX layer by CVD

of [2.2]-*p*-cyclophane. Subsequent removal of the soluble core template polymer nanofiber by extraction results in PPX nanotubes. Using this approach we recently showed the successful immobilization of catalytically active and readily recyclable generation 5 PAMAM dendrimers caged in poly(*p*-xylylene) nanotubes.[11] Herein we report preparation of ethynyl-functionalized PPX-nanotubes by applying the TUFT process. Subsequent chemical modification of these PPX nanotubes allows for conjugation of catalysts. The obtained tubes feature a high surface area, show high catalytic activity and are readily recyclable. As first test reactions we investigated the TEMPO-catalyzed oxidation[12] of benzyl alcohol and the CuAAC[13] of benzyl azide with phenyl propargyl ether.

4.3 Results and Discussion

Ethynyl-functionalized PPX[6] was obtained by the TUFT process.[10] The underlying concept is illustrated in Figure 4.1. 4-Ethynyl-[2.2]-*p*-cyclophane **5** was readily
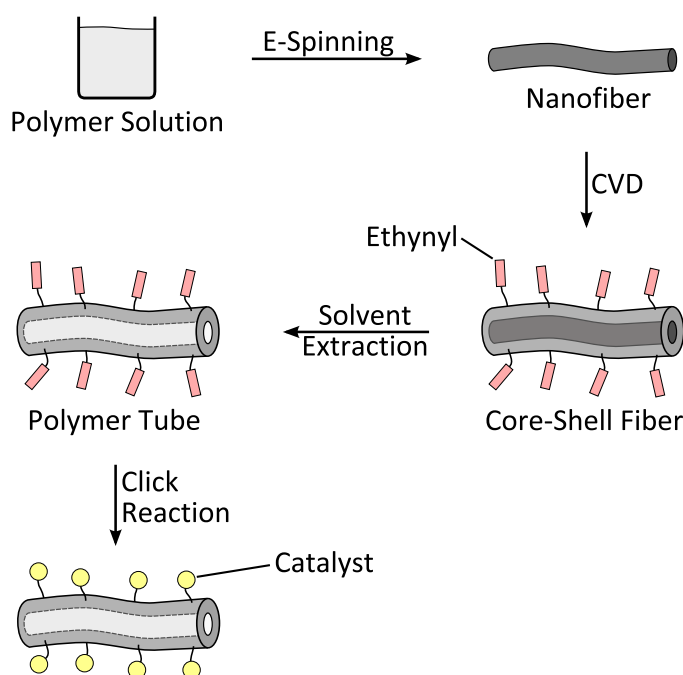

Figure 4.1. The TUFT process using electrospun nanofibers as templates and subsequent chemical vapor deposition of ethynyl-functionalized [2.2]-*p*-cyclophane. Solvent extraction of the inner core material leads to the corresponding ethynyl-functionalized PPX tubes.

prepared according to Hopf et al.[6a] starting with [2.2]-*p*-cyclophane **1** (Scheme 4.1).

Bromination of **1** gave 4-bromo-[2.2]-*p*-cyclophane **2** which was further converted
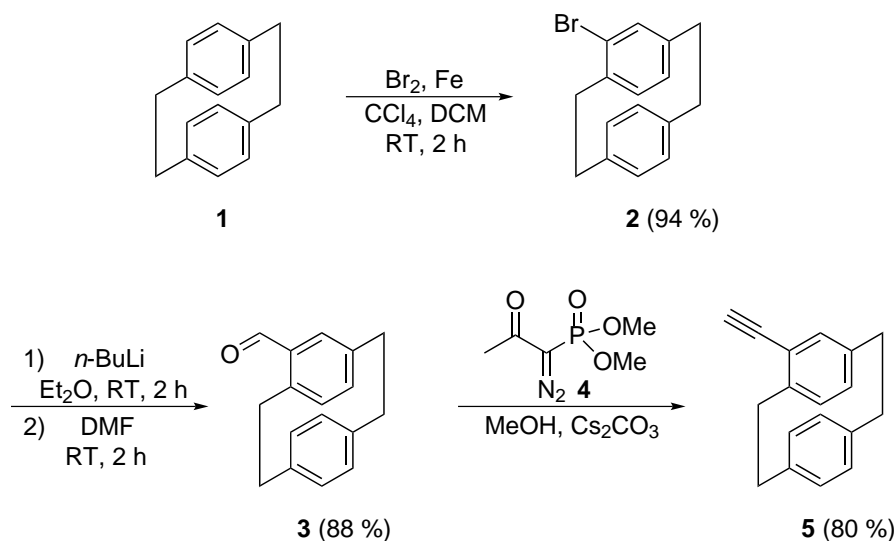
Scheme 4.1. Preparation of 4-ethynyl-[2.2]-*p*-cyclophane **5**.

in good yield via bromine lithium exchange and subsequent addition of dimethyl-formamide to 4-formyl-[2.2]-*p*-cyclophane **3**. In the final step the aldehyde was treated with diazocarbonyl phosphonate **4** under basic conditions to provide 4-ethynyl-[2.2]-*p*-cyclophane **5** in 80 % yield. For template nanofiber formation we chose poly(ethylene oxide) (PEO) which is known in the electrospinning process.[9] To this end, an aqueous solution of 10 wt% PEO was electrospun to uniform fibers free of beads, as shown in Figure 4.2 (left). The average diameter of the fibers was 415 ± 59 nm, featuring a high surface area.[14] The PEO fibers were then coated with 4-ethynyl-[2.2]-*p*-cyclophane **5** using the CVD process (Scheme 4.2).[5] The resulting core-shell fibers (Figure 4.2, right) were homogeneously coated and free of visible pores or cracks. The average diameter was 645 ± 15 nm, hence the PPX layer thickness was calculated to lie at around 115 nm. As opposed to the deposited PPX-type shell, the inner PEO template was soluble in water and could easily be removed via solvent extraction in agreement with previous studies which showed that the PPX membrane can be permeated by non-globular structures and polymers,[15] whereas sterically demanding dendrimers remain encapsulated inside the PPX confinements.[11] Gravimetric measurements confirmed the successful extraction of the PEO template material. Electron scanning micrographs of
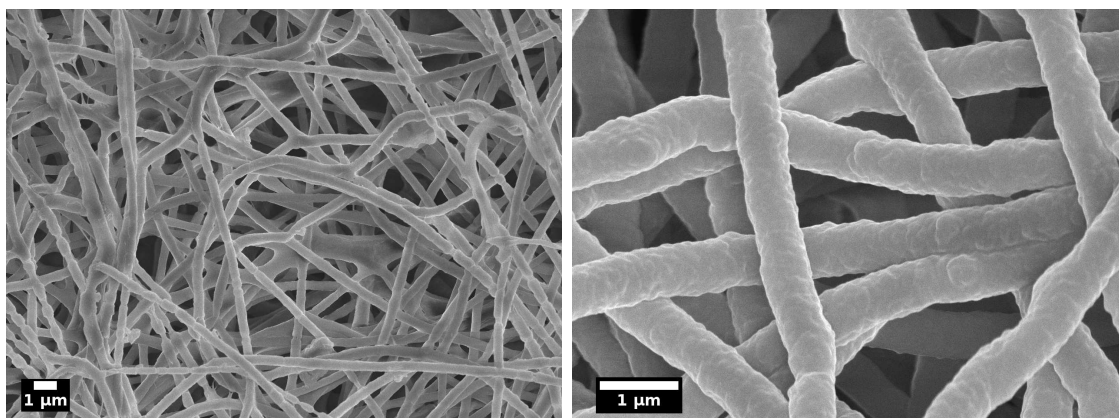
Figure 4.2. Scanning electron micrographs of electrospun PEO nanofibers (left) and the corresponding core-shell fibers after deposition of ethynyl-functionalized PPX derived from **5** (right).

the resulting sample after freeze-fracturing showed both cross- and longitudinal sections of the hollow tubes (Figure 4.3). For conjugation of the PPX-tubes **6**,
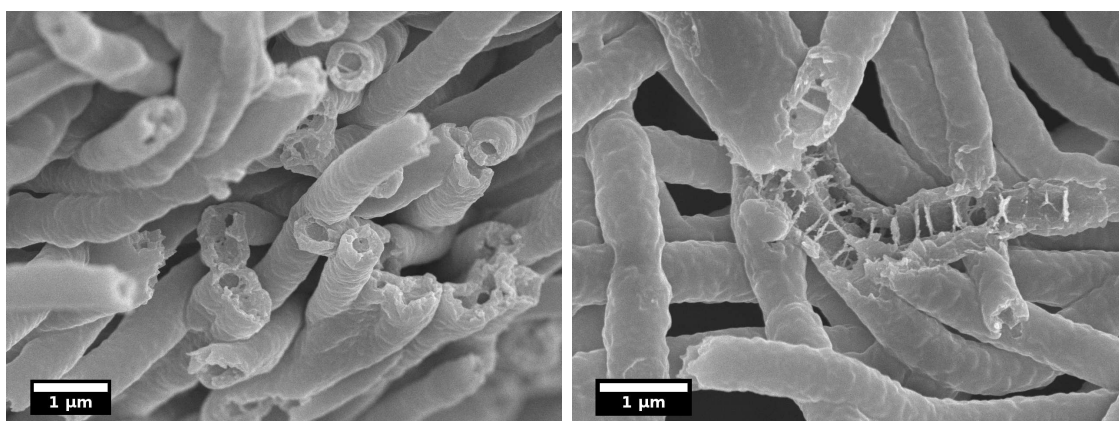

Figure 4.3. Scanning electron micrographs of the ethynyl-functionalized PPX tubes. As a result of the freeze-fracturing of the sample, both cross-sections and longi-tudinal sections were visible.

an azidyl-functionalized TEMPO-derivative **9** was prepared (Scheme 4.3). To this end, commercially available *N*-acetamido-TEMPO **7** was hydrolyzed under basic conditions (KOH). The resulting amine was then acylated with 6-bromo-hexanoic acid chloride to give **8** which was then further converted to azide **9** upon treatment
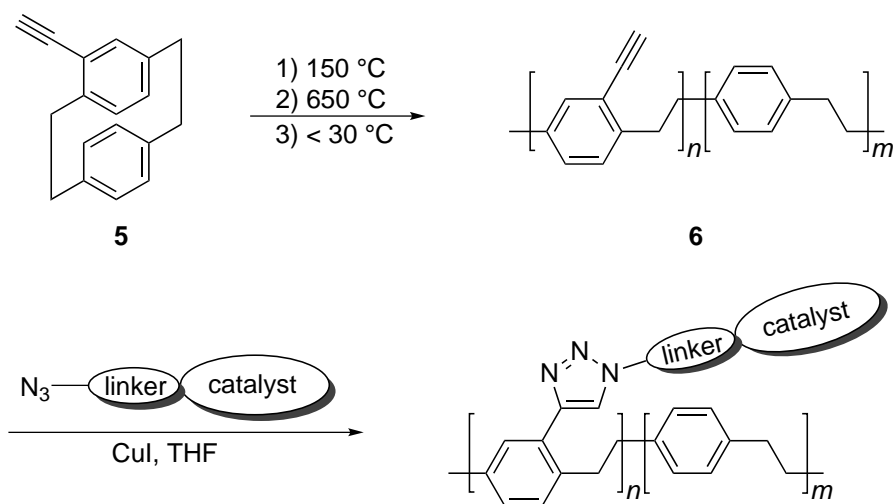
Scheme 4.2. CVD of **5** to give ethynyl-functionalized PPX **6** and subsequent CuAAC.
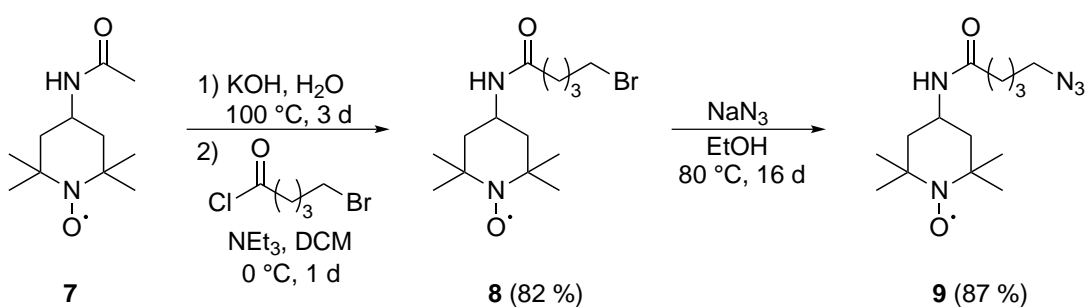
Scheme 4.3. Synthesis of TEMPO-derivative **9**.

with NaN$_3$ (Scheme 3). Conjugation of the azide **9** to the PPX nanotubes **6** via CuAAC turned out to be challenging. Standard click conditions using CuSO$_4$ · 5 H$_2$O (6 mol%) in the presence of sodium ascorbate as reducing reagent were not suitable for this transformation. Using a Cu(I)-salt (CuI, 6 mol%) was also not effective. A careful literature search revealed that the CuAAC at surfaces is mostly conducted by using azide-functionalized solid phases whereas the alkyne is generally used in excess as soluble component.[13b] This is opposite to our current case. We assumed that the click reaction at the nanotubes occurs very slowly and that the oxidation of the catalytic active Cu(I)-species might be a problem under the applied conditions. Therefore, the CuAAC was repeated under careful exclusion of air under argon atmosphere using CuI (6 mol%) as catalyst. We were pleased to find that cycloaddition proceeded albeit very slowly. Reaction for 2 days provided catalyst system **A**, in which about 62 % of the alkyne moieties were functionalized by the TEMPO-derivative **9** via a triazole moiety (for general structure see Scheme 4.2). The degree of functionalization was estimated gravimetrically and by elemental analysis.

With the catalyst system **A** in hand, we investigated oxidation of benzyl alcohol under Anelli conditions using **A** (around 2.5 mol nitroxide), NaOCl as stoichiometric cooxidant, KBr and NaHCO$_3$ (Scheme 4.4, for apparatus used, see the Supporting Information).[16] Benzaldehyde was formed in over 95 % yield and the hybrid
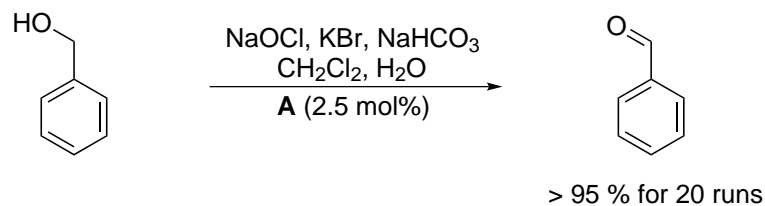
> 95 % for 20 runs

Scheme 4.4. Oxidation of benzyl alcohol using catalyst **A** under Anelli conditions.[16]

material **A** was readily recovered (see Supporting Information). Tube material **A** was successfully reused for 20 runs without loss of activity (yields were determined by GC analysis, Figure 4.4). The loss in activity for run 9 (yield dropped to 83 %) was caused by using an old and likely partly decomposed solution of NaOCl.[17] After 20 runs the fiber mat was intensively washed and then dried under reduced pres-
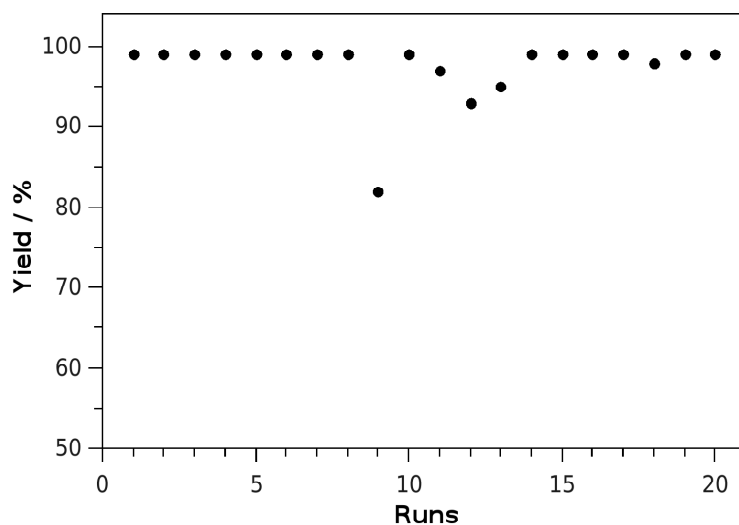
Figure 4.4. Recycling study: benzyl alcohol oxidation with nanotube **A** as catalyst (nitroxide concentration about 2.5 mol%).

sure. To our surprise, despite the high activity, only 74 wt% of the initial TEMPO-functionalized nanotubes were recovered. The isolated fiber mat was fragile and brittle. Scanning electron micrographs of the nanotubes showed a large change in morphology (Figure 4.5): Fiber mats were porous and showed partially coalesced structures (compare with Figure 4.3) likely caused by the harsh oxidizing conditions applied.[18] However, despite the partly destructed structure of the tubes, system **A**
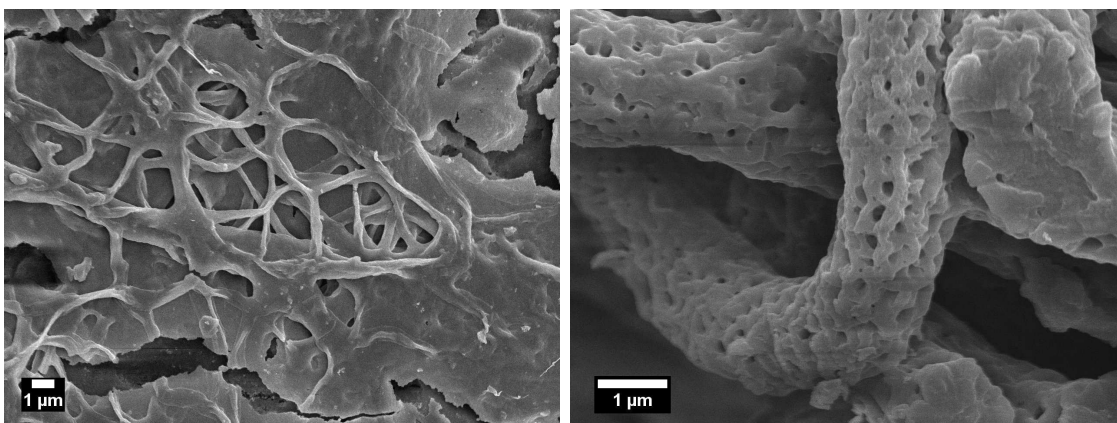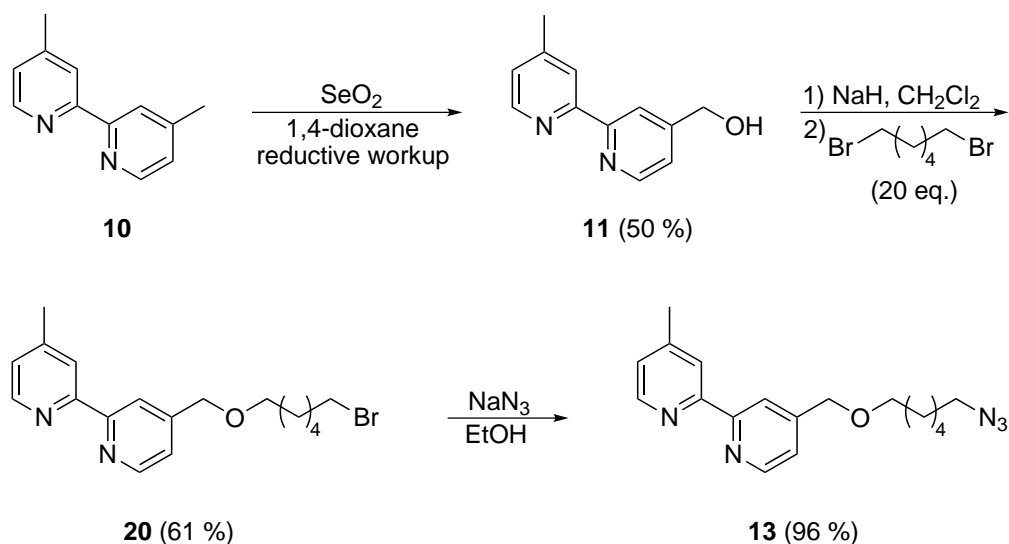

Figure 4.5. Scanning electron micrographs of catalyst system **A** after 20 runs.

was still catalytically active in the 20th run.

Encouraged by the successful preparation of the TEMPO-functionalized system **A**, we decided to conjugate the bipyridine ligand **13** to the PPX nanotubes **6** (Scheme 4.5). To this end, commercially available bipyridine **10** was first oxidized

Scheme 4.5. Synthesis of the azido bipyridine derivative **13**.

by SeO$_2$ to alcohol **11**. *O*-alkylation with 1,6-dibromohexane provided **12** which was further reacted with NaN$_3$ to eventually give azido bipyridine **13** that was isolated in 29 % over three steps. The modification of ethynyl-functionalized nanotubes **6** with azido bipyridine **13** was performed in analogy to the TEMPO-conjugation discussed above using 20 mol% CuI under argon atmosphere resulting in bipyridine modified nanotubes. To remove the Cu-complexes formed during the CuAAC the bipyridine-functionalized nanotubes were intensively washed with a solution of ethylenediaminetetraacetic acid (EDTA, 0.2 mol L^{-1}) in THF. Elemental analysis revealed a degree of functionalization of about 27 %. The successful covalent modification of the alkyne-functionalized tube material with the bipyridine ligand offers a platform for the immobilization of metal salts. Along these lines, the nanotubes were stirred for one day in a solution of Cu(II)SO$_4$ to provide Cu-bipyridine complexes covalently bound to the PPX nanotubes which are hereafter called as catalyst system **B**. To remove nonligated physisorbed Cu(II)SO$_4$, the tubes were intensively washed. To test the activity and reusability of catalyst system **B**, we chose the Cu(I)-catalyzed cycloaddition of phenyl propargyl ether (**14**) with benzyl

azide (**15**) to give triazole **16** as test reaction (Scheme 4.6). In order to activate the
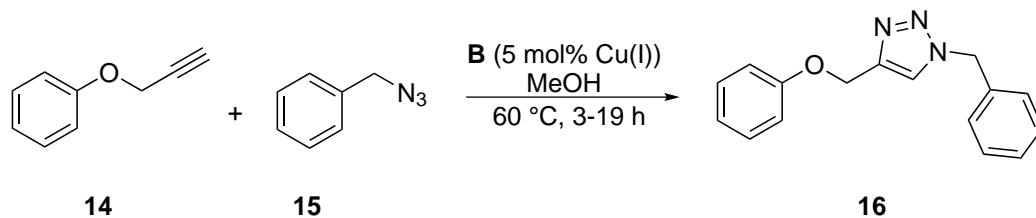
Scheme 4.6. CuAAC of phenyl propargyl ether (**14**) with benzyl azide (**15**) by using catalyst system **B**.

Cu-catalyst sodium L-ascorbate was added as reducing reagent and a nearly quantitative conversion to the triazole **16** was obtained (at around 5 mol% Cu-loading). Initial reactions were conducted for 19 h but we noted later that high conversion (> 90 %) is achieved within 3 h. Importantly, catalyst system **B** was successfully recycled 17 times without a significant drop in activity (> 90 %, see Supporting Information). To test whether the cycloaddition is catalyzed by the tube material with immobilized Cu(I) and not by Cu-salt which might have leached out of the tube material into the solution, a control experiment was performed: catalyst system **B** was removed after a conversion of about 25 % and stirring was continued for 190 min in the absence of the catalyst. Then the catalyst **B** was added again to the mixture and reaction progress was monitored by gas chromatography (see Figure 4.6, black squares). The analysis clearly revealed that the reaction did not stop completely after removal of the tube material **B** indicating that little Cu-salt was leaching out of the tube material, however reaction rate dropped significantly. After adding catalyst system **B**, the initial activity was restored. After 18 runs the fiber mat was intensively washed and then dried under reduced pressure. The isolated fiber mat turned out to be fragile and brittle. SEM-analysis of the used nanotubes clearly showed that the tube structure is still existing (Figure 4.7) in agreement with the experimental findings that the catalyst system **B** was still very active in the CuAAC in the 18th run. In contrast to the TEMPO-bleach process discussed above, the milder conditions of the CuAAC did not lead to a destruction of the tube material.
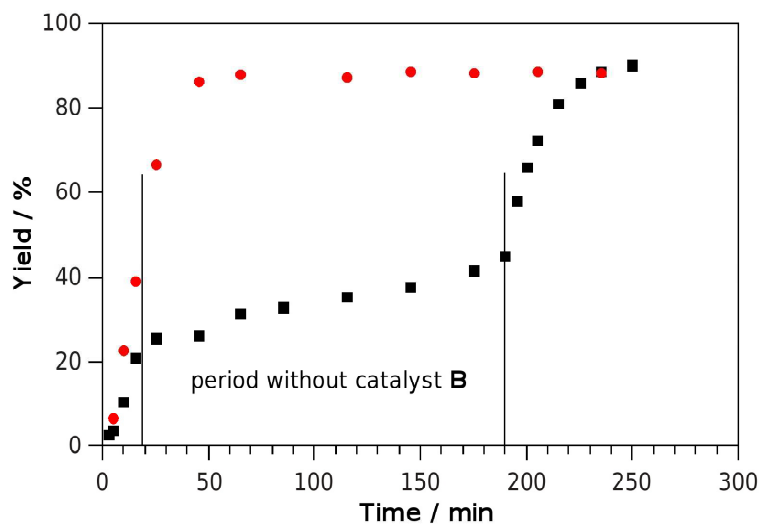
Figure 4.6. Reaction progress of a standard experiment (red circles) and an experiment (black squares) where catalyst system **B** was removed at about 25 % conversion and then readded again after 190 min.
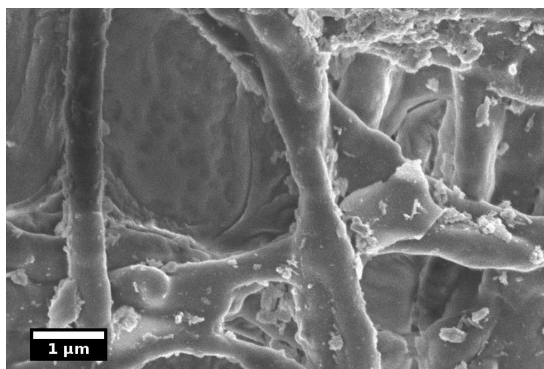

Figure 4.7. Scanning electron micrograph of catalyst system **B** which was used for 18 experiments.

4.4 Conclusion

In this paper we presented a new concept for the immobilization of catalysts into poly(*p*-xylylene) nanotubes. The novel approach uses the electrospinning technique for the preparation of polymer template nanofibers which are subsequently coated with ethynyl-functionalized PPX via CVD. In the last step the core template fibers are removed by extraction leading to ethynyl-functionalized nanotubes. These nanotubes, which have a high surface area, can be further chemically modified using the CuAAC. Conjugation of a TEMPO-derivative provided a catalyst system which was successfully used as recyclable catalyst for oxidation of benzyl alcohol. The tube material was very robust since after 20 runs under oxidizing conditions (bleach), catalyst activity was still very high. The CuAAC also allowed immobilizing a bipyridine ligand. Cu-complexation gave a tube material which showed activity as recyclable catalyst in the CuAAC of phenyl propargyl ether with benzyl azide. We are confident that the immobilization concept presented should be broadly applicable and will allow immobilizing various catalysts. This is due to the general applicability of the surface CuAAC which we used for conjugation of the catalytically active moieties to the PPX nanotubes. Work along this line is underway.

4.5 Experimental Section

Electrospinning of Poly(ethylene oxide) Template Nanofibers

An aqueous solution containing $10 \, \text{wt\%}$ PEO ($M_w = 300,000 \, \text{g} \, \text{mol}^{-1}$) was electrospun using a custom made single-nozzle electrospinning setup. The collector electrode, a round metal plate of $9 \, \text{cm}$ diameter, was covered with aluminum foil and mounted below a downward facing $1 \, \text{mL}$ syringe equipped with a $0.9 \, \text{mm}$ cannula. The gap between the two electrodes was $20 \, \text{cm}$ and the applied voltage was $20 \, \text{kV}$. At room temperature and $20 \, \%$ relative humidity, the feed rate was set to $0.25 \, \text{mL} \, \text{h}^{-1}$ resulting in the deposition of PEO nanofibers onto the collector foil.

Chemical Vapor Deposition of Ethynyl-Functionalized Poly(*p*- xylylene)

Rectangular pieces of 4.5×5.5 cm of the prepared PEO fiber mats were mounted inside the deposition chamber and subsequently coated with ethynyl-functionalized PPX using a custom made CVD setup (see the Supporting Information). The vaporization chamber was filled with 150 mg of the ethynyl-functionalized [2.2]-*p*-cyclophane precursor and set to 100 °C. The following pyrolysis zone was set to 580 °C. Whereas the deposition chamber was kept at room temperature, the connecting transportation zone was set to 300 °C. The pressure was kept below 2.0×10^{-2} mbar and after 1 h, the vaporization temperature was raised 10 °C every 30 min until 150 °C. After the CVD setup reached room temperature, the coated fiber mats were flipped and the back layer was subsequently coated as described above. The resulting core-shell fiber mats were homogeneously coated and slightly yellow.

Solvent Extraction of the inner Polymer Template

The prepared core-shell fiber mats were introduced into water in order to extract the inner PEO fibers. The aqueous phase was renewed every 24 h until the weight was consistent.

General Procedure for the Oxidation of Benzyl Alcohol using Catalyst System A

A solution (3.66 mL) of benzyl alcohol (0.40 mol L^{-1}, 1.47 mmol, 1.0 eq.) and hexadecane (0.40 mol L^{-1}, 1.47 mmol, 1.0 eq.; internal standard) in dichloromethane was mixed with a solution of KBr (aq., 0.5 mol L^{-1}, 0.29 mL, 0.15 mmol, 0.1 eq.) at 0 °C. Then a solution of NaOCl (aq., 0.35 mol L^{-1}, 5.24 mL, buffered by NaHCO$_3$ to pH 8.9, 1.83 mmol, 1.25 eq.) was added at 0 °C. The TEMPO-functionalized PPX-nanotubes **A** (20.0 mg, 36.6 mmol, 2.5 mol% nitroxide) were fixed in a Teflon holder (see Figure 4.8 in the Supporting Information) and dipped into the reaction mixture. By removal of the catalyst **A** the reaction was stopped and the product was isolated by rinsing the fiber mat with dichloromethane (3 × 5 mL). The combined phases were dried over MgSO$_4$. Conversion of the reaction was determined by GC

analysis.

General Procedure for the CuAAC with Catalyst System B

Catalyst system **B** (72.0 mg, 12 mmol, 5 mol% copper) was fixed using the custom made sample mount and a solution of benzyl azide (0.25 mmol, 1.0 eq.) and phenyl propargyl ether (0.27 mmol, 1.1 eq.) in dry methanol (5 mL) were added. In the first reaction cycle after longer storage time of the fiber mat, sodium L-ascorbate (5 mg, 0.02 mmol, 0.1 eq.) was added to the solution to reduce oxidized Cu(II) to Cu(I). The reaction mixture was heated to 60 °C for 3–19 h. Subsequently, the sample mount and the tube material were washed several times with methanol and the washed tube material was dried carefully by passing an argon stream followed by drying under vacuum. After removal of the solvent from the reaction mixture, the obtained residue was dissolved in CDCl$_3$ and yield was determined by ^{1}H NMR spectroscopy by using dibromomethane as an internal standard.

4.6 Acknowledgments

4.7 References

[1] Immobilization of catalysts: (a) J. M. Fraile, J. I. García, J. A. Mayoral, *Chem. Rev.* **2009**, *109*, 360; (b) A. F. Trinidade, P. M. P. Gois, C. A. M. Alfonso, *Chem. Rev.* **2009**, *109*, 418; (c) R. Akiyama, S. Kobayashi, *Chem. Rev.* **2009**, *109*, 594.

[2] Immobilization of organocatalysts: (a) M. Benaglia, A. Puglisi, F. Cozzi, *Chem. Rev.* **2003**, *103*, 3401; (b) M. Gruttadauria, F. Giacalone, R. Noto, *Chem. Soc. Rev.* **2008**, *37*, 1666; (c) T. E. Kristensen, T. Hansen, *Eur. J. Org. Chem.* **2010**, *17*, 3179.

[3] C. J. Brown, A. C. Farthing, *Nature* **1949**, *164*, 915.

[4] H. Hopf, *Angew. Chem. Int. Ed.* **2008**, *47*, 9808.

[5] W. F. Gorham, *J. Polym. Sci., Part A-1: Polym. Chem.* **1966**, *4*, 3027.

[6]   (a) L. Bandorenko, I. Dix, H. Hinrichs, H. Hopf, *Synthesis* **2004**, *16*, 2751; (b) H. Nandivada, H.-Y. Chen, L. Bandorenko, J. Lahann, *Angew. Chem. Int. Ed.* **2006**, *45*, 3360; (c) H.-Y. Chen, J. H. Lai, X. Jiang, J. Lahann, *Adv. Mater.* **2008**, *20*, 3474.

[7]   X. Dong, J. Lahann, *Macromol. Rapid Commun.* **2012**, *33*, 1459.

[8]   (a) M. Stasiak, C. Röben, N. Rosenberger, F. Schleth, A. Studer, A. Greiner, J. H. Wendorff, *Polymer* **2007**, *48*, 5208; (b) M. Stasiak, A. Studer, A. Greiner, J. H. Wendorff, *Chem.-Eur. J.* **2007**, *13*, 6150; (c) C. Röben, M. Stasiak, B. Janza, A. Greiner, J. H. Wendorff, A. Studer, *Synthesis* **2008**, *14*, 2163.

[9]   Reviews for electrospinning: (a) D. Li, Y. Xia, *Adv. Mater.* **2004**, *16*, 1151; (b) A. Greiner, J. H. Wendorff, *Angew. Chem. Int. Ed.* **2007**, *46*, 5670.

[10]   M. Bognitzki, H. Hou, M. Ishaque, T. Frese, M. Hellwig, C. Schwarte, A. Scharper, J. H. Wendorff, A. Greiner, *Adv. Mater.* **2000**, *12*, 637.

[11]   J. P. Lindner, C. Röben, A. Studer, M. Stasiak, R. Ronge, A. Greiner, J. H. Wendorff, *Angew. Chem. Int. Ed.* **2009**, *48*, 8874.

[12]   Reviews: (a) T. Vogler, A. Studer, *Synthesis* **2008**, *13*, 1979; (b) L. Tebben, A. Studer, *Angew. Chem. Int. Ed.* **2011**, *50*, 5034; (c) A. E. J. de Nooy, A. C. Besemer, H. van Bekkum, *Synthesis* **1996**, *10*, 1153; (d) W. Adam, C. R. Saha-Möler, P. A. Ganeshpure, *Chem. Rev.* **2001**, *101*, 3499; (e) R. A. Sheldon, I. W. C. E. Arends, G.-T. ten Brink, A. Dijksman, *Acc. Chem. Res.* **2002**, *35*, 774.

[13]   (a) V. V. Rostovtsev, L. G. Green, V. V. Folkin, K. B. Sharpless, *Angew. Chem. Int. Ed.* **2002**, *41*, 2596; (b) M. Medal, C. W. Tornøe, *Chem. Rev.* **2008**, *108*, 2952.

[14]   Z.-M. Huang, Y.-Z. Zhang, M. Kotaki, S. Ramakrishna, *Compos. Sci. Technol.* **2003**, *63*, 2223.

[15]   (a) P. Hanefeld, F. Sittner, W. Ensinger, A. Greiner, *e-Polymers* **2006**, *26*, 1; (b) A. Greiner, J. H. Wendorff, A. L. Yarin, E. Zussman, *Appl. Microbiol. Biotechnol.* **2006**, *71*, 387.

[16] P. Lucio Anelli, C. Biffi, F. Montanari, S. Quici, *J. Org. Chem.* **1987**, *52*, 2559.

[17] In other experiments we observed a very high yield over 12 runs, clearly showing the slightly decreased yield in 9 was caused by the lower quality of the NaOCl solution as mentioned in the text.

[18] The insolubility of the tube material makes analysis of the tube material very difficult. IR (FT-ATR) did not give any structural information on how the tube material was demaged. Elemental analysis before (C = 68.74 %, H = 7.21, N = 8.00) and after catalysis (C = 68.31 %, H = 7.35, N = 7.77) showed that the relative amount of C and N slightly decreased. We believe that under the harsh oxidizing conditions CH-oxidation at the benzylic sites and subsequent oxidative C-C-cleavage is slowly occuring which leads of the destruction of the material and eventually to material loss as observed in the experiment. The lower N and C content is then caused by a larger content of O (calculated increase is 0.52 %). Since the catalyst is covalently bound, the loss of activity after extensive use of the tube material will be caused by a lower concentration of catalyst due to damage and loss of tube material after multiple use.

4.8 Supporting Information

Materials and Chemicals

Water: deionized water. Poly(ethylene oxide): Acros, $M_w = 300,000 \, \text{g} \, \text{mol}^{-1}$. THF was freshly distilled from K, Et_2O was freshly distilled from K/Na, benzene was freshly distilled from Na, and CH_2Cl_2 was distilled from P_2O_5. All other solvents and reagents were purified according to standard procedures or were used as received from Aldrich, Fluka, Alfa Aesar, or Acros.

General Methods

All reactions involving air- or moisture-sensitive reagents were carried out in heat-gun-dried glassware under an argon atmosphere and were performed by using stan-

dard Schlenk techniques. ^{1}H NMR and ^{13}C NMR spectra were recorded on a Bruker DPX-300 (^{1}H: 300 MHz, ^{13}C: 75 MHz), a Varian Inova 500 (^{1}H: 500 MHz, ^{13}C: 125 MHz), or Varian Unity plus 600 (^{1}H: 600 MHz, ^{13}C: 150 MHz). Chemical shifts δ in ppm are referenced to the solvent residual peak. Thin layer chromatography (TLC) was carried out on Merck silica gel 60 F_{254} plates; detection by UV or dipping into a solution of $KMnO_4$ (1.5 g), $NaHCO_3$ (5.0 g) in H_2O (400 mL) followed by heating. Flash chromatography (FC) was carried out on Merck silica gel 60 (40–63 µm) at about 1.5 bar. All solvents for FC and extraction were distilled before use. HRMS (m/z) were performed using a Bruker MicroTof and a LTQ Orbitrap XL (nanospray inlet, 1.1 kV, resolution: 30000). IR-spectra were recorded on a Digilab FTS 4000, equipped with a Specac MKII Golden Gate Single Reflection ATR System. GC analyses were carried out on a Hewlett Peckard HP 6890 Series equipped with a HP 5 column (30 m × 0.32 mm, film thickness 0.25 µm) using hydrogen as carrier gas.

Chemical Vapor Deposition Setup

For the CVD process, a 90 cm long quartz glass tube was connected to a cylindrical deposition chamber (borosilicate glass) of 5.5 cm inner diameter and a 8 cm long vaporization chamber (borosilicate glass) using ground glass joints. The deposition chamber was connected to three cold traps followed by an oil vacuum pump (Edwards S Two Stage). The pressure was measured using a vacuum gauge (Edwards Pirani 1001 and Pirani Gauge PRL10). Both the vaporization chamber and the glass tube were placed in a 115 cm long oven (Pyrolus AT) featuring three 38 cm long, individually controllable furnaces (vaporization zone, pyrolysis chamber, and transportation zone). The deposition chamber was kept outside the oven at room temperature.

Scanning Electron Microscopy

Scanning electron micrographs were recorded on a JSM-7500F (JEOL). The preset Plastics (with coating) was selected, and the acceleration voltage was set to 2 kV. The column mode SEM (r-Filter SM) was used, and the probe current was set to LC 7. The corresponding software was PC-SEM (JEOL, version 2.0.0.8). In order

to determine the average fiber diameter of a fiber mat, 100 fibers were measured using ImageJ (National Institute of Health, USA, version 1.44c).

Special Apparatus used for the Catalytic Cycles and the Functionalization of the Nanotubes

Figure 4.8. Special apparatus used for the functionalization of the nanotubes and the catalytic cycles.

General Procedures

Immobilization of Catalysts or Ligands onto Ethynyl-Functionalized PPX Nanotubes by CuAAC (GP 1): A custom-made reactor (see Figure 4.8) was charged with ethynyl-functionalized poly-p-xylylene (PPX, 1 eq.) and flushed with argon for 1 h. THF (5 mL) and CuI (0.06 eq.) were added under an argon atmosphere. After 2 h the azide (2 eq.) dissolved in THF (1 mL) was added and the reaction mixture was stirred for 48 h at room temperature (RT). The modified PPX-nanotubes were rinsed with THF (10×5 mL). The washed nanotubes were dried under reduced pressure; conversion was determined by elemental analysis and gravimetrically.

Oxidation of Benzyl Alcohol using Catalytic System A (GP 2): A solution (3.66 mL) of benzyl alcohol (0.40 mol L^{-1}, 1.47 mmol, 1.0 eq.) and hexadecane (internal standard; 0.40 mol L^{-1}, 1.47 mmol, 1.0 eq.) in dichloromethane was mixed with a solution of KBr (aq., 0.5 mol L^{-1}, 0.29 mL, 0.15 mmol, 0.1 eq.) at 0 °C. Then a solution of NaOCl (aq., 0.35 mol L^{-1}, 5.24 mL, buffered by NaHCO$_3$ to pH 8.9, 1.83 mmol, 1.25 eq.) was added at 0 °C. The TEMPO-functionalized PPX-nanotubes (20.0 mg, 36.6 µmol, 2.5 mol% nitroxide) were fixed in a Teflon holder (see Figure 4.8) and dipped into the reaction mixture. By removal of the catalytic system **A** the reaction was stopped and the product was isolated by rinsing the fiber mat with dichloromethane (3 × 5 mL). The combined phases were separated and dried over MgSO$_4$. Conversion of the reaction was determined by GC analysis.

CuAAC by Catalytic System B (GP 3): For the CuAAC catalytic system **B** (72.0 mg, 12 µmol, 5 mol% copper) was fixed in a special apparatus and a solution of benzyl azide (**15**) (0.25 mmol, 1.0 eq.) and phenyl propargyl ether (**14**) (0.27 mmol, 1.1 eq.) in dry methanol (5 mL) were added. In the first reaction cycle after longer storage time of the fiber mat, sodium ʟ-ascorbate (5 mg, 0.02 mmol, 0.1 eq.) was added to the solution to reduce oxidized Cu(II) to Cu(I). The reaction mixture was heated to 60 °C for 3–19 h. Subsequently, the sample mount and the tube material were washed several times with methanol and the washed tube material was dried carefully by passing an argon stream followed by drying under vacuum. After removing the solvent from the reaction mixture, the obtained residue was dissolved in CDCl$_3$ and yield was determined by ^{1}H NMR spectroscopy by using dibromomethane as an internal standard.

Preparation of Starting Materials

***p*-Toluenesulfonyl Azide:**
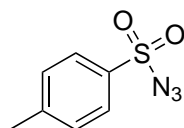
According to Regitz et al.[1] NaN_3 (6.0 g, 31.6 mmol, 1.1 eq.) was dissolved in water (6 mL) and ethanol (9 mL). A heated 45 °C solution of *p*-toluenesulfonyl chloride (4.2 g, 22.1 mmol, 1.0 eq.) in ethanol (22 mL) was added and stirred for 2.5 h. After the reaction was finished the solvent was removed under reduced pressure. The residue was dissolved in water (20 mL) and extracted by dichloromethane (3×20 mL). The combined organic phases were dried over $MgSO_4$ and the solvent was removed under reduced pressure to afford *p*-toluenesulfonyl azide as a white solid (6.1 g, 30.9 mmol, 98 %). The product was used without further purification.

Dimethyldiazo-2-oxopropyl Phosphonate (4):
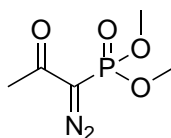
NaH (60 % in liquid paraffin, 1.0 g, 25.3 mmol, 1.1 eq.) was dissolved in benzene at 0 °C (60 mL) and tetrahydrofuran (10 mL). A solution of dimethyl-2-oxopropyl-phosphonate (4.0 g, 24.1 mmol, 1.0 eq.) in benzene (20 mL) was added drop wise and the reaction mixture was stirred at 0 °C for 1 h. Then, *p*-toluenesulfonyl azide (5.0 g, 25.3 mmol, 1.05 eq.) was added and stirred for 2 h. The mixture was filtered over celite and solvent was removed under reduced pressure. FC (pentane/EtOAc = 1:1) gave phosphonate **4** (3.2 g, 16.9 mmol, 72 %) as a white solid.

^{1}H NMR (300 MHz, $CDCl_3$, 300 K): δ = 3.78 (d, J = 11.9 Hz, 6H, $2 \times OCH_3$), 2.20 ppm (s, 3H, CH_3). The physical data are in agreement with those reported in the literature.[2]

4-Bromo-[2.2]-*p*-cyclophane (2):
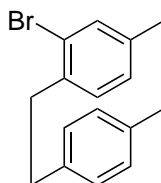
According to Ernst et al.[3] [2.2]-*p*-cyclophane **1** (4.0 g, 19.2 mmol, 1.0 eq.) and a catalytic amount of iron powder were dissolved in dichloromethane (90 mL) and carbon tetrachloride (30 mL). Bromine (1.0 mL, 19.2 mmol, 1.0 eq.) was added slowly under vigorous stirring. After 2 h the reaction mixture was quenched a solution of NaHCO$_3$ (aq., sat., 2 × 25 mL) and the phases were separated. The organic layer was extracted with water (25 mL), a solution of NaCl (aq., sat., 25 mL) and dried over MgSO$_4$. The solvent was removed under reduced pressure. FC (pentane/Et$_2$O) gave bromide **2** (5.2 g, 18.0 mmol, 94 %) as a colorless solid.

IR (Film): 3033 w, 2958 w, 2926 s, 2888 m, 2850 m, 1894 w, 1586 m, 1543 m, 1497 m, 1476 m, 1449 w, 1432 m, 1409 m, 1391 s, 1321 w, 1238 w, 1187 m, 1156 w, 1124 w, 1092 w, 1035 s, 956 w, 942 w, 904 s, 860 w, 840 s, 793 s, 708 s, 699 s, 610 s, 576 cm^{-1} m. ^{1}H NMR (300 MHz, CDCl$_3$, 300 K): δ = 7.17 (m, 1H, Ar-*H*), 6.61–6.40 (m, 6H, Ar-*H*), 3.47 (m, 1H, C*H$_2$*CCBr), 3.28–3.16 (m, 1H, C*H$_2$*CCBr), 3.17–3.01 (m, 4H, 2 × C*H$_2$*), 2.98–2.75 ppm (m, 2H, C*H$_2$*). The physical data are in agreement with those reported in the literature.[4]

4-Formyl-[2.2]-*p*-cyclophane (3):
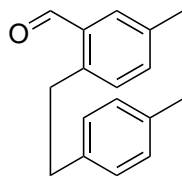


According to Brink et al.[5] bromide **2** (3.0 g, 10.4 mmol, 1.0 eq.) was dissolved in diethyl ether (70 mL) and a solution of *n*-butyl lithium (1.6 mol L^{-1} in *n*-hexane, 13 mL, 20.8 mmol, 2.0 eq.) was added dropwise at 0 °C. The mixture was stirred for 2 h, followed by the addition of dimethylformamide (1.6 mL, 20.8 mmol, 2.0 eq.). After 1.5 h the reaction was quenched by adding a solution of NH$_4$Cl (aq., sat., 45 mL). The phases were separated and the aqueous phase was extracted with diethyl ether (3 × 40 mL). The combined organic phases were dried over MgSO$_4$ and the solvent was removed under reduced pressure. FC (pentane/Et$_2$O) gave aldehyde **3** (2.1 g, 8.7 mmol, 84 %) as a colorless solid.

IR (Film): 3009 w, 2952 w, 2926 m, 2889 w, 2852 w, 2747 w, 1677 s, 1589 m, 1554 w, 1497 w, 1436 w, 1410 w, 1321 w, 1283 w, 1226 m, 1181 w, 1158 w, 1142 m, 1115

w, 1102 w, 977 w, 943 w, 907 m, 874 m, 795 s, 773 m, 742 w, 719 s, 659 w, 635 s, 623 s, 574 cm^{-1} m. ^{1}H NMR (300 MHz, CDCl$_3$, 300 K): δ = 9.95 (s, 1H, CH_O), 7.01 (d, J = 2.0 Hz, 1H, Aryl-H), 6.73 (dd, J = 7.8, 2.0 Hz, 1H, Aryl-H), 6.63–6.53 (m, 3H, Aryl-H), 6.53–6.47 (m, 2H, Aryl-H), 6.40 (qd, J = 7.9, 1.8 Hz, 2H, CH_2CH$_O$), 4.19–4.04 (m, 1H, CH_aCH$_b$CCCOH), 3.33–2.87 ppm (m, 7H, CH$_a$CH_bCCCOH, 3× CH$_2$). The physical data are in agreement with those reported in the literature.[6]

4-Ethinyl-[2.2]-*p*-cyclophane (5):
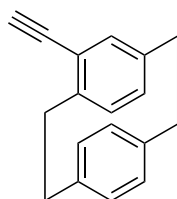
According to Hopf et al.[7] aldehyde **3** (3.0 g, 12.7 mmol, 1.0 eq.) and Cs$_2$CO$_3$ (8.3 g, 25.4 mmol, 2.0 eq.) were dissolved in methanol (250 mL). Then, phosphonate **4** (3.7 g, 19.1 mmol, 1.5 eq.) was added to the mixture and stirred for 4 h at 40 °C. The solvent was removed under reduced pressure and the residue was dissolved in water (100 mL) and pentane (100 mL). The phases were separated and the aqueous phase was extracted with pentane (3 × 75 mL). The combined organic phases were dried over MgSO$_4$ and the solvent was removed under reduced pressure. FC (pentane/DCM = 30:1) gave alkyne **5** (2.4 g, 10.2 mmol, 80 %) as a colorless solid.

IR (Film): 3300 m, 3034 w, 3012 w, 2954 w, 2929 m, 2890 w, 2852 w, 2099 w, 1676 w, 1589 w, 1500 w, 1481 w, 1449 w, 1431 w, 1411 w, 1307 w, 1206 m, 1188 w, 1154 w, 1087 w, 943 m, 908 s, 864 m, 796 m, 716 s, 649 s, 605 s, 585 cm^{-1} s. ^{1}H NMR (300 MHz, CDCl$_3$, 300 K): δ = 6.93 (dd, J = 7.8, 1.7 Hz, 1H, Aryl-H), 6.51–6.36 (m, 6H, Aryl-H), 3.51 (ddd, J = 13.0, 10.3, 2.8 Hz, 1H, CH_aCH$_b$CH$_2$CCCCH), 3.21 (s, 1H, CCCH), 3.20–3.10 (m, 1H, CH$_a$CH_bCH$_2$CCCCH)), 3.09–2.71 ppm (m, 6H, 3 × CH_2). The physical data are in agreement with those reported in the literature.[7]
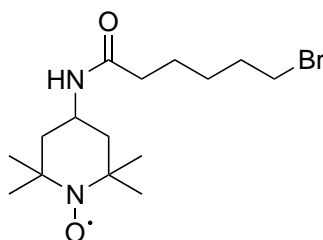
4-Amino-TEMPO:
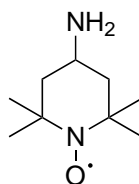
N-Acetamido-TEMPO **7** (8.0 g, 37.5 mmol, 1.0 eq.) and KOH (25.3 g, 450 mmol, 12.0 eq.) were dissolved in water (375 mL) and stirred for 72 h at reflux. After cooling down to RT K_2CO_3 was added (50 g, 360 mmol, 9.6 eq.) and the mixture was extracted with diethyl ether (3 × 150 mL). The organic phases were combined and dried over $MgSO_4$. By removal of the solvent under reduced pressure nitroxide (5.5 g, 32.3 mmol, 86 %) was obtained as a red solid.

IR (Film): 3365 w, 3301 w, 2971 s, 2934 s, 2916 s, 1641 w, 1584 w, 1461 s, 1361 s, 1332 m, 1304 w, 1243 s, 1221 s, 1178 s, 1132 w, 1088 w, 1052 w, 940 w, 873 s, 856 s, 813 s, 680 cm^{-1} m. MS (ESI): m/z = 172 ([M+H]$^+$). HRMS (ESI): calculated for $[C_9H_{19}N_2OH]^+$ m/z = 172.1570; found m/z = 172.1592. The physical data are in agreement with those reported in the literature.[8]

**6-(1-Hydroxy-2,2,6,6-tetramethylpiperidine-4-ylcarbamoyl)bromhexane (8):**

4-Amino-TEMPO (2.0 g, 11.7 mmol, 1.0 eq.) and trietyhlamine (2.74 g, 12.8 mmol, 1.1 eq.) were dissolved in dichloromethane. Next, 6-bromohexanoyl chloride (3.55 g, 35 mmol, 3.0 eq.) was added at 0 °C. The mixture was stirred for 1 h at RT, subsequently quenched with HCl (aq., 1 mol L^{-1}, 15 mL) and extracted with dichloromethane (3 × 15 mL). The combined organic phases were dried over $MgSO_4$ and the solvent was removed under reduced pressure. FC (DCM/MeOH = 20:1) gave nitroxide **8** (3.9 g, 11.1 mmol, 95 %) as a red viscous oil.

IR (Film): 3329 m, 3056 m, 2937 m, 2858 m, 1639 s, 1546 s, 1448 m, 1360 m, 1300 m, 1400 m, 1178 m, 1123 w, 1087 w, 1041 w, 1003 w, 936 w, 841 w, 724 m, 692

m, 620 m, 576 cm^{-1} w. MS (ESI): $m/z = 370$ ([M+Na]$^+$). HRMS (ESI): calculated for [C$_{15}$H$_{28}$BrN$_2$O$_2$Na]$^+$ $m/z = 370.1226$; found $m/z = 370.1219$

6-(1-Hydroxy-2,2,6,6-tetramethylpiperidine-4-ylcarbamoyl)azidohexane (9):
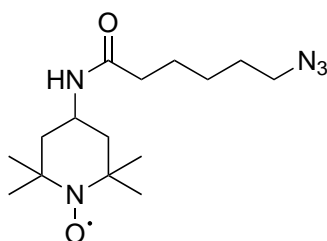
Nitroxide **8** (2.0 g, 5.7 mmol, 1.0 eq.) and NaN$_3$ (1.5 g, 23.0 mmol, 4.0 eq.) were dissolved ethanol (25 mL) and stirred for 16 h at reflux. The precipitation was filtered and the solvent removed under reduced pressure. The residue was dissolved in water (15 mL) and diethyl ether (10 mL). The phases were separated and the aqueous phase was extracted with diethyl ether (210 mL). The combined organic phases were dried over MgSO$_4$ and solvent was removed under reduced pressure. Azide **9** (1.5 g, 4.9 mmol, 87 %) was obtained as a red solid.

IR (Film): 3298 w, 3072 w, 2986 m, 2935 m, 2864 w, 2093 s, 1642 s, 1539 s, 1460 m, 1361 m, 1298 m, 1261 s, 1241 s, 1179 m, 1110 w, 976 w, 897 w, 725 m, 637 m, 564 cm^{-1} s. MS (ESI): $m/z = 333$ ([M+Na]$^+$). HRMS (ESI): calculated for [C$_{15}$H$_{28}$N$_5$O$_2$Na]$^+$ $m/z = 333.2135$; found $m/z = 333.2138$. Elemental analysis in % calculated for C$_{15}$H$_{28}$N$_5$O$_2$: C 58.04, H 9.09, N 22.56; found: C 57.69, H 9.15, N 22.30.

Synthesis of Catalytic System A
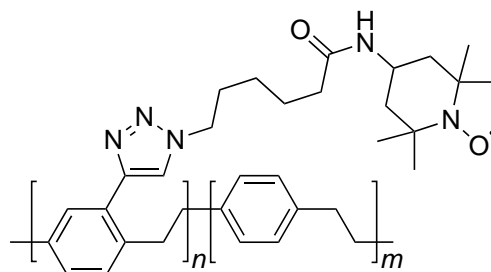
According to GP 1, with TEMPO-azide **9** (40.0 mg, 129.0 μmol). Catalytic system **A** (31.7 mg) was isolated by intensive washing with THF and drying under reduced pressure. Elemental analysis revealed a degree of functionalization of 62 % (calculated by the nitrogen content of the functionalized fiber mat).

Elemental analysis in % calculated for complete functionalization: C 73.03, H 8.17, N 12.90; found: C 68.74, H 7.21, N 8.00.

4-Hydroxymethyl-4'-methyl-2,2'-bipyridine (11)
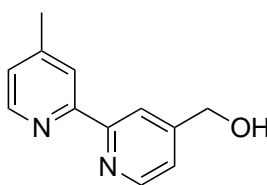
According to Åkermark et al.,[9] 4,4'-dimethyl-2,2'-bipyridine **10** (2.0 g, 11.0 mmol, 1.0 eq.) was suspended in 100 ml of 1,4-dioxane and 2.0 g selenium dioxide (1.6 eq., 18.0 mmol) was added at RT vigorous under stirring. The mixture was heated for 24 h at reflux. After cooling down to RT the reaction mixture was treated carefully with $NaBH_4$ (0.4 g, 11 mmol, 1.0 eq.) and NaOH (aq., 2 mol L^{-1}, 5 ml) at 0 °C. The precipitation was filtered and the solvent was removed under reduced pressure. Residuals were dissolved in chloroform and filtered again to remove selenium byproducts. FC (DCM/MeOH = 9:1) gave bipyridine **11** (1.1 g, 5.5 mmol, 50 %) as a colorless solid.

IR (Film): 3154 m, 3062 w, 3006 w, 2920 w, 2880 w, 2825 w, 1598 s, 1557 m, 1457 m, 1375 s, 1321 m, 1275 m, 1246 m, 1157 m, 1111 m, 1060 s, 993 s, 908 m, 823 s, 813 s, 737 m, 720 m, 695 m, 669 m, 581 cm^{-1} m. ^{1}H NMR (300 MHz, CDCl$_3$, 300 K): δ = 8.56 (d, J = 5.0 Hz, 1H, Aryl-H), 8.48 (d, J = 5.1 Hz, 1H, Aryl-H), 8.30 (s, 1H, Aryl-H), 8.18 (d, J = 1.7 Hz, 1H, Aryl-H), 7.34–7.23 (m, 1H, Aryl-H), 7.13 (dd, J = 5.2, 1.7 Hz, 1H, Aryl-H), 4.75 (s, 2H, CH_2OH), 3.95 (br s, 1H, CH$_2$OH), 2.42 ppm (s, 3H, CH_3). ^{13}C NMR (75 MHz, CDCl$_3$, 300 K): δ = 155.8 (CH), 155.5 (CH), 151.7 (CH), 149.1 (CH), 148.7 (CH), 148.6 (CH), 124.9 (CH), 122.4 (CH), 121.3 (CH), 118.8 (CH), 63.4 (CH$_2$), 21.2 ppm (CH$_3$). MS (ESI): m/z = 223 ([M+Na]$^+$), 201 ([M+H]$^+$). HRMS (ESI): calculated for [C$_{12}$H$_{12}$N$_2$ONa]$^+$

$m/z = 223.0842$; found $m/z = 223.0844$. The physical data are in agreement with those reported in the literature.[9]

4-(((6-Bromohexyl)oxy)methyl)-4'-methyl-2,2'-bipyridine (12)
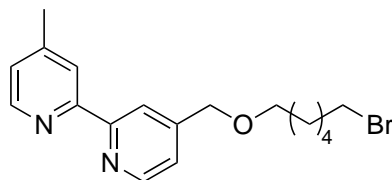
Bipyridine **11** (0.5 g, 2.5 mmol, 1.0 eq.) was dissolved in tetrahydrofuran (10 ml). NaH (0.2 g, 3.7 mmol, 1.5 eq.) was added slowly under stirring. The reaction mixture was added dropwise into a solution of 1,6-dibromohexane (2.3 ml, 15.0 mmol, 6.0 eq.) in tetrahydrofuran (5 mL) and stirred for 1 h. After removal of the solvent under reduced pressure bromide **12** (0.6 g, 1.5 mmol, 61 %) was isolated by FC (DCM/MeOH = 9:1) as a colorless solid.

IR (Film): 3180 m, 3008 w, 2934 m, 2744 w, 1597 s, 1557 m, 1445 s, 1373 s, 1327 m, 1285 m, 1247 m, 1216 m, 1158 w, 1108 m, 1074 m, 1037 s, 992 m, 927 w, 897 m, 848 m, 819 s, 667 m, 642 m, 576 s, 525 cm^{-1} s. ^{1}H NMR (300 MHz, CDCl$_3$, 300 K): δ = 8.63 (d, $J = 5.0$ Hz, 1H, Aryl-H), 8.52 (d, $J = 4.9$ Hz, 1H, Aryl-H), 8.30 (s, 1H, Aryl-H), 8.22 (s, 1H, Aryl-H), 7.40–7.27 (m, 1H, Aryl-H), 7.19–6.97 (m, 1H, Aryl-H), 4.58 (s, 2H, CCH_2O), 3.51 (t, $J = 6.4$ Hz, 2H, CH_2Br), 3.39 (t, $J = 6.8$ Hz, 2H, OCH_2CH$_2$), 2.42 (s, 3H, CCH_3), 1.85 (q, $J = 6.9$ Hz, 2H, CH_2CH$_2$Br), 1.64 (q, $J = 6.6$ Hz, 2H, OCH$_2$CH_2), 1.52–1.35 ppm (m, 4H, 2 × CH_2). ^{13}C NMR (75 MHz, CDCl$_3$, 300 K): δ = 156.0 (C), 155.7 (C), 149.4 (CH), 149.1 (CH), 149.0 (C), 148.2 (C), 124.8 (CH), 122.1 (CH), 121.9 (CH), 119.5 (CH), 71.6 (CH$_2$), 71.0 (CH$_2$), 33.9 (CH$_2$), 32.9 (CH$_2$), 29.7 (CH$_2$), 28.1 (CH$_2$), 25.5 (CH$_2$), 21.3 ppm (CH$_3$). MS (ESI): $m/z = 363$ ([M+H]$^+$). HRMS (ESI): calculated for [C$_{18}$H$_{23}$BrN$_2$OH]$^+$ m/z = 363.1067; found $m/z = 363.1064$.

4-(((6-Azidohexyl)oxy)methyl)-4'-methyl-2,2'-bipyridine (13)
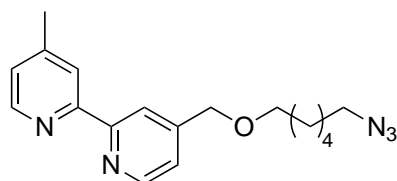
Bromide **12** (300 mg, 0.8 mmol, 1 eq.) and NaN$_3$ (210 mg, 3.3 mmol, 4 eq.) were dissolved in ethanol (10 mL) and stirred for 24 h at reflux. After cooling to RT the solvent was removed under reduced pressure and the residue was dissolved in water (15 mL) and dichloromethane (15 mL). Phases were separated and the aqueous phase was extracted with dichloromethane (2 × 15 mL). The combined organic phases were were dried over MgSO$_4$ and the solvent removed under reduced pressure. FC (DCM/MeOH = 20:1) gave azide **13** (250 mg, 0.77 mmol, 96 %) as a colorless oil.

IR (Film): 2935 m, 2860 m, 2092 s, 1729 w, 1596 s, 1555 m, 1458 m, 1376 m, 1252 s, 1182 w, 1101 s, 991 m, 900 w, 822 s, 744 w, 670 m, 588 cm^{-1} w. ^{1}H NMR (300 MHz, CDCl$_3$, 300 K): δ = 8.64 (d, J = 5.0 Hz, 1H, Aryl-H), 8.53 (d, J = 4.9 Hz, 1H, Aryl-H), 8.31 (s, 1H, Aryl-H), 8.23 (s, 1H, Aryl-H), 7.33 (d, J = 4.9 Hz, 1H, Aryl-H), 7.13 (d, J = 4.9 Hz, 1H, Aryl-H), 4.59 (s, 2H, CCH_2O), 3.53 (t, J = 6.4 Hz, 2H, CH_2N$_3$), 3.26 (t, J = 6.9 Hz, 2H, OCH_2CH$_2$), 2.44 (s, 3H, CCH_3), 1.64 (m, 4H, CH_2CH$_2$N$_3$, OCH$_2$CH_2), 1.52–1.33 ppm (m, 4H, 2 × CH_2). ^{13}C NMR (75 MHz, CDCl$_3$, 300 K): δ = 156.4 (C), 155.9 (C), 149.3 (CH), 149.0 (CH), 148.9 (C), 148.1 (C), 124.7 (CH), 122.0 (CH), 121.8 (CH), 119.4 (CH), 71.5 (CH$_2$), 70.9 (CH$_2$), 51.4 (CH$_2$), 29.6 (CH$_2$), 28.8 (CH$_2$), 26.6 (CH$_2$), 25.8 (CH$_2$), 21.2 ppm (CH$_3$). MS (ESI): m/z = 326 ([M+H]$^+$), 348 ([M+Na]$^+$). HRMS (ESI): calculated for [C$_{18}$H$_{23}$N$_5$ONa]$^+$ m/z = 348.1795; found m/z = 348.1799.

Synthesis of Catalytic System B
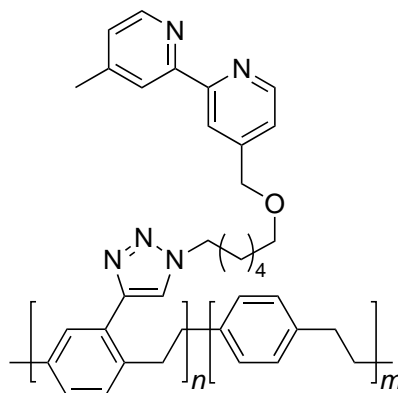
According to GP 1, with bipyridine-derivate **13** (150.0 mg, 461.0 µmol). Catalytic system **B** (72.0 mg) was isolated by intensive washing with THF and drying under reduced pressure. Elemental analysis revealed a degree of functionalization of 27 % (calculated by the nitrogen content of the functionalized fiber mat).

Elemental analysis in % calculated for complete functionalization: C 73.03, H 8.17, N 12.90; found: C 69.94, H 7.81, N 3.48.

^{1}H NMR and ^{13}C NMR Spectra of all new Compounds

4-(((6-Bromohexylo)xy)methyl)-4'-methyl-2,2'-bipyridine (12):
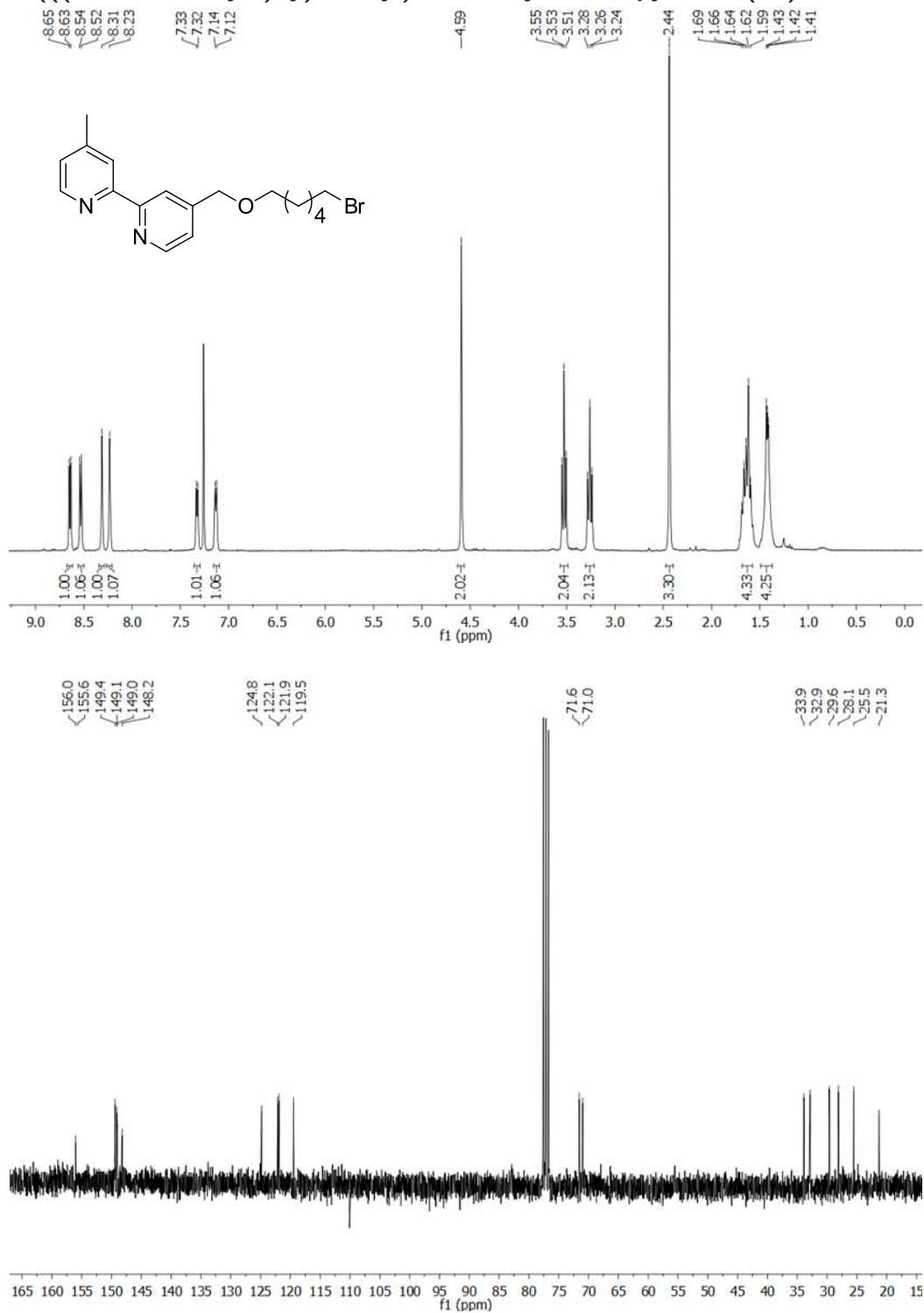
4-(((6-Azidohexyl)oxy)methyl)-4'-methyl-2,2'-bipyridine (13):

4.9 References (Supporting Information)

[1] M. Regitz, J. Hocker, A. Liedhegener, *Org. Synth.* **1968**, *48*, 36.

[2] W. R. F. Goundry, J. E. Baldwin, V. Lee, *Tetrahedron* **2003**, *59*, 1719.

[3] L. Ernst, L. Wittkowski, *Eur. J. Org. Chem.* **1999**, *7*, 1653.

[4] J. W. Graskemper, B. Wang, L. Qin, K. D. Neumann, S. G. DiMagno, *Org. Lett.* **2001**, *13*, 3158.

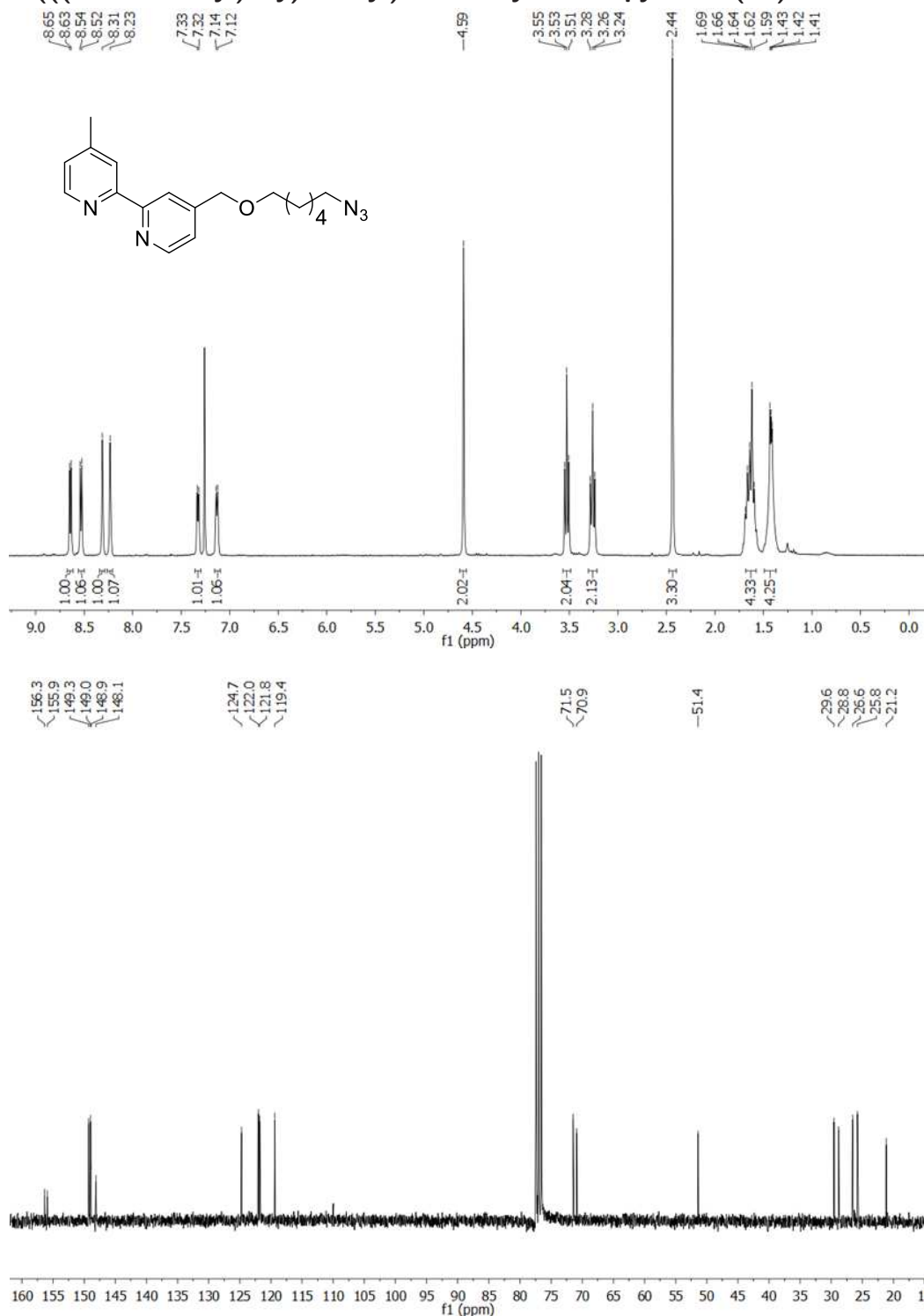[5] M. Brink, *Synthesis* **1975**, *12*, 807.

[6] H. Nandivada, H.-Y. Chen, J. Lahann, *Macromol. Rapid Commun.* **2005**, *26*, 1794.

[7] L. Bondarenko, I. Dix, H. Hinrichs, H. Hopf, *Synthesis* **2004**, *16*, 2751.

[8] J. Zakrzewski, J. Hupko, K. Kryezka, *Monatsh. Chem.* **2003**, *134*, 843.

[9] K. E. Berg, A. Tran, M. K. Raymond, M. Abrahamsson, J. Wolny, S. Redon, M. Andersson, L. Sun, S. Styring, L. Hammarström, H. Toftlund, B. Åkermark, *Eur. J. Inorg. Chem.* **2001**, *12*, 1019.

5 Transition Metal-Functionalized Dendrimers Encapsulated in PPX Tubes as Reusable Catalysts

Fabian Mitschang,[a] Barbara K. Dettlaff,[b] Jean-Pierre Lindner,[b] Armido Studer,[b,] Andreas Greiner[a,*]*

[a]Makromolekulare Chemie II, Universität Bayreuth, Universitätsstraße 30, 95440 Bayreuth, Germany.

[b]Organisch-Chemisches Institut, Westfälische Wilhelms-Universität Münster, Corrensstraße 40, 48149 Münster, Germany.

*Corresponding Authors:
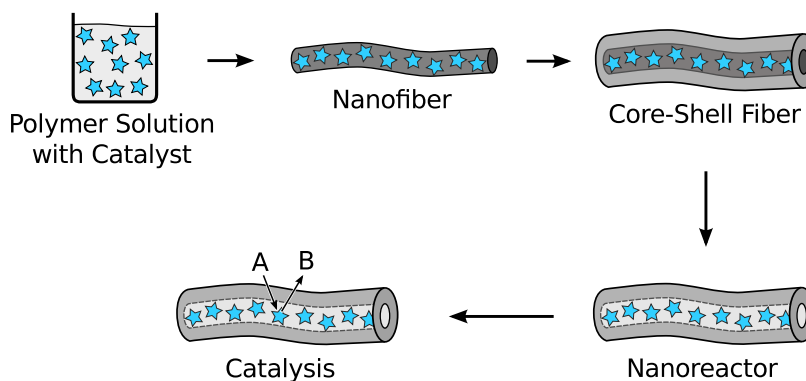
A. Greiner: E-mail: greiner@uni-bayreuth.de; Fax: +49-921-553393.

A. Studer: E-mail: studer@uni-muenster.de; Fax: +49-251-8336523.

5.1 Abstract

Composite nanofibers of polyurethane and catalytically active Pd- or Cu-functionalized poly(amido amine) dendrimers were electrospun and subsequently coated with poly(*p*-xylylene) by the chemical vapor deposition. After removal of the inner

polyurethane template matrix, the dendrimers remained encapsulated inside the confinement and the leaching behavior of the caged dendritic catalysts was studied. The tube system was successfully used as a readily reusable tea bag type catalyst for Suzuki-Miyaura couplings and alkyne/azide click reactions.

5.2 Introduction

Nowadays there are many potent catalysts for various reactions available yet catalyst recycling often remains a considerable challenge. Many times it is favorable and often even necessary to apply sophisticated purification protocols in order to remove expensive and toxic catalysts from the products to obtain the desired product properties.[1–3] A valuable approach to overcome this problem is to conjugate the catalyst to an insoluble support with a high surface area, such as zeolites, charcoal, or porous pellets which allows for easy catalyst removal after successful reaction.[4,5] Alternatively, the catalyst can be encapsulated inside of nanoparticles, dendrimers, or sol-gel supports for its convenient recovery after the reaction.[6–9] Continuous semipermeable nanotubes have also been successfully applied to confine catalysts.[10,11] In contrast to immobilized catalysts that are covalently bound, confined catalysts can diffuse freely in their cages and show therefore reactivity profiles comparable to homogeneous systems. Hence they have properties of a homogeneous catalyst in terms of reactivity and reveal also properties of a heterogeneous system in terms of simple catalyst recovery.[12] Moreover, the tube material can potentially function as a selective membrane[13,14] and therefore could lead to substrate selection during the reaction.

Herein, we report the preparation of poly(p-xylylene) (PPX) tube-encapsulated Pd- and Cu-functionalized poly(amido amine) (PAMAM) dendrimers and their application as reusable catalyst systems in two different reaction types.

5.3 Results and Discussion

In a previous study, we showed that immobilized dendrimers are retained by PPX membranes only if the hydrodynamic diameter of the dendrimer is large enough.[11] Whereas PAMAM dendrimers of generation 4 (PAMAM G4) leached out of PPX

tubes used as membrane reactors, PAMAM dendrimers of the fifth generation (PAMAM G5) remained immobilized inside the confinements. Therefore, we used PAMAM of generation 5 for the present studies. Commercially available amino-terminated PAMAM G5 dendrimer (**1**) was converted to diphenylphosphine-functionalized PAMAM-PPh$_2$ (**4**) using a modified Reetz protocol[15] by reacting PAMAM with diphenylphosphine (**3**) and paraformaldehyde (**2**) in a MeOH/toluene solvent mixture (Scheme 5.1). The resulting PAMAM-PPh$_2$ (**4**) was character-
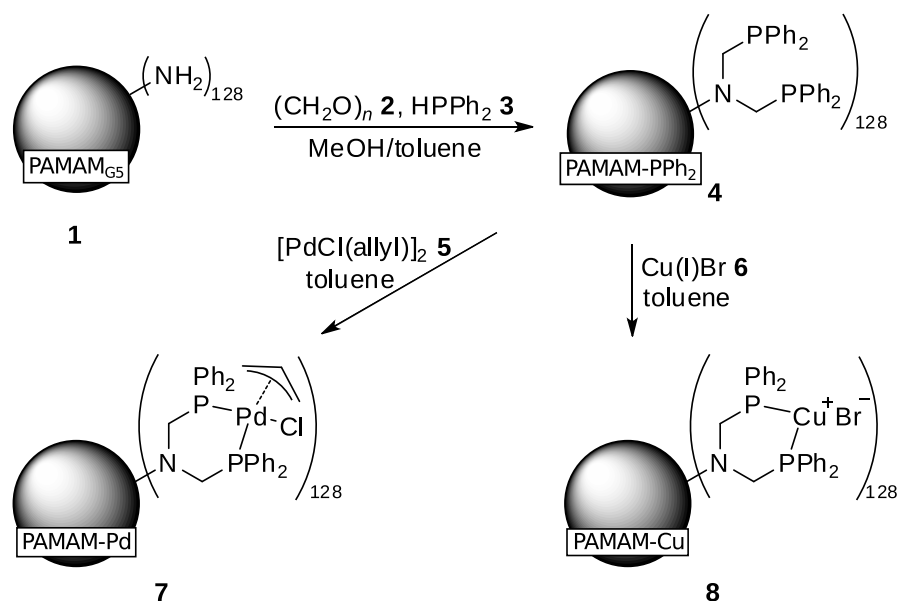
Scheme 5.1. Preparation of the PAMAM-Pd and PAMAM-Cu catalysts **7** and **8**, respectively.

ized by NMR spectroscopy, IR spectroscopy and MALDI-TOF mass spectrometric analysis. All data, especially the sharp signal in the ^{31}P NMR spectrum at -27.8 ppm clearly showed the successful conversion. Subsequent treatment of **4** with [Pd(allyl)Cl]$_2$ (**5**) or Cu^{I}Br (**6**) provided the corresponding PAMAM-Pd and PAMAM-Cu complexes, **7** and **8**, respectively. In both cases, a significant shift of the P-resonance in the ^{31}P NMR spectrum from -27.8 ppm to 2.3 ppm for PAMAM-Pd (**7**) and to -25.8 ppm for PAMAM-Cu (**8**) was noted, indicating the successful complexation of **4** by the two different metal salts used.

In order to prepare a catalyst system consisting of PPX tubes with encapsulated transition metal complexes, the tubes by fiber templates (TUFT) process[16] was used, as illustrated in Figure 5.1. In a first step, composite nanofibers of the func-
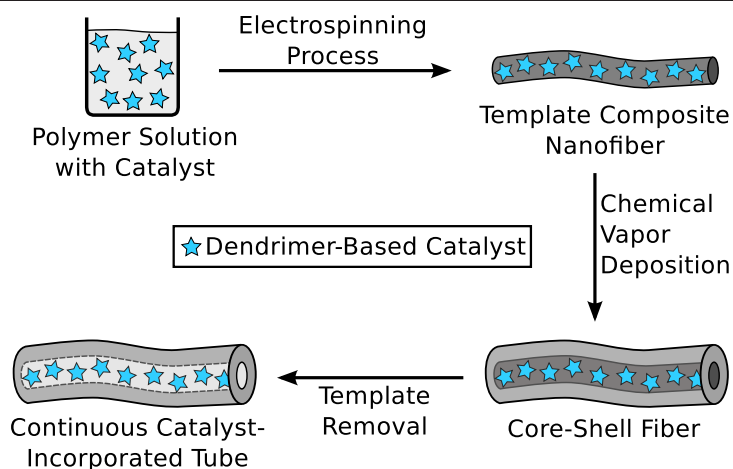
Figure 5.1. Illustration of the underlying TUFT concept used for the preparation of PPX tube encapsulated transition metal catalysts (stars denote the dendritic catalysts **7** and **8**).

tionalized dendrimers **7** or **8** within a suitable polymer matrix were electrospun.[17,18] The obtained fibers were then coated with PPX by using the chemical vapor deposition (CVD) process.[19,20] PPX is a suitable catalyst support due to the high resistance against both water and organic solvents,[21] its thermal stability up to 220 °C,[22] and its high gap penetration capability.[23] Extraction of the inner polymer template finally resulted in PPX tubes with encapsulated functionalized dendrimers **7** and **8**.

Prior to the preparation of the composite nanofibers, a suitable template polymer had to be identified. Since the dendritic catalysts **7** and **8** were only soluble in dimethylformamide (DMF) a template polymer which was soluble in DMF had to be found. Furthermore, that polymer must be compatible with the electrospinning process and should be suitable for the TUFT process resulting in nanofiber mats featuring good mechanical properties. After extensive experimentation we found polyurethane (PU) as an ideal template material for the preparation of the catalyst-incorporated composite nanofibers. Single-nozzle electrospinning of 10 wt% PU and 5 wt% PAMAM-catalyst **7** or **8** dissolved in DMF resulted in the corresponding fiber mats shown in Figure 5.2. The uniform PU/PAMAM-Pd composite fibers had an average diameter of 383 ± 93 nm, whereas the Cu-containing fibers showed a diameter of 130 ± 74 nm. Interestingly, the PU/PAMAM-Cu fibers were not well isolated but rather fused together, forming a cross-linked network. Neither of the
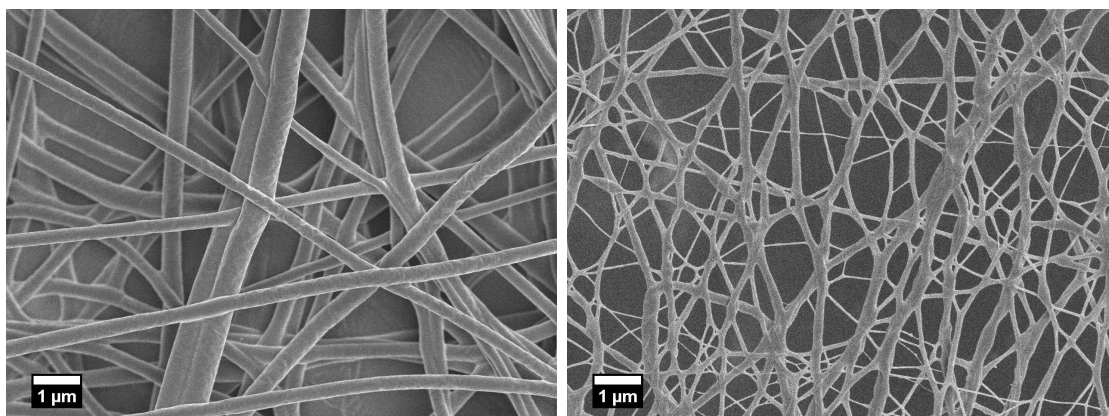
Figure 5.2. Scanning electron micrographs of electrospun composite fiber mats containing 2/3 PU and 1/3 incorporated PAMAM-Pd **7** (left) and PAMAM-Cu **8** (right).

samples showed the formation of beads.

The prepared composite fiber mats were then coated with PPX using the CVD process. The corresponding pressure was 8.8 kPa, the vaporization temperature was 150 °C, the pyrolysis temperature was 650 °C, and the deposition temperature was below 30 °C. To ensure a homogeneous PPX distribution throughout each sample, the fiber mats were coated from both sides. As shown in the scanning electron micrographs in Figure 5.3, the deposited PPX layer was free of visible cracks and covered the template fibers uniformly. The layer thickness was determined us-
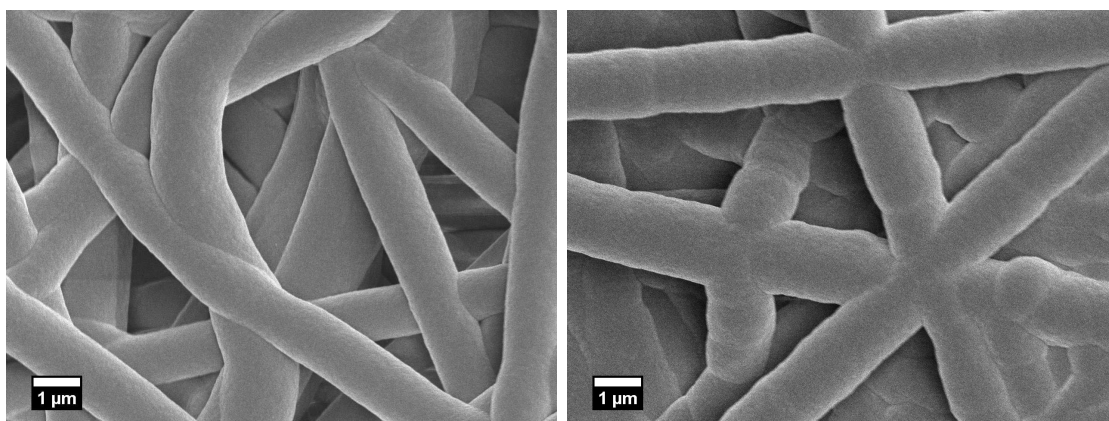
Figure 5.3. Scanning electron micrographs of PU-PPX core-shell fibers with incorporated PAMAM-Pd (left) and PAMAM-Cu (right).

ing a profilometer and scanning electron microscopy. These analyses revealed that

the PU/PAMAM-Pd fibers were coated with 424 nm of PPX, whereas the Cu-containing composite fibers had an average PPX shell thickness of 672 nm. The corresponding fiber diameters were 1231 ± 114 nm and 1474 ± 49 nm, respectively.

As opposed to the large, spherical dendrimers, linear polymers have been shown to be able to permeate PPX membranes by diffusion.[11][24] Hence, in order to prepare hollow PPX tubes and, respectively, catalyst incorporated nanoconfinements, the inner template material was extracted using a suitable solvent. The fiber mats were fixated using a custom-made sample mount (see Supporting Information) and subsequently immersed in tetrahydrofuran (THF) under vigorous stirring. The solvent was exchanged every 24 h until the weight of the mats remained constant (up to seven cycles). Since the original template fibers consisted of 33 wt% of the catalysts, the remaining PPX tubes were not completely hollow but rather filled with the corresponding dendrimers. As a result, no cross sections of hollow tubes could be observed. Transmission electron microscopy was used to depict the core-shell character of the obtained system (Figure 5.4).
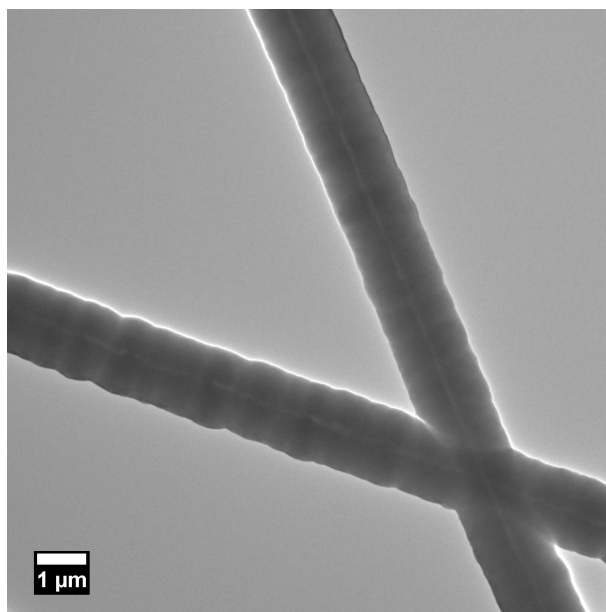
Figure 5.4. Transmission electron micrograph of the obtained PPX tubes filled with dendrimer catalyst **8**.

Inductively coupled plasma mass spectrometry (ICP-MS) was used to study the leaching behavior of the incorporated metal catalysts. Even though leaching oc-

curred in both cases during the initial washing cycles, the amount of extracted catalyst declined rapidly as the solvent was renewed (see Figure 5.5). As a result,
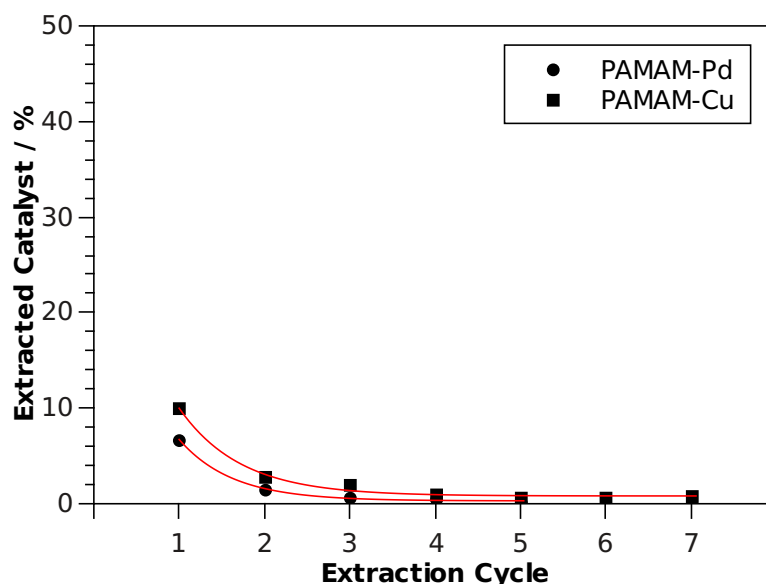
Figure 5.5. Leaching behavior of the PPX tube encapsulated catalysts PAMAM-Pd **7** (**7**@PPX) and PAMAM-Cu **8** (**8**@PPX), respectively.

90 wt% PAMAM-Pd **7** and, respectively, 82 wt% PAMAM-Cu **8** remained immobilized inside the PPX confinements. In this way, it was possible to prepare tube material **7**@PPX and **8**@PPX which contained up to 15 wt% of the metalated PAMAM catalyst.

The activity and reusability of the new catalysts were tested in catalysis. The Suzuki-Miyaura coupling reaction[25] and the Cu(I)-catalyzed Huisgen azide/alkyne cycloaddition,[26] depicted in Scheme 5.2, were selected as test reactions. We found that the Suzuki-Miyaura coupling is best conducted in MeOH in the presence of NaOMe at 60 °C. Reaction for 3 h using 2 mol% (with respect to Pd) of **7**@PPX immersed into the reaction mixture provided good yields of the corresponding biphenyls **15**–**19** (Table 5.1).

Suzuki-Miyaura coupling worked well for aryl bromides (**11**, **12**) and aryl iodides (**9**, **10**) whereas the less reactive aryl chlorides were not converted under the applied conditions (not shown). The catalytically active fiber mat could be reused after simple washing (detailed leaching studies will be discussed below). The cy-

a)

R^1—⟨benzene⟩—X + (HO)$_2$B—⟨benzene, R^2⟩—R^3 $\xrightarrow[\substack{\text{NaOMe, MeOH,} \\ \text{3h, 60 °C}}]{\textbf{7}@\text{PPX}}$ R^1—⟨biphenyl, R^2⟩—R^3

9 R^1 = H, X = I   **13** R^2 = H, R^3 = CH$_3$ **15** R^1 = H, R^2 = H, R^3 = CH$_3$
10 R^1 = NO$_2$, X = I   **14** R^2 = CH$_3$, R^3 = H   **16** R^1 = H, R^2 = CH$_3$, R^3 = H
11 R^1 = CHO, X = Br   **17** R^1 = NO$_2$, R^2 = H, R^3 = CH$_3$
12 R^1 = CH$_3$, X = Br   **18** R^1 = CHO, R^2 = H, R^3 = CH$_3$
        19 R^1 = CH$_3$, R^2 = H, R^3 = CH$_3$

b)

⟨benzyl⟩—N$_3$ + H≡≡—R^1 $\xrightarrow[\substack{\text{MeOH, 60 °C} \\ \text{24 - 48 h}}]{\textbf{8}@\text{PPX}}$ ⟨benzyl-triazole⟩—R^1

20   **21** R^1 = CH$_2$OPh   **25** R^1 = CH$_2$OPh
        22 R^1 = Ph   **26** R^1 = Ph
        23 R^1 = CH$_2$OCH$_3$ **27** R^1 = CH$_2$OCH$_3$
        24 R^1 = CH$_2$NH$_2$ **28** R^1 = CH$_2$NH$_2$
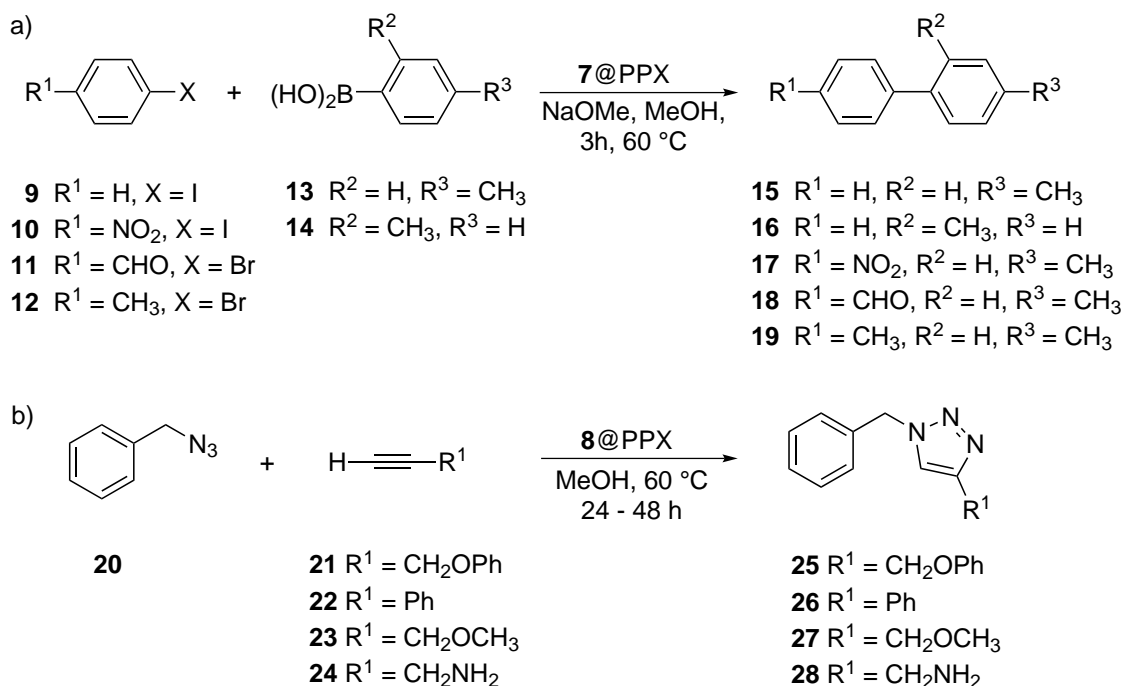
Scheme 5.2. Model reactions used to study the encapsulated catalysts: (a) Suzuki-Miyaura coupling with encapsulated PAMAM-Pd (**7**); (b) Click reactions with encapsulated PAMAM-Cu (**8**).

cloaddition reactions were performed in MeOH for 24 to 48 h at 60 °C using 0.9 mol% of the immobilized catalyst **8**@PPX and **20** was chosen as azide component in these transformations. With the alkynes **21**–**24** the corresponding triazoles **25**–**28** were obtained in excellent yields (see Table 5.1). The PPX-tube material did not show any influence on yield and rate of the reaction, as two test runs using nonimmobilized PAMAM-Pd (**7**) and PAMAM-Cu (**8**) showed similar results (Table 5.1).

To study the long-term stability and Pd-leaching behavior of the fiber mat **7**@PPX under Suzuki-Miyaura coupling conditions, the tube material was reused 16 times. For this study 4-bromobenzylaldehyde (**11**) and 4-methylphenylboronic acid (**13**) were chosen as reaction partners and couplings were conducted under optimized conditions (MeOH, NaOMe, 60 °C, 3 h). After each cycle the catalyst fiber mat was thoroughly washed with MeOH. Yields determined by NMR spectroscopy for each cycle are shown in Figure 5.6. It is noticeable that the yield slightly decreased upon repeated use of the catalyst system. Although after removal of the

Table 5.1. Selected catalytic reactions and conditions chosen (solvent = MeOH, reaction temperature = 60 °C).

Catalyst	Reactant 1	Reactant 2	Product	t / h	Yield / %
7@PPX	9	13	15	3	88
7@PPX	9	14	16	3	77
7@PPX	10	13	17	3	80
7@PPX	11	13	18	3	82
7@PPX	12	13	19	3	75
8@PPX	20	21	25	24	99
8@PPX	20	22	26	28	81
8@PPX	20	23	27	48	quan.[a]
8@PPX	20	24	28	48	quan.[a]
7	11	13	18	3	86
8	20	21	25	22	85

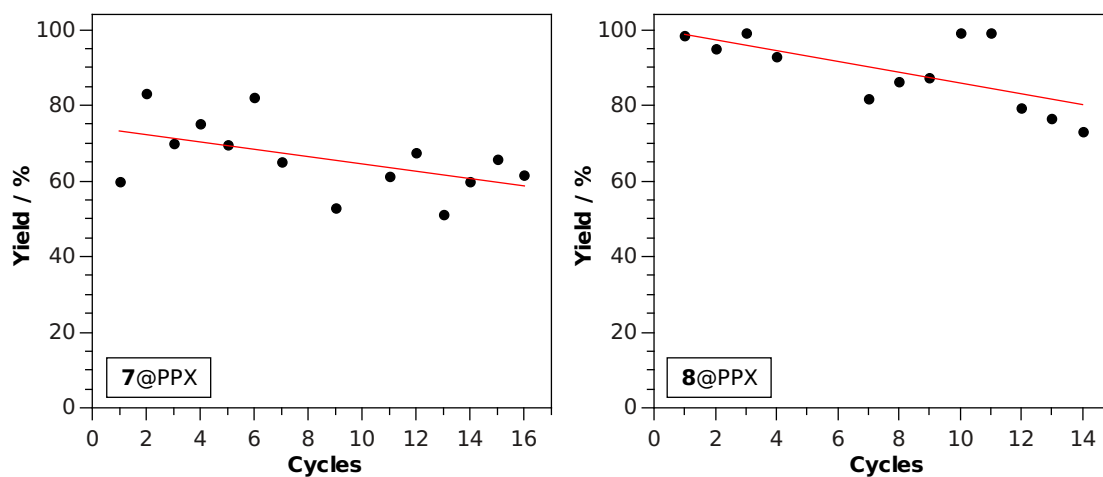[a]The yield was determined by GC analysis.

Figure 5.6. Catalytic activity and reusability with (left) **7**@PPX in the reaction of **11** with **14** and (right) **8**@PPX in the reaction of **20** with **21**.

PU-template fibers during catalyst preparation no further Pd metal was washed out after the fourth extraction cycle using THF as proved by ICP-MS measurements (see Figure 5.5), we believe that under the Suzuki-Miyaura reaction condition traces of metal may be liberated out of the mats into the solution which would explain the decrease in yield after multiple use of the fiber mat. Indeed, after stopping the reaction at low conversion by removal of the fiber mat **7**@PPX, we observed further conversion of the reaction which indicated that traces of the Pd-catalyst were released from the tube system during the reaction.

To test the long-term stability and reusability of the PAMAM-Cu system **8**@PPX, the reaction between benzyl azide (**20**) and propargyl phenyl ether (**21**) to give triazole **25** was selected. As shown in Figure 5.6 (right), the tube material was successfully reused for 14 cycles. As with the Pd-system, a slight decrease in yield was noted upon repeated usage of the fiber mat. In addition, it was noted that upon storage of the fiber mat for a longer period of time slow oxidation from Cu(I) to Cu(II) occurred which caused a substantial drop in activity (for runs 5 (41 %) and 6 (18 %), not shown in Figure 5.6 (right)). However, addition of sodium L-ascorbate as reducing reagent restored the high activity of the tube material. Hence, after longer storage the mat has to be reactivated with a reducing reagent to regain the high activity.

As shown in Figure 5.7, both catalyst systems were still intact after multiple reaction cycles (16, and, respectively, 14 cycles). Despite marginal deposits, the PPX
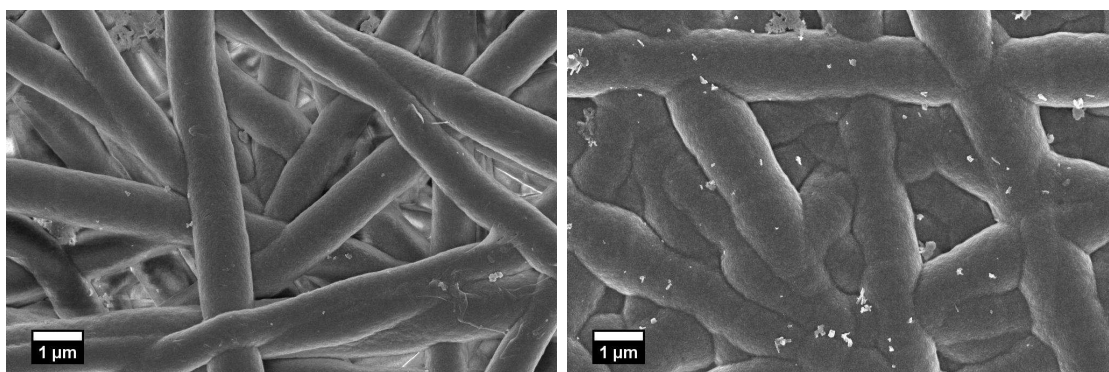

Figure 5.7. Scanning electron micrographs of the used tube catalyst systems (left: **7**@PPX after 16 cycles; right: **8**@PPX after 14 cycles). Despite marginal deposits the PPX surface did not show abrasion and was still intact.

surface did not show cracks or abrasion, hence the PPX confinements are highly compatible with the chosen conditions of the Suzuki-Miyaura and click reactions.

5.4 Conclusion

Palladium- and copper-based catalysts were successfully ligated with generation 5 PAMAM dendrimers. Electrospinning of the metalated dendrimers with polyurethane provided defect-free polymer nanofibers which were used as templates for chemical vapor deposition with PPX resulting in the corresponding core-shell fibers with an average diameter of 1231 and 1474 nm, respectively. After removal of the inner template polyurethane fiber material with THF, the extracts were analyzed by ICP-MS to study the leaching behavior. Whereas the first extraction cycle was accompanied by Pd-leaching, leaching rapidly dropped to a negligible amount. 90 wt% of the Pd-functionalized dendrimers and, respectively, 82 wt% of PAMAM-Cu remained caged inside the PPX tubes. The Pd-containing tube material was an efficient reusable catalyst for various Suzuki-Miyaura couplings. Fiber mats were success-fully reused up to 16 times. The Cu-containing tubes allowed catalyzing the azide/alkyne cycloaddition and were reused up to 14 times. However, for both catalyst systems tested a slight decrease of the yield after multiple runs was noted. It was shown that under the applied reaction conditions, Pd and Cu slowly leached out of the fiber mats. The PPX surface showed a high resistance to abrasion and was still intact after many catalytic cycles. Future studies will therefore be devoted to the development of PAMAM-based ligands with improved affinities to the catalytically active metal species.

5.5 Experimental Section

Materials and Analytical Methods

For detailed information on the materials used as well as on the analytical methods please see the Supporting Information.

Preparation of PAMAM-PPh$_2$ (4)

p-Formaldehyde (**2**) (8.1 mg, 0.26 mmol, 2.3 eq.) and diphenylphosphine (**3**) (45 µL, 0.26 mmol, 2.3 eq.) in dry and degassed methanol were stirred for 30 min at 65 °C and after cooling to room temperature generation 5 PAMAM-NH$_2$ **1** in methanol (5 wt%, 500 µL, 8.7×10^{-4} mmol, 0.11 mmol NH$_2$-groups, 1 eq.) was added. After 20 min, a colorless solid precipitated which was dissolved by addition of dry and degassed toluene (2 mL). The solution was heated for 19 h to 60 °C, subsequently concentrated to 0.4 mL in vacuo, and methanol (2 mL) was added to the residue resulting in a colorless suspension which was transferred into a centrifugal tube. The precipitated dendrimer was centrifuged (15 min, 5300 rpm) and dried under vacuum. PPh$_2$-modified dendrimer **4** (61.1 mg, 7.7×10^{-4} mmol, 88 %) was isolated as a foam.

^{1}H NMR (300 MHz, CDCl$_3$): δ [ppm] = 7.31–7.20 (m, 1024H, phenyl), 7.16–7.04 (m, 1536H, phenyl), 5.85–6.15 (m, 84H, NH), 3.54–3.34 (m, 424H, CH$_2$), 3.22–2.94 (m, 512H, CH$_2$), 2.91–2.72 (m, 364H, CH$_2$), 2.70–2.35 (m, 624H, CH$_2$). 2.29–2.08 (m, 512H, NCH$_2$P), 1.96–1.70 (m, 168H, CH$_2$CO). ^{31}P NMR (300 MHz, CDCl$_3$): δ [ppm] = -28.5. IR (film): [cm^{-1}] = 3271 w, 3053 w, 2934 w, 2822 w, 1643 m, 1542 m, 1433 s, 1360 m, 1246 m, 1182 m, 1122 m, 1093 m, 999 s, 909 m, 857 m, 729 s, 692 s, 550 m.

Preparation of PAMAM-Pd (7)

Diphenylphosphine-PAMAM **4** (67.4 mg, 8.5×10^{-4} mmol, 0.11 mmol PPh$_2$ units, 1 eq.) was dissolved in dry toluene (1 mL) and [Pd(allyl)Cl]$_2$ (**5**) (18.3 mg, 0.05 mmol, 0.5 eq.) in dry toluene (1 mL) was slowly added. The suspension was stirred at room temperature for 19 h, centrifuged (10 min, 5300 rpm) and the supernatant solution was removed. For purification, the precipitate was suspended twice in toluene (2 mL), again centrifuged and subsequently dried under vacuum. PAMAM-Pd (**7**) (51.2 mg, 5.0×10^{-4} mmol, 59 %) was isolated as a pale yellow solid.

^{1}H NMR (300 MHz, CDCl$_3$): δ [ppm] = 7.78–7.32 (m, 1024H, phenyl), 7.32–7.04 (m, 1536H, phenyl), 5.65–5.45 (m, 84H, NH), 4.18–3.82 (m, 336H, CH$_2$), 3.80–3.35 (m, 292H, CH$_2$), 3.35–2.95 (m, 454H, CH$_2$), 2.92–2.36 (m, 1126H, CH$_2$). ^{31}P NMR

(300 MHz, CDCl$_3$): δ [ppm] = 2.3.

Preparation of PAMAM-Cu (8)

Diphenylphosphine-PAMAM (**4**) (65.4 mg, 8.2 × 10^{-4} mmol, 0.10 mmol PPh$_2$ units, 1 eq.) was dissolved in dry toluene (1 mL) and copper(I) bromide (**6**) (15.1 mg, 0.10 mmol, 1 eq.) in dry toluene (1 mL) was slowly added. The suspension was stirred at room temperature for 19 h, centrifuged (10 min, 5300 rpm), and the supernatant solution was removed. For purification, the precipitate was suspended twice in toluene (2 mL), again centrifuged and subsequently dried under vacuum. PAMAM-Cu (8) (52.2 mg, 5.3 × 10^{-4} mmol, 63 %) was isolated as a colorless solid.

^{1}H NMR (300 MHz, DMF-d$_7$): δ [ppm] = 8.30–7.30 (m, 2560H, phenyl), 4.25–3.20 (m, 1296H, CH$_2$), 2.51–1.85 (m, 824H, CH$_2$). ^{31}P NMR (300 MHz, DMF-d$_7$): δ [ppm] = 28.1 and -25.8.

Electrospinning of Catalyst-PU Composite Nanofibers

Mixtures of 10 wt% PU (1.24 × 10^5 g mol^{-1}) and 5 wt% PAMAM-catalyst were dissolved in DMF and stirred under an argon atmosphere for 16 h. In order to prepare the composite nanofibers, a custom-made single-nozzle electrospinning setup[16] was used. The best results were achieved with an outer needle-diameter of 0.9 mm and an electrode gap of 10 cm. The collector electrode was a perpendicular aluminum plate, spinning with 6 rotations per minute. On top of the collector electrode was a trimmed piece of baking paper carrying a square metal frame (edge length 9 cm). The corresponding voltage was 2 kV, whereas the voltage of the needle was set to 22 kV. The temperature was about 25 °C, and 1 mL syringes were used at a flow rate of 6. A connected dehumidifier lowered the relative humidity below 20 %. After 30–40 min, the baking paper was trimmed to the size of the metal frame and carefully separated from the electrospun fibers. As a result, the metal frame carried a 9 × 9 cm fiber mat with homogeneously distributed composite fibers. The prepared fiber mats were stored under an argon atmosphere. Scanning electron microscopy (SEM) was used to measure the average fiber diameter. The PAMAM-Pd incorporated fibers had a diameter of 383 ± 93 nm, whereas the PAMAM-Cu-PU composite fibers had a diameter of 130 ± 74 nm. There were no beads visible.

Chemical Vapor Deposition of PPX

Prior to the chemical vapor deposition of PPX, the weight of the fiber mats had to be determined. Hence, the fibers were transferred from the metal frames onto a light, rigid polymer grid and subsequently weighed. Then the fiber mats were fixed to a square aluminum piece ($9 \times 9 \times 1\,cm$) using 4 needles. The prepared samples were placed inside the deposition chamber of the used Labcoater 1 (Specialty Coating Systems). The temperature of the evaporation chamber was set to $150\,°C$, whereas the temperature of the pyrolysis chamber/furnace was $650\,°C$. At a temperature below $30\,°C$ and a pressure of $8.8\,kPa$, PPX was deposited onto the composite fibers. Generally an amount of $0.60\,g - 1.00\,g$ of the corresponding precursor [2.2]paracyclophane resulted in $200–350\,nm$ of PPX. After the deposition process, the fiber mats were flipped and subsequently coated from the other side in order to provide a homogeneous PPX distribution throughout the whole sample. Various core-shell fiber mats were prepared featuring different PPX thicknesses. SEM measurements of the coated PU/PAMAM-Pd composite fibers revealed an average fiber diameter of $1231 \pm 161\,nm$, whereas the Cu-containing system had a diameter of $1474 \pm 49\,nm$. The coating was smooth and free of visible cracks.

Template Extraction

To extract the inner PU template, each core-shell fiber mat was fixed using a custom-made sample mount (see Supporting Information) and subsequently immersed in THF at room temperature. The solvent was vigorously stirred for $24\,h$, removed, and the samples were rinsed. The described extraction process was repeated 5–7 times until no further weight loss could be measured. The extraction fractions were analyzed by ICP-MS to quantify traces of the extracted transition metals. To this end, the extracts were dried and an aqueous solution of nitric acid ($1\,wt\%$) was added to transfer the corresponding transition metals into the aqueous phase. The aqueous phase was then analyzed. As a result, we found that $90\,wt\%$ PAMAM-Pd and, respectively, $82\,wt\%$ PAMAM-Cu remained immobilized inside the PPX confinements.

General Procedure for Suzuki-Miyaura Couplings with Tube Material 7@PPX

For all Suzuki-Miyaura couplings the Pd-containing tube material **7**@PPX (5.0 mg PAMAM-Pd (**7**), 6.2×10^{-3} mmol Pd, 0.02 eq.) was fixed in the custom-made sample mount and a solution of aryl halide (0.25 mmol, 1 eq.), boronic acid (0.37 mmol, 1.5 eq.) and sodium methoxide (0.75 mmol, 3 eq.) in dry methanol (5 mL) was added under argon atmosphere. The reaction mixture was heated to 60 °C for 3 h. Subsequently, the sample mount and the tube material were washed several times with methanol and the washed tube material was dried carefully by passing an argon stream followed by drying under vacuum. After removal of the solvent from the reaction mixture, the obtained residue was dissolved in water and dichloromethane. The water layer was extracted with dichloromethane (2×15 mL) and the combined organic layers were washed with saturated NaCl solution (20 mL), dried over MgSO$_4$, filtrated and the solvent was removed under vacuum, which led to the desired coupling product. The yield was determined by ^{1}H NMR spectroscopy by using dibromomethane as an internal standard.

General Procedure for the Azide/Alkyne Cycloaddition with Tube Material 8@PPX

For all cycloadditions the Cu-containing tube material **8**@PPX (1.68 mg PAMAM-Cu (**8**), 2.2×10^{-3} mmol Cu, 0.9 eq.) was fixed in the custom-made sample mount and a solution of benzyl azide (0.25 mmol, 1 eq.) and the corresponding alkyne (0.27 mmol, 1.1 eq.) in dry methanol (5 mL) was added. In cases of longer storage time of the fiber mat, sodium L-ascorbate (5 mg, 0.02 mmol, 0.1 eq.) was added to the solution to reduce oxidized Cu(II) to Cu(I). The reaction mixture was heated to 60 °C for 24–48 h. Subsequently, the sample mount and the tube material were washed several times with methanol and the washed tube material was dried carefully by passing an argon stream followed by drying under vacuum. After removal of the solvent from the reaction mixture, the obtained residue was dissolved in CDCl$_3$ and yield was determined by ^{1}H NMR spectroscopy by using dibromomethane as an internal standard.

5.6 Acknowledgments

5.7 References

[1] B. Clapham, T. S. Reger, K. D. Janda, *Tetrahedron* **2001**, *57*, 4637.

[2] B. Bendjemil, E. Borowiak-Palen, A. Graff, T. Pichler, M. Guerioune, J. Fink, M. Knupfer, *Appl. Phys. A: Mater. Sci. Process.* **2004**, *78*, 311.

[3] K. J. Borah, P. Dutta, R. Borah, *Bull. Korean Chem. Soc.* **2011**, *32*, 225.

[4] S. L. Poe, M. Kobašlija, D. T. McQuade, *J. Am. Chem. Soc.* **2006**, *128*, 15586.

[5] A. Corma, H. Gracia, *Top. Catal.* **2008**, *48*, 8.

[6] S. J. Brodwater, S. L. Roth, K. E. Price, M. Kobašlija, D. T. McQuade, *Org. Biomol. Chem.* **2005**, *3*, 2899.

[7] B. Hekms, S. J. Guillaudeu, Y. Xie, M. McMurdo, C. J. Hawker, J. M. J. Fréchet, *Angew. Chem. Int. Ed.* **2005**, *44*, 6384.

[8] S. L. Poe, M. Kobašlija, D. T. McQuade, *J. Am. Chem. Soc.* **2007**, *129*, 9216.

[9] R. van Heerbeck, P. C. J. Kamer, P. van Leeuwen, J. N. H. Reek, *Chem. Rev.* **2002**, *102*, 3717.

[10] J.-M. Nhut, L. Pesant, J.-P. Tessonnier, G. Winé, J. Guille, C. Pham-Huu, M.-J. Ledoux, *Appl. Catal., A* **2003**, *254*, 345.

[11] J.-P. Lindner, C. Röben, A. Studer, M. Stadiak, R. Ronge, A. Greiner, J. H. Wendorff, *Angew. Chem. Int. Ed.* **2009**, *48*, 8874.

[12] N. Madhaven, T. Takatani, C. D. Sherrill, M. Weck, *Chem.-Eur. J.* **2009**, *15*, 1186.

[13] K. Schröck, S. Schulze, A. Schlemmer, K.-M. Weitzel, *J. Phys. D: Appl. Phys.* **2010**, *43*, 025501.

[14]   P. Hanefeld, F. Sittner, W. Ensinger, A. Greiner, *e-Polymers* **2006**, *26*, 1.

[15]   M. T. Reetz, G. Lohmer, R. Schwickardi, *Angew. Chem. Int. Ed.* **1997**, *36*, 1526.

[16]   M. Bognitzki, H. Hou, M. Isahaque, T. Frese, M. Hellwig, C. Schwarte, A. Schaper, J. H. Wendorff, A. Greiner, *Adv. Mater.* **2000**, *12*, 637.

[17]   S. Agarwal, A. Greiner, J. H. Wendorff, *Prog. Polym. Sci.* **2013**, *38*, 963.

[18]   Z.-M. Huang, Y.-Z. Zhang, M. Kotaki, S. Ramakrishna, *Compos. Sci. Technol.* **2003**, *63*, 2223.

[19]   W. F. Gorham, *J. Polym. Sci., Part A: Polym. Chem.* **1966**, *4*, 3027.

[20]   P. Simon, S. Mang, A. Hasenhindl, W. Gronski, A. Greiner, *Macromolecules* **1998**, *31*, 8775.

[21]   A. Greiner, S. Mang, V. Schäfer, P. Simon, *Acta Polym.* **1997**, *48*, 1.

[22]   H. Hopf, *Angew. Chem. Int. Ed.* **2008**, *47*, 9808.

[23]   J. Lahann, D. Klee, H. Höcker, *Materialwiss. Wirkstofftech.* **1999**, *30*, 763.

[24]   A. Greiner, J. H. Wendorff, A. L. Yarin, E. Zussmann, *Appl. Microbiol. Biotechnol.* **2006**, *71*, 387.

[25]   N. Miyaura, A. Suzuki, *Chem. Rev.* **1995**, *95*, 2457.

[26]   M. Mendal, C. W. Tornøe, *Chem. Rev.* **2008**, *108*, 2952.

5.8 Supporting Information

General Information

All reactions involving air- or moisture-sensitive reagents or intermediates were carried out in dried glassware under argon atmosphere and were carried out using standard Schlenk techniques. All solvents for extraction and flash chromatography were distilled before use. All other solvents and reagents were used as received from the corresponding suppliers. Amino-terminated PAMAM G5 dendrimers with an ethylenediamine core were ordered from Sigma Aldrich as 5 wt% MeOH solution.

TLC was carried out on Merck silica gel $60\,F_{254}$ plates, detection by UV, iodine vapor, or dipping into a solution of $NaHCO_3$ (5.0 g), $KMnO_4$ (1.5 g) and H_2O (0.20 L) follow by heating. Flash chromatography was carried out using Merck or Fluka silica gel 60 (40–63 µm) with an argon pressure of about 1.1–1.5 bar. Centrifugation was carried out on a Heraeus microprocessor controlled laboratory centrifuge Labofuge 200. ^{1}H-, ^{13}C- and ^{31}P-NMR spectra were recorded on a Bruker DPX 300 or a Bruker Varian 200 spectrometer. Chemical shifts δ in ppm are referenced to the TMS signal at 0 ppm as an internal standard. IR spectra were recorded on a Varian 3100 FT-IR equipped with a MKII Golden Gate Single Reflection ATR unit. ESI-MS and HRMS were performed using a Bruker MicroTof, MALDI spectra were recorded with an Autoflex Speed TOF-MS (Bruker Daltonics) in linear mode. GC analyses were carried out on a Hewlett Packard HP 6890 Series GC System equipped with an HP 5 column (30 m × 0.32 mm, film thickness 0.25 µm) using hydrogen as carrier gas. For the CVD process, [2.2]paracyclophane (Specialty Coating Systems, Parylene N) was used. The poly(urethane) template polymer was commercially available Desmopan® DP 9370AU (Bayer).

Scanning Electron Microscopy

Scanning electron micrographs were recorded using a JSM-7500F (JEOL). For the selected samples, the preset *Plastics (with coating)* was used. The acceleration voltage was set to 2 kV. The column mode was SEM (r-Filter SM), and the probe current was set to LC 7. In order to control the SEM, the software PC-SEM (JEOL, version 2.0.0.8) was used. To determine the average nanofiber diameter of a sample, 100 fibers were measured using ImageJ (National Institute of Health, USA, version 1.44c).

Inductively Coupled Plasma Mass Spectrometry

In order to quantify the amounts of leached palladium and copper, respectively, the corresponding solutions were analyzed using ICP-MS (Dipl.-Chem. David Nette, research group Prof. Andreas Seubert, Philipps-Universität Marburg). The samples were nebulized using a PFA Micro Flow and a Scott-type spray chamber. The used spectrometer was a 7500ce (Agilent, no-gas mode). The device was calibrated prior

to the measurements using an ICP palladium standard solution and, respectively, an ICP multi-element standard solution (Merck, $1000\,\mathrm{mg\,L^{-1}}$). Hence, a dilution series of both standards was prepared using aqueous nitric acid (0.7 % in ultra-pure water). The calibration range was 1–$100\,\mathrm{\mu g\,L^{-1}}$ of the corresponding metals. The internal standard was yttrium (Bernd Kraft GmbH, $1000\,\mathrm{\mu g\,L^{-1}}$). An amount of $10\,\mathrm{\mu g\,L^{-1}}$ of yttrium was added to each sample.

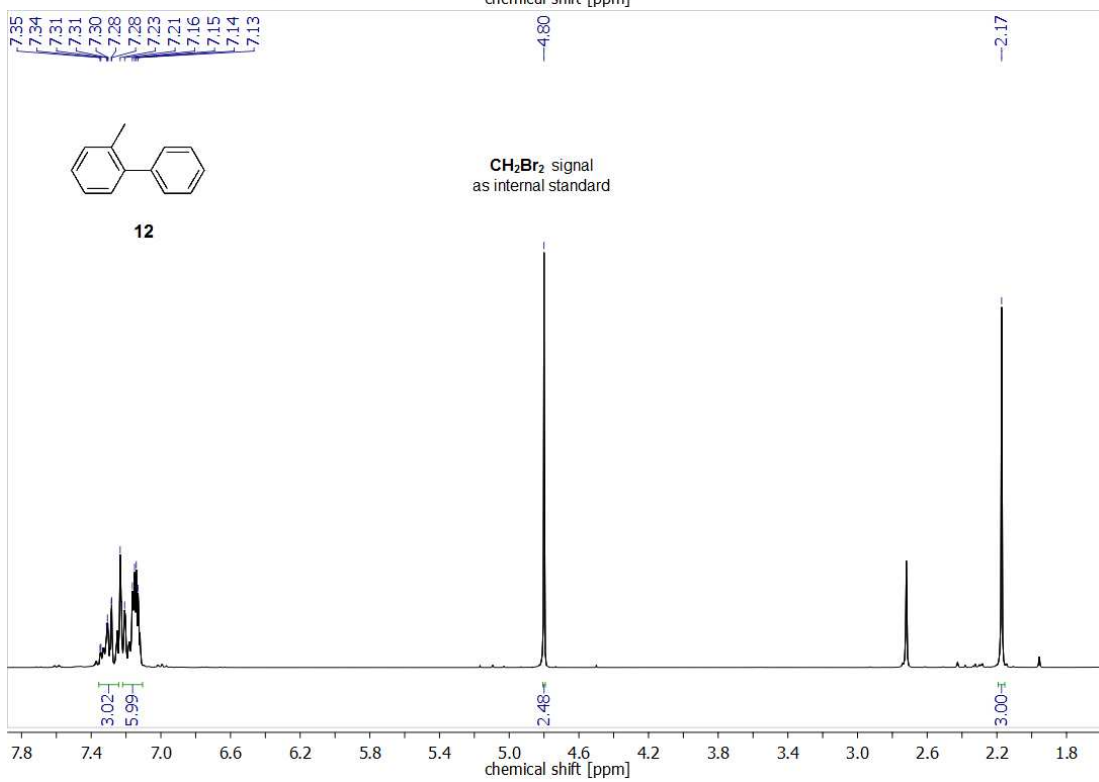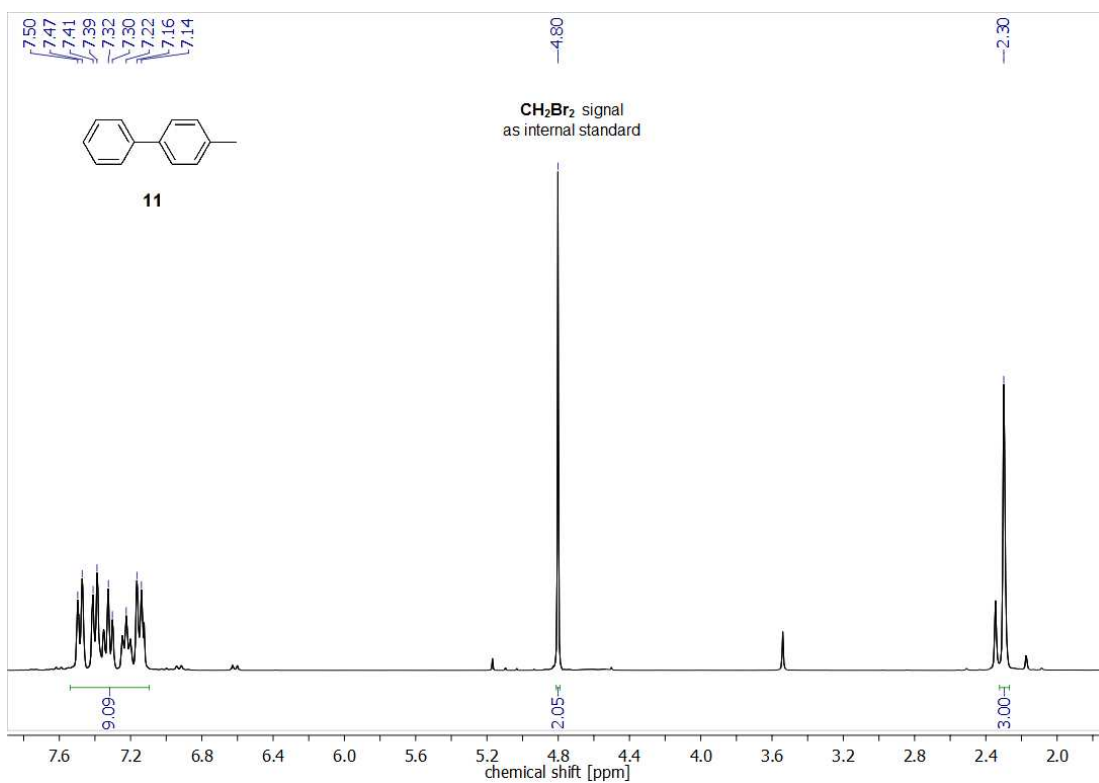**Extractions and Catalytic Reactions**

For the extraction of the inner template PU fibers of the prepared core-shell systems and for the catalytic reactions, the custom made sample mount shown in Figure 5.8 was used. The tube material was moistened with the corresponding solvent, carefully folded under argon and placed inside the perforated Teflon chamber. The glass parts were borosilicate glass. A slim magnetic stir bar was used to vigorously stir the solvent and reactants, respectively. After the extraction cycles or reactions, the material was transferred onto a filter paper and subsequently dried under a continuous argon flow, until most of the solvent was evaporated. Further, the tube material was dried under reduced pressure. Generally, the samples were stored under argon atmosphere to prevent oxidation.
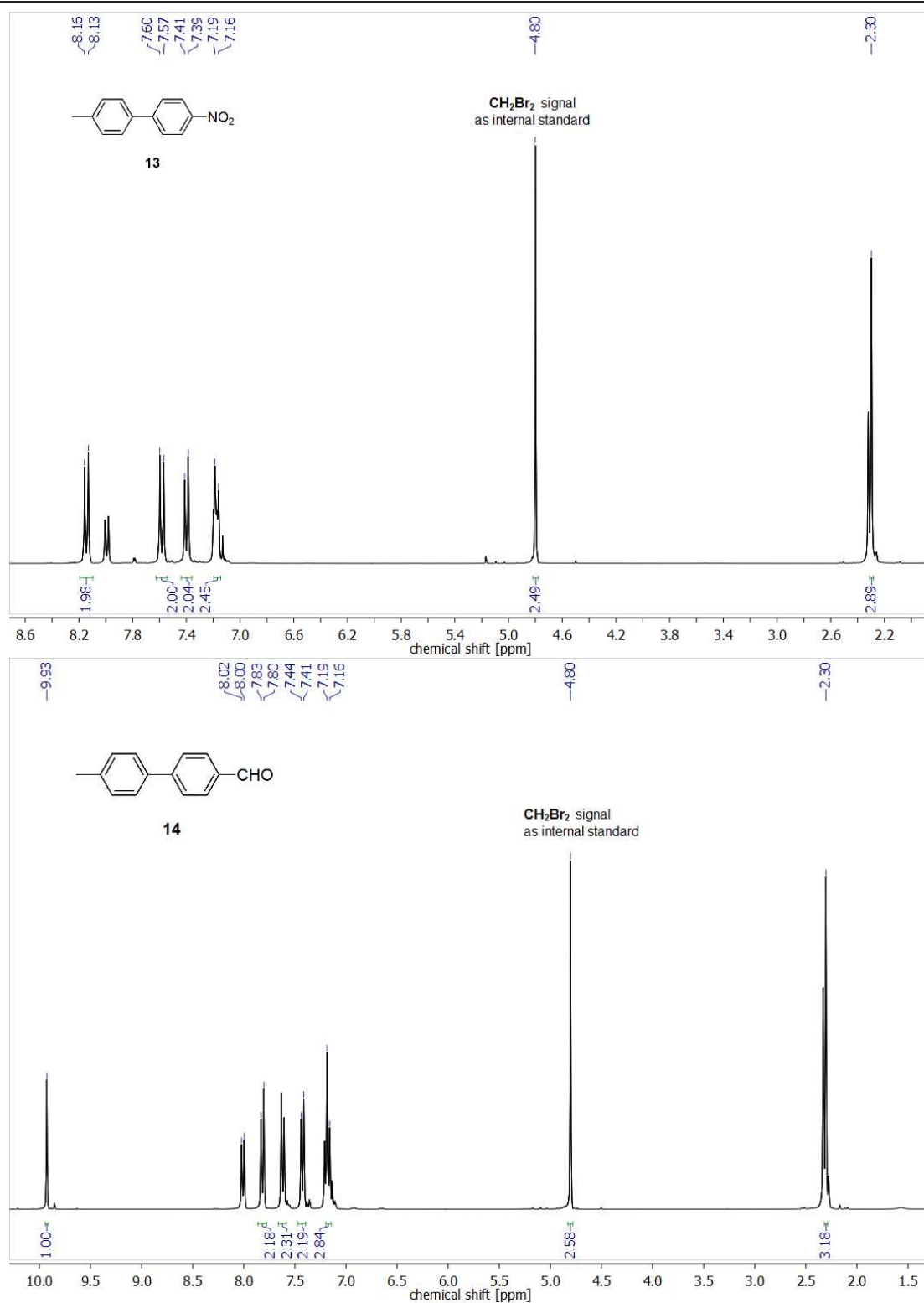
Figure 5.8. The tube material (white square, ca. 7×7 cm) was folded and placed inside the white Teflon chamber of the custom made sample mount (right).

Estimation of Catalytic Reactions' Yields based on NMR Spectra
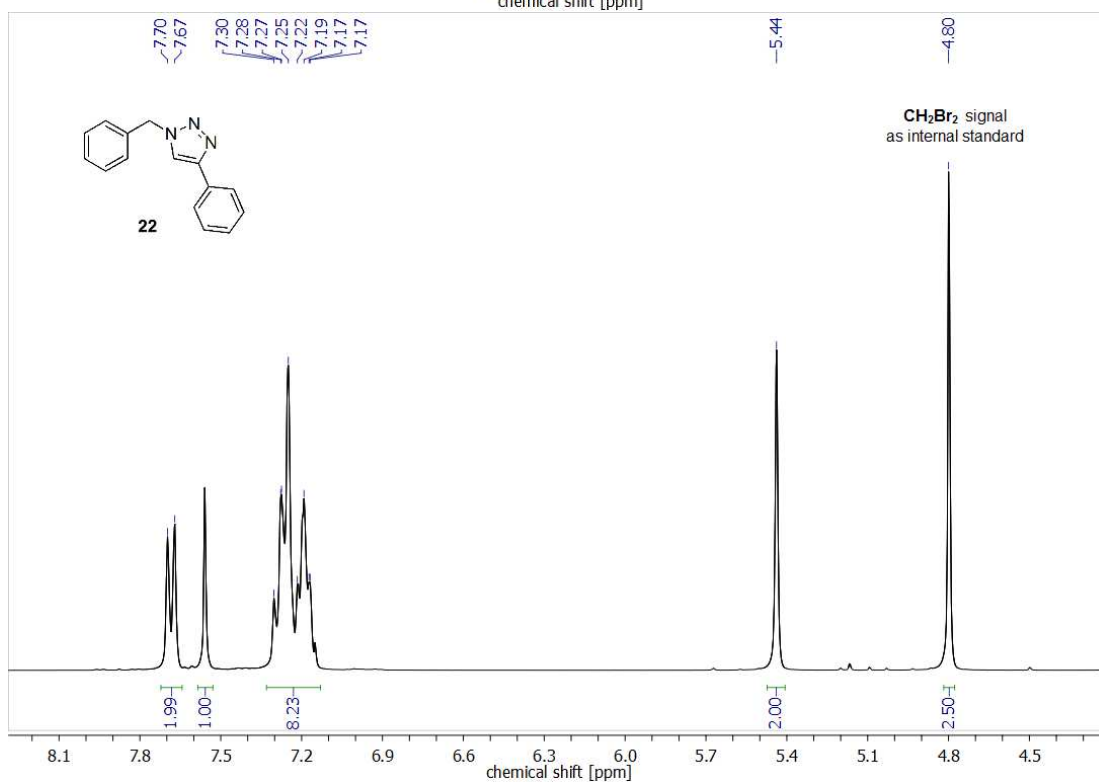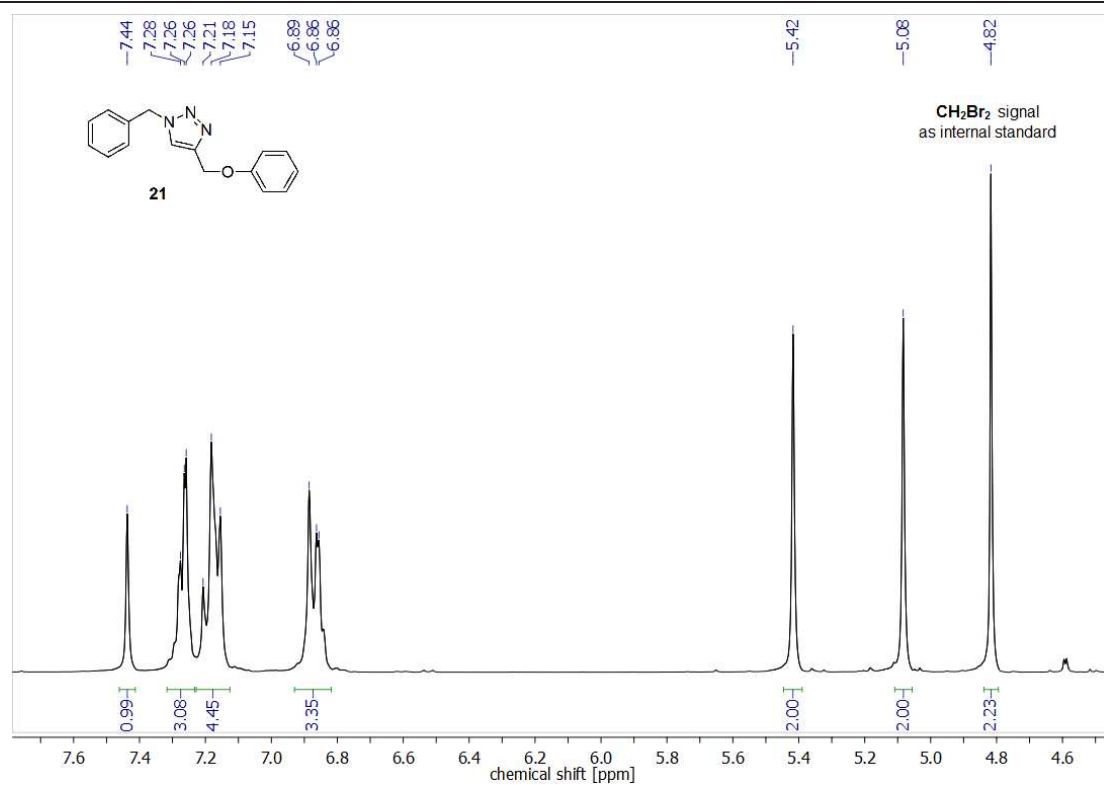
6 Tea Bag-Like Polymer Nanoreactors Filled with Gold Nanoparticles

Fabian Mitschang, Holger Schmalz, Seema Agarwal, Andreas Greiner

Makromolekulare Chemie II, Universität Bayreuth, Universitätsstraße 30, 95440 Bayreuth, Germany.

*Corresponding Author: E-mail: greiner@uni-bayreuth.de; Fax: +49-921-553393.

6.1 Abstract

Gold-containing polymer nanotubes, which showed both catalytic activity and resistance to leaching, were prepared by the tubes by fiber templates (TUFT) process. For this purpose, electrospun polymer nonwovens with incorporated poly(L-lactide)-stabilized gold nanoparticles were coated with poly(p-xylylene) by the chemical vapor deposition process, and then the inner fiber templates were removed. The resulting polymer tubes carried encapsulated gold nanoparticles which were shown to be immobilized and featured pronounced catalytic activity towards the hydrolytic oxidation of dimethylphenylsilane and the alcoholysis of dimethylphenylsilane with n-butanol. The macroscopic nonwovens could be used as tea bag-like catalyst systems and showed excellent reusability.

6.2 Introduction

Gold nanoparticles and -wires are of great interest in the nanosciences due to their potential in microsensorics, microelectronics, catalysis, and biomedical applications.[1,2] However, since nanomaterials tend to agglomerate in order to minimize their surface energy,[3] a variety of methods for stabilization have been established, such as steric and electrostatic stabilization.[4] Polymer-stabilized gold nanoparticles allow for their incorporation in polymer matrices as well as the preparation of homogeneous dispersions.[5] In many cases, the nanomaterials must be immobilized onto carriers. There is a demand for tea bag-like catalyst systems for multiple batch production cycles as well as for reactive filter systems for continuous production.[6,7] Suitable catalyst supports could be either porous materials like membranes and zeolites or fabrics with thin fiber diameters and hence a high surface area.[8] Further, fully encapsulated catalysts can display selectivity and prevent potential incompatibilities.[9]

A promising hybrid system that also sets a great challenge for synthesis consists of continuous polymer nanotubes with encapsulated nanoparticles. Most of the research on the interactions between nanoparticles and nanotubes, as well as on the incorporation of nanoparticles into nanotubes, is based on single- and multiwalled carbon nanotubes.[10] In addition, there are corresponding studies on inorganic nanotubes, such as titanium dioxide tubes,[11] and on polymer nanotubes, where the length of the tubes is highly restricted.[12] Noble-metal nanoparticles have been encapsulated by the use of electrospun polymer fibers doped with precursor salts following the concept of the tubes by fiber templates (TUFT) process.[13]

Herein, we report the preparation of highly efficient heterogeneous tea bag-like gold-nanoparticle-based catalysts by the TUFT process. We studied in detail the preparation of well-dispersed gold nanoparticles, their immobilization in poly(L-lactide) (PLLA) composite fibers, their coating with poly(*p*-xylylene) (PPX) by chemical vapor deposition (CVD), and the subsequent quantitative removal of PLLA by pyrolysis. The leaching of gold nanoparticles from the resulting PPX tubes was studied as well as their catalytic activity.

6.3 Results and Discussion

Figure 6.1 illustrates the underlying concept based on the TUFT process.[14] First, a dispersion of poly(L-lactide)-stabilized gold nanoparticles (PLLA@Au) and the template matrix polymer PLLA were electrospun using a high voltage potential difference.[15] It is important to emphasize that electrospinning polymers like PLLA generally results in macroscopic nonwovens which makes them particularly useful in handling as tea bag-like catalysts. After the resulting composite nanofibers had
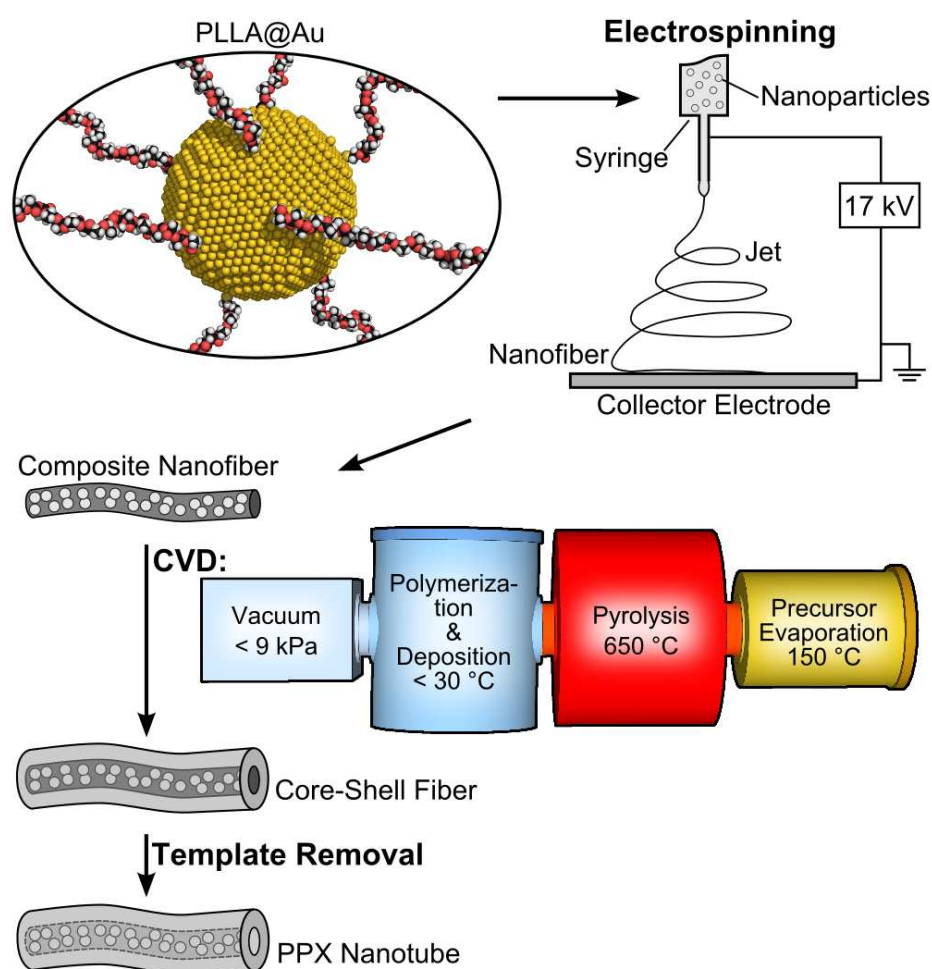

Figure 6.1. Electrospun composite nanofibers with incorporated PLLA-stabilized gold nanoparticles were coated with poly(*p*-xylylene) using the chemical vapor deposition process. Subsequently, the inner PLLA template material was removed by thermal degradation resulting in gold-containing PPX tubes.

been coated with PPX by CVD,[16] the inner PLLA template material was removed quantitatively by thermal degradation,[17] resulting in PPX tubes with encapsulated gold nanoparticles.

The availability of well-dispersed gold nanoparticles is crucial for the preparation of composite nanofibers by electrospinning. Therefore, PLLA-stabilized gold nanoparticles (PLLA@Au) were prepared based on PLLA featuring a thiol end-group (PLLA-SH) (Figure 6.2a). The corresponding PLLA-SH precursor was synthesized in analogy to poly(DL-lactide) with a thiol end-group[18] but under modified conditions. The bulk polymerization was carried out for 5 days at 130 °C using an aluminum catalyst and a protected thiol as the initiator. As determined by NMR spectroscopy, the molecular weight of the prepared PLLA-SH was about $2400 \, \text{g mol}^{-1}$. Gel permeation chromatography (GPC, poly(methyl methacrylate) calibration) showed a dispersity $Đ_M$ of 1.25. Subsequent reduction of chloroauric acid using lithium triethylborohydride[19] in the presence of PLLA-SH yielded in PLLA@Au. The nanoparticles were isolated as a deep purple solid and showed an excellent redispersibility as well as a pronounced stability in organic solvents such as dichloromethane, trichloromethane, and tetrahydrofuran. Thermogravimetric analysis (TGA) indicated a gold content about 20 wt%, whereas elemental analysis by atomic absorption spectroscopy indicated 18 wt% gold. The corresponding transmission electron microscopy (TEM) images as well as the results of the characterization by GPC coupled with a diode array detector[20] are shown in Figure 6.2.

The spherical gold nanoparticles had an average diameter of $(9.5 \pm 2.8) \, \text{nm}$ as determined by TEM image analysis. The corresponding spacing of the lattice planes was 0.24 nm, which matched the (111) planes of face-centered cubic gold.[2,21] Using GPC coupled with a diode array detector, it was found that poly(L-lactide) was indeed attached to the gold nanoparticles, due to the combined characteristic absorption of nanoparticulate gold (see below) and PLLA (325 nm) at 25.3 min. Moreover, free PLLA-SH, which was eluted at 32 min, presumably arose either because of exchange reactions (the sample was measured in dimethylformamide in the presence of lithium bromide) or due to incomplete grafting of the polymer onto the gold surface. Further, both the X-ray powder diffraction pattern and the UV/Vis spectrum of PLLA@Au confirmed the presence of nanometer-scale particles

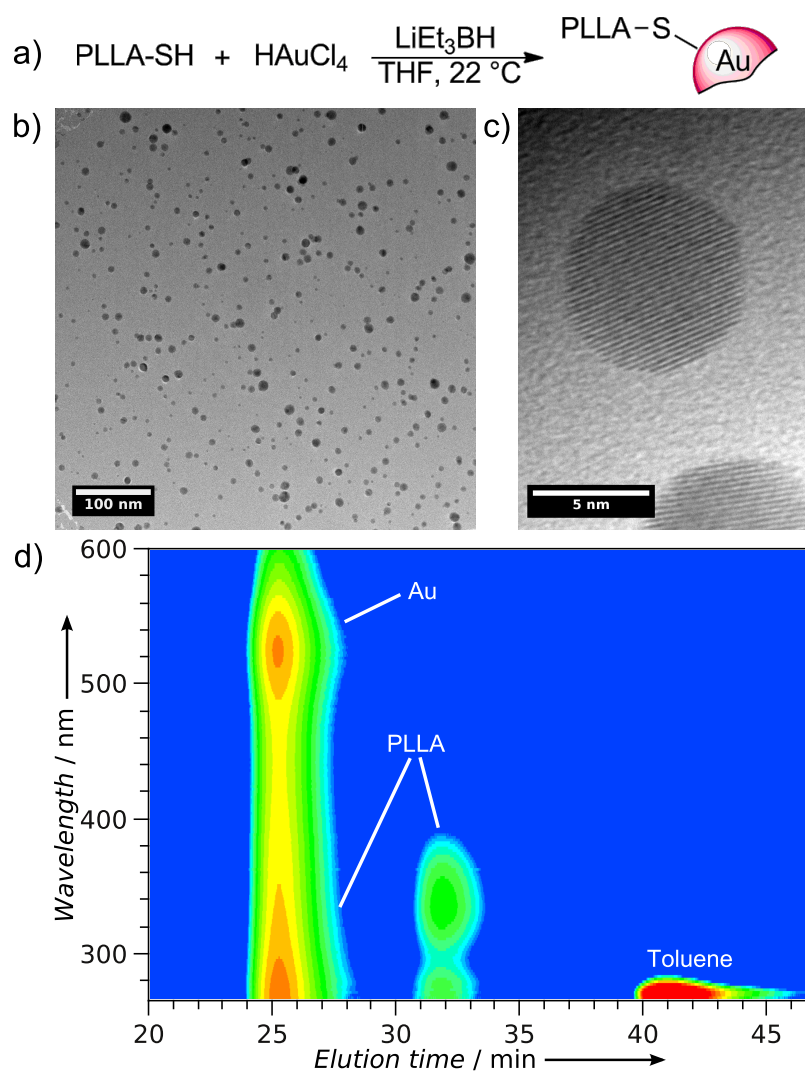**Figure 6.2.** Synthesis and characterization of PLLA@Au. a) In situ preparation of the nanoparticles based on PLLA-SH. b) TEM image showing homogeneously dispersed particles. c) High-resolution TEM image revealing the characteristic lattice planes of gold particles. d) Measurement conducted with a GPC coupled with a diode array detector proving the connection between PLLA and the gold particles.

(Supporting Information, Figure 6.4 and Figure 6.5). Aside from the characteristic pattern of the semicrystalline PLLA,[22] the corresponding reflections of the gold particles showed distinct line broadening.[23] In addition, the UV/Vis spectrum showed the characteristic plasmon resonance absorption of nanoparticulate gold at 522 nm.[24]

Composite nanofibers were electrospun from a dispersion of 10 wt% PLLA@Au, 0.5 wt% PLLA, and 0.25 wt% of the salt tetraoctylammonium bromide (TOAB), which is soluble in organic solvent. The free polymer was necessary to improve the mechanical properties of the fibers, whereas the salt suppressed the formation of beads.[25] Scanning electron microscopy (SEM) revealed an average fiber diameter of (322 ± 72) nm (Figure 6.3a). Further, the composite fibers were free of beads and consisted of 19 wt% gold, as determined by TGA. According to the TEM picture in Figure 6.3b, the gold nanoparticles were homogeneously distributed throughout the PLLA matrix.

After the composite fibers had been coated with PPX, the resulting fibers had an average diameter of (711 ± 46) nm (Figure 6.3c). These core-shell fibers were annealed under reduced pressure at 280 °C, in order to remove the template PLLA material, which resulted in PPX tubes with an average diameter of (730 ± 83) nm. IR spectroscopy confirmed the quantitative removal of the PLLA (Supporting Information, Figure 6.6). The tubular structure was clearly proven by SEM (Figure 6.3d). Further, TEM analysis also confirmed the tubular structure and indicated the presence of gold nanoparticles inside the PPX tubes (Figure 6.3e). Subsequent TGA measurements confirmed a gold content of 9 wt%. The encapsulated particles were found to be immobilized when in contact with organic solvents, such as di- or trichloromethane (see the Supporting Information for UV/Vis spectra, Figure 6.7). Due to the absence of leaching, these gold nanoparticle PPX tubes should be suitable for various applications, for example as novel reusable tea bag-like catalyst systems.

To study the applicability of this tea bag-like catalyst, the alcoholysis of dimethylphenylsilane with *n*-butanol,[26] as well as the well-studied hydrolytic oxidation of dimethylphenylsilane,[27] were used as model reactions (Scheme 6.1). Even at room temperature the catalyst system showed high catalytic activity, which also
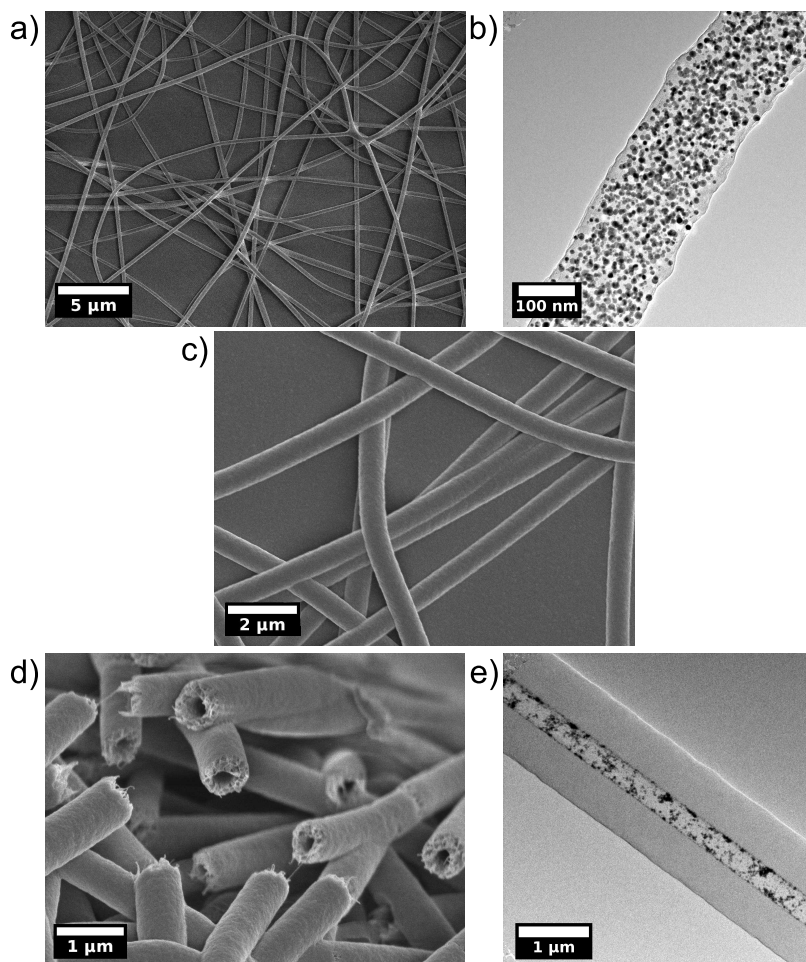
Figure 6.3. Electron micrographs before, during, and after the TUFT process: a) SEM image of electrospun composite nanofibers and b) TEM image of the fibers. c) SEM image of the PPX-coated composite fibers. d) SEM image of the gold-containing PPX tubes after template removal and subsequent freeze-fracturing. e) TEM image of the PPX tubes.
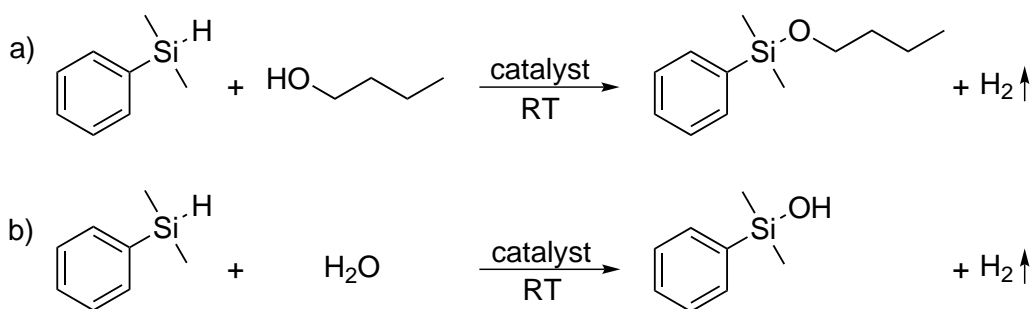
Scheme 6.1. Model reactions for the non-immobilized PLLA@Au nanoparticles as well as for the gold-containing PPX nanoreactors. a) Alcoholysis of dimethylphenylsilane with *n*-butanol. b) Hydrolytic oxidation of dimethylphenylsilane.

proved the reactants' ready access to the inside of the PPX nanotubes. The gold-catalyzed alcoholysis of dimethylphenylsilane (Scheme 6.1a, 6.6 mol% gold with respect to the silane) yielded the adduct butoxydimethylphenylsilane in quantitative yield after 26 h, whereas the reaction catalyzed by non-immobilized PLLA@Au nanoparticles required 5 h for quantitative conversion. At 100 °C, the same reaction (based on 0.05 mol% immobilized gold) required 5 h for complete conversion of the silane. In comparison, for non-encapsulated gold nanoparticles on an aluminum oxide support (3–5 nm mean diameter, 0.05 mol% gold with respect to the silane), quantitative conversion required only 3 h (at 100 °C).[26] However, the cited catalyst system was only used at 100 °C, whereas the prepared PPX tubes were also suitable for catalysis at room temperature, as mentioned above. Further, we speculate that the semipermeable PPX tubes[7] can be used for selective catalysis. Since the gold nanoparticles are fully encapsulated rather than surface-immobilized, a second catalyst could be attached to the shell of the PPX tubes[28] allowing for site-isolated tandem catalysis.[29]

Using the PPX-encapsulated gold catalyst system, we observed excellent catalytic activity for the hydrolytic oxidation of dimethylphenylsilane (Scheme 6.1b). At room temperature, the corresponding adduct, dimethylphenylsilanol, was formed in quantitative yield after 3.5 h (0.87 mol% gold with respect to the silane), whereas at 80 °C the same reaction (with 0.83 mol% gold) required 1.5 h for complete conversion. In comparison, alternative gold-based catalyst systems, such as nanograined metallic glass[30] and hydroxyapatite-supported gold nanoparticles,[31] required 24 h for 93 % conversion (RT, 0.87 mol% nanograined gold with respect to the silane) and 3 h at 80 °C for quantitative conversion (2 nm mean particle diameter, 0.83 mol% nanoparticulate gold with respect to the silane), respectively. In both cases, neither disiloxanes nor other by-products could be found, and in the absence of gold nanoparticles, no product was formed. Upon removal of the tea bag-like catalyst during the reaction, product formation stopped immediately, confirming that the catalyst does not leach. When the removed catalyst was then added to the reaction mixture, conversion recommenced until quantitative conversion was achieved. Further, in order to study the reusability of the catalyst system, the silane alcoholysis was repeated 18 times using the same sample of PPX-encapsulated gold nanopar-

ticles. Even after 18 cycles, the reaction time required for complete conversion did not increase. Moreover, the weight of the PPX catalyst system remained constant, hence the nanoparticle-based PPX nanoreactors demonstrated excellent reusability.

6.4 Conclusion

In conclusion, PLLA-SH was synthesized and subsequently used for the stabilization of gold nanoparticles. Electrospun gold-containing nanofibers were coated with PPX using the CVD process, and the template PLLA material was then removed quantitatively. The resulting PPX tubes were obtained as macroscopic nonwovens and successfully immobilized the encapsulated gold nanoparticles. Despite the insoluble PPX shell, the inside of the gold-loaded tubes was shown to be accessible to the reactants and was used for both the catalytic hydrolytic oxidation of dimethylphenylsilane and for the corresponding silane alcoholysis with *n*-butanol. The tea bag-like catalyst system featured solid performance in the alcoholysis and excellent catalytic activity with regard to the hydrolytic oxidation even at room temperature. No disiloxanes were formed, and no catalyst leaching occurred. The catalyst system was reused 18 times with no decrease in activity. Since PPX membranes have been shown to be size selective,[7] these novel catalyst-confining systems obtained by the highly flexible TUFT process have huge potential for the preparation of other catalysts based on nanoparticles, bacteria, enzymes, and dendrimers. The combination of different catalysts in one system and the potential for substrate selectivity are as yet unexplored and are topics of current research.

6.5 Acknowledgments

6.6 References

[1] a) N. A. Kotov, J. O. Winter, I. P. Clements, E. Jan, B. P. Timko, S. Campidelli, S. Pathak, A. Mazzatenta, C. M. Lieber, M. Prato, R. V. Bellamkonda, G. A. Silva, N. W. S. Kam, F. Patolsky, L. Ballerini, *Adv. Mater.* **2009**, *21*, 3970; b) D. T. Thompson, *Nano Today* **2007**, *2*, 40.

[2]   G.-M. Kim, A. Wutzler, H.-J. Radusch, G. H. Michler, P. Simon, R. A. Sperling, W. J. Parak, *Chem. Mater.* **2005**, *17*, 4949.

[3]   W. Caseri, *Macromol. Rapid Commun.* **2000**, *21*, 705.

[4]   a) C. Lourenco, M. Teixeira, S. Simões, R. Gaspar, *Int. J. Pharm.* **1996**, *138*, 1; b) J. Hang, L. Shi, X. Feng, L. Xiao, *Powder Technol.* **2009**, *192*, 166.

[5]   a) M. K. Corbierre, N. S. Cameron, M. Sutton, S. G. J. Mochrie, L. B. Lurio, A. Rühm, R. B. Lennox, *J. Am. Chem. Soc.* **2001**, *123*, 10411; b) D.-H. Han, C.-Y. Pan, *J. Polym. Sci., Part A: Polym. Chem.* **2008**, *46*, 341.

[6]   a) M. Gaab, S. Bellemin-Laponnaz, L. Gade, *Chem. Eur. J.* **2009**, *15*, 5450; b) M. Stratakis, H. Garcia, *Chem. Rev.* **2012**, *112*, 4469.

[7]   a) M. Stasiak, A. Studer, A. Greiner, J. H. Wendorff, *Chem. Eur. J.* **2007**, *13*, 6150; b) J.-P. Lindner, C. Röben, A. Studer, M. Stasiak, R. Ronge, A. Greiner, J. H. Wendorff, *Angew. Chem. Int. Ed.* **2009**, *48*, 8874.

[8]   a) Z. Xie, Z. Liu, Y. Wang, Q. Yang, L. Xu, W. Ding, *Int. J. Mol. Sci.* **2010**, *11*, 2152; b) A.-H. Lu, F. Schüth, *Adv. Mater.* **2006**, *18*, 1793; c) M. Graeser, E. Pippel, A. Greiner, J. H. Wendorff, *Macromolecules* **2007**, *40*, 6032.

[9]   a) S. H. Joo, J. Y. Park, C.-K. Tsung, Y. Yamada, P. Yang, G. A. Somorjai, *Nat. Mater.* **2009**, *8*, 126; b) S. Ikeda, Y. Ikoma, H. Kobayashi, T. Harada, T. Torimoto, B. Ohtani, M. Matsumura, *Chem. Commun.* **2007**, *36*, 3753.

[10] a) A. La Torre, G. A. Rance, J. El Harfi, J. Li, D. J. Irvine, P. D. Brown, A. N. Khlobystov, *Nanoscale* **2010**, *2*, 1006; b) Y.-J. Gu, W.-T. Wong, *J. Nanosci. Nanotechnol.* **2009**, *9*, 2066.

[11] K. Shin, Y. Jun, G. Y. Han, J. H. Park, *J. Nanosci. Nanotechnol.* **2009**, *9*, 7436.

[12] H. Kong, J. Song, J. Jang, *Macromol. Rapid Commun.* **2009**, *30*, 1350.

[13] Z. Sun, J. Zeng, H. Hou, H. Wickel, J. H. Wendorff, A. Greiner, *Progr. Colloid Polym. Sci.* **2005**, *130*, 15.

[14] a) M. Bognitzki, H. Hou, M. Isahaque, T. Frese, M. Hellwig, C. Schwarte, A. Schaper, J. H. Wendorff, A. Greiner, *Adv. Mater.* **2000**, *12*, 637; b) H. Hou, Z. Jun, A. Reuning, A. Schaper, J. H. Wendorff, A. Greiner, *Macromolecules* **2002**, *35*, 2429.

[15] a) X. Zong, K. Kim, D. Fang, S. Ran, B. S. Hsiao, B. Chu, *Polymer* **2002**, *43*, 4403; b) E.-R. Kenawy, G. L. Bowlin, K. Mansfield, J. Layman, D. G. Simpson, E. H. Sanders, G.W. Wnek, *J. Control. Release* **2002**, *81*, 57; c) J. Zeng, H. Hou, A. Schaper, J. H. Wendorff, A. Greiner, *e-Polymers* **2003**, *3*, 102.

[16] A. Greiner, S. Mang, O. Schäfer, P. Simon, *Acta Polym.* **1997**, *48*, 1.

[17] H. Abe, N. Takahashi, K. J. Kim, M. Mochizuki, Y. Doi, *Biomacromolecules* **2004**, *5*, 1606.

[18] S. Aryal, K. C. R. Bahadur, N. Bhattarai, B. M. Lee, H. Y. Kim, *Chem. Phys.* **2006**, *98*, 463.

[19] C. K. Yee, R. Jordan, A. Ulman, H. White, A. King, M. Rafailovich, J. Sokolov, *Langmuir* **1999**, *15*, 3486.

[20] S. Bokern, J. Getze, S. Agarwal, A. Greiner, *Polymer* **2011**, *52*, 912.

[21] R. P. Andres, J. D. Bielefeld, J. Henderson, D. B. Janes, V. R. Kolagunta, C. P. Kubiak, W. J. Mahoney, R. G. Osifchin, *Science* **1996**, *273*, 1690.

[22] N. Ogata, S. Yamaguchi, N. Shimada, G. Lu, T. Iwata, K. Nakane, T. Ogihara, *J. Appl. Polym. Sci.* **2007**, *104*, 1640.

[23] a) P. Jiang, S. Xie, J. Yao, S. Pang, H. Gao, *J. Phys. D: Appl. Phys.* **2001**, *34*, 2255; b) J. I. Langford, A. J. C. Wilson, *J. Appl. Crystallogr.* **1978**, *11*, 102.

[24] G. A. Rance, D. H. Marsh, A. N. Khlobystov, *Chem. Phys. Lett.* **2008**, *460*, 230.

[25] X. Zong, K. Kim, D. Fang, S. Ran, B. S. Hsiao, B. Chu, *Polymer* **2002**, *43*, 4403.

[26] P. Raffa, C. Evangelisti, G. Vitulli, P. Salvadori, *Tetrahedron Lett.* **2008**, *49*, 3221.

[27] T. Y. Lee, L. Dang, Z. Zhou, C. H. Yeung, Z. Lin, C. P. Lau, *Eur. J. Inorg. Chem.* **2010**, *36*, 5675.

[28] J. A. M. Hepperle, F. Mitschang, A. K. Bier, B. K. Dettlaff, A. Greiner, A. Studer, *RSC Adv.* **2013**, *3*, 25976.

[29] S. L. Poe, M. Kobašlija, D. T. McQuade, *J. Am. Chem. Soc.* **2006**, *128*, 15586.

[30] N. Chen, R. Frank, N. Asao, D. V. Louzguine-Luzgin, P. Sharma, J. Q. Wang, G. Q. Xie, Y. Ishikawa, N. Hatakeyama, Y. C. Lin, M. Esashi, Y. Yamamoto, A. Inoue, *Acta Mater.* **2011**, *59*, 6433.

[31] T. Mitsudome, A. Noujima, T. Mizugaki, K. Jitsukawa, K. Kaneda, *Chem. Commun.* **2009**, *35*, 5302.

6.7 Supporting Information

Materials

Aluminum isopropoxide: Merck, for synthesis. Argon: Air Liquide, 99.999 %. Chloro-auric acid: Sigma-Aldrich, p.a., $\geq 49\,\%$ Au basis. Dichloromethane: BASF, purified by distillation. Dimethylphenylsilane: Aldrich, $\geq 98\,\%$. Dimethyl sulfoxide-d6: Deutero. 1-Fluoro-2,4-dinitrobenzene: Acros Organics, 98 %. (*S,S*)-Lactide: Aldrich, 98 %. Lithium triethylborohydride: Aldrich, $1\,\text{mol}\,\text{L}^{-1}$ in tetrahydrofuran. 2-Mercapto-ethanol: Acros Organics, 99 %. Methanol: BASF, purified by distillation. [2.2]Pa-racyclophane: Specialty Coating Systems, Parylene N. Poly(L-lactide): Boehringer Ingelheim, Resomer® L210S. Tetrahydrofuran: BASF, dried over Solvona® (Dr. Bilger Umweltconsulting GmbH), purified by distillation. Tetraoctylammonium bromide: Fluka. Toluene: BASF, dried over calcium hydride (ABCR, 92 %), purified by distillation. Trichloromethane: BASF, purified by distillation. Trichloromethane-d: Roth. Triethylamine: BASF, purified by distillation.

Methods

Differential Scanning Calorimetry: A DSC 821^e (Mettler Toledo) was used in combination with 40 µL aluminum crucibles (Mettler Toledo) under nitrogen atmosphere. Calibration was conducted using indium, *n*-octane and zinc standards. The amount of each sample was between 9 mg and 12 mg and the scanning rate was 10 K min^{-1}. The glass transition temperature T_g, the crystallization temperature T_c, and the melting temperature T_m were determined using the software Star^e (Mettler Toledo, version 9.20). For T_c and T_m the peak maximum was used.

Elemental Analysis: The amount of both S and Au was determined by the analytical service facility (Department of Chemistry, Philipps-University Marburg). Whereas Au was analyzed by atomic absorption spectroscopy, S was determined by photometric titration.

Fourier Transform Infrared Spectroscopy: Spectra were recorded using a FTIR spectrometer (Digilab, Excalibur Series) with an attenuated total reflectance (ATR) unit (Pike Technologies, MIRacle). Software: WinIRPro (Digilab, version 3.3.1).

Gas Chromatography: A gas chromatograph GC-2010Plus (Shimadzu) equipped with a 30 m capillary column (0.25 mm inner diameter, 0.25 µm film thickness) was used in combination with a flame ionization detector (255 °C). Nitrogen was used as a carrier gas (1 mL min^{-1}), whereas a combination of both synthetic air and hydrogen was used for the combustion. The injector temperature was 250 °C. The reaction mixtures were dissolved in acetone (2 µL mL^{-1}) and 1 µL was measured from 50 °C (1 min) up to 250 °C with a heating rate of 10 K min^{-1}. Software: LabSolutions (Shimadzu, version 5.54 SP2).

Gas Chromatography-Mass Spectrometry: A gas chromatograph 7890B (Agilent Technologies) equipped with a 30 m capillary column (0.25 mm inner diameter, 0.25 µm film thickness) was used in combination with a mass spectrometer 5977A (Agilent Technologies, electron ionization detector). Helium was used as a carrier gas (1 mL min^{-1}). The injector temperature was 250 °C. The reaction mix-

tures were dissolved in acetone ($2\,\mu L\,mL^{-1}$) and $1\,\mu L$ was measured from $50\,°C$ ($2\,min$) up to $200\,°C$ with a heating rate of $10\,K\,min^{-1}$. Software: Maestro 1 GC-MSD/EnhancedMassHunter (Gerstel, version 1.4.23.11).

Gel Permeation Chromatography: GPC measurements were carried out at $30\,°C$ with 1 drop of toluene as internal standard. Polymers were characterized using trichloromethane (Fischer Scientific, HPLC grade) as the eluent ($1\,g\,L^{-1}$), 3 SDV columns (Polymer Standards Service, LinearXL $20\,\mu$), a Smartline 1000 (Knauer, $10\,mL$ pump head) pump (flow rate $1.0\,mL\,min^{-1}$) and a refractive index detector (Knauer, RI 2300). Software: WinGPC Unity (Polymer Standards Service, Build 5403). Calibration: Poly(methyl methacrylate) standards (Polymer Standards Service). The nanoparticles were characterized using the eluent dimethylformamide ($1.0\,g\,L^{-1}$, flow rate $1.0\,mL\,min^{-1}$) coupled with a diode array detector (HP, 1040A HPLC Detection System, 260–600 nm, 1 spectrum each 3 seconds). 3 SDV columns (Polymer Standards Service, 10E4, 10E6 and 1000) were used, calibrated with polystyrene standards. Software: WinGPC Unity (Polymer Standards Service, Build 6807).

Nuclear Magnetic Resonance Spectroscopy: Both ^{1}H NMR ($300\,MHz$) and ^{13}C NMR ($75\,MHz$) spectra were recorded on a Bruker Avance 300 UltraShield™ spectrometer at room temperature in deuterated trichloromethane (50–$60\,g\,L^{-1}$) using Icon-NMR (Bruker BioSpin, version 4.1.b.6, build 1). In order to evaluate the spectra, TopSpin (Bruker BioSpin, version 3.0.b.7) was used. Calibration was performed using the trichloromethane signal at $7.26\,ppm$ (^{1}H NMR) and $77.0\,ppm$ (^{13}C NMR), respectively.

Scanning Electron Microscopy: Micrographs were recorded on a JSM-7500F (JEOL) using the software PC-SEM (JEOL, version 2.0.0.8) and the preset *Plastics (with coating)* (mode: SEM, r-filter: SB, accelerating voltage: $2\,kV$, sample current: LC 7). The samples were sputtered with platinum for $90\,s$ using the built-in sputter deposition chamber. Evaluation of the micrographs was conducted using ImageJ (National Institute of Health, USA, version 1.44c), measuring at least 100 fibers and tubes, respectively, each.

Thermogravimetric Analysis: The measurements were carried out on a thermobalance TGA/SDTA 851^e (Mettler Toledo) using 70 µm corundum crucibles and about 9–12 mg of each sample. The heating rate was set to 10 K min^{-1} and the samples were measured under a nitrogen atmosphere from 20 °C up to 800 °C. Software: Star^e (Mettler Toledo, version 9.20).

Transmission Electron Microscopy: Micrographs were recorded on a JEM 3010 (JEOL) using a CCD camera (2048×2048 pixels) and the software DigitalMicrograph$^{\text{TM}}$ (Gatan, version 3.4.3). A LaB$_6$ single crystal cathode (voltage: 300 kV, current density 7–33 pA cm^{-2}) was used for both the nanoparticles (on carbon coated copper grids (Quantifoil Micro Tools, Quantifoil® Cu 300 mesh)) and the fibers/tubes (on uncoated copper grids (Ted Pella, Athene Grids, 3.05 mm, 400 mesh)). Evaluation of the micrographs was conducted using ImageJ (National Institute of Health, USA, version 1.44c), measuring at least 100 particles or fibers/tubes, respectively.

UV-Visible Spectroscopy: UV-vis spectra were recorded with quartz glass cuvettes using a spectrometer Lambda 9 (PerkinElmer) at room temperature from 260 nm up to 800 nm. The samples were dissolved and dispersed, respectively, in dichloromethane, trichloromethane, or tetrahydrofuran (0.08 g L^{-1}). Software: Lambda-SPX/P Scan (Ascanis, version 1.7).

X-Ray Powder Diffraction: Measurements were carried out on an X-ray powder diffractometer X'Pert Pro PW3040/60 (Philips, Cu-K$_\alpha$) at room temperature using a voltage of 40 kV and a current of 40 mA, respectively. The measured angle 2Θ was 10–90°. Software: X'Pert Data Collector (PANalytical, version 2.2f).

Syntheses and Supplementary Analytical Data

2-((2,4-Dinitrophenyl)thio)ethanol:[1] 1.41 mL (20 mmol) of 2-mercaptoethanol were dissolved in 16 mL of trichloromethane, followed by slow addition to a mixture of 2.54 mL (20 mmol) of 1-fluoro-2,4-dinitrobenzene and 5.6 mL (40 mmol) of triethylamine in 24 mL of trichloromethane. After stirring at room temperature for

16 h, aqueous hydrochloric acid (1.0 mol L^{-1}) was added until pH 7 was reached. The mixture was washed twice with water and yellow crystals were collected from the organic phase. Recrystallization from trichloromethane and drying under reduced pressure at 50 °C gave 2.45 g (10 mmol, 50 %) of the protected thiol as needle shaped yellow crystals.

^{1}H NMR (300 MHz, CDCl$_3$, 25 °C) = 9.08 (d, ^2J(C,H) = 2.5 Hz, 1 H; Ar H), 8.38 (dd, ^3J(H,H) = 6.5 Hz, ^2J(C,H) = 2.5 Hz, 1 H; Ar H), 7.69 (d, ^3J(H,H) = 9.0 Hz, 1 H; Ar H), 4.04 (q, ^3J(H,H) = 5.7 Hz, 2 H; CH$_2$), 3.31 (t, ^3J(H,H) = 6.0 Hz, 2 H; CH$_2$), 1.93 ppm (t, ^3J(H,H) = 5.5 Hz, 1 H; OH); ^{13}C NMR (75 MHz, CDCl$_3$, 25 °C) = 158.0 (C-NO$_2$), 147.5 (Ar CS), 128.6 (Ar CH), 128.4 (Ar CH), 123.1 (Ar CH), 61.6 (CH$_2$OH), 36.7 ppm (CH$_2$S); FTIR (attenuated total reflectance (ATR)): ν = 3294 (m, broad), 3095 (m), 3062 (m), 2971 (w), 2936 (w), 2856 (w), 1587 (s), 1527 (s), 1509 (s), 1467 (m), 1412 (m), 1392 (m), 1335 (s), 1289 (s), 1246 (s), 1151 (m), 1129 (m), 1097 (m), 1052 (s), 1017 (m), 992 (m), 955 (w), 915 (s), 857 (m), 828 (s), 749 (m), 729 (s), 694 (w), 666 (m), 603 cm^{-1} (m); UV-vis (tetrahydrofuran): $\lambda_{\max}$ = 337, 269 nm.

Poly(L-lactide) with a Protected Thiol End-Group: A dispersion of 489 mg (2.0 mmol, 3 eq.) of the prepared 2-((2,4-dinitrophenyl)thio)ethanol in 10 mL of dry toluene was added to a solution of 136 mg (0.67 mmol) of aluminum isopropoxide in 5 mL of dry toluene and stirred for 1 h at 100 °C. Subsequently, formed propan-2-ol was distilled off from the reaction mixture at 130 °C. Again, 10 mL of dry toluene were added and removed at 130 °C. The distillation was performed one more time and a dispersion of 10 g of (*S*,*S*)-lactide in 10 mL of dry toluene was added. After the solvent was removed under reduced pressure, the reaction mixture was stirred under argon for 120 h at 130 °C, resulting in a white solid. The crude product was dissolved in 50 mL of tetrahydrofuran, precipitated in heptane, and dried under reduced pressure at 50 °C for 18 h to give 7.70 g (77 %) of the white poly(L-lactide) with a protected thiol end-group.

^{1}H NMR (300 MHz, CDCl$_3$, 25 °C) = 9.06 (d, ^2J(C,H) = 3 Hz, 1 H; Ar H), 8.40 (dd, ^3J(H,H) = 9 Hz, ^2J(C,H) = 3 Hz, 1 H; Ar H), 7.71 (d, ^3J(H,H) = 9 Hz, 1 H; Ar H), 5.14 (q, ^3J(H,H) = 7 Hz, 35 H; CH), 4.49–4.25 (m, 3 H), 3.32 (t, ^3J(H,H) =

7 Hz, 2 H; CH$_2$), 2.74 (br s, 1 H; OH), 1.64–1.42 ppm (m, 108 H, CH$_3$), $M_{\text{n,NMR}}$ = 2800 g mol^{-1}; ^{13}C NMR (75 MHz, CDCl$_3$, 25 °C) = 175.1 (OC=O), 169.6 (OC=O), 145.2 (Ar C), 144.9 (Ar C), 144.2 (Ar C), 127.4 (Ar C), 126.8 (Ar C), 121.9 (Ar C), 68.9 (CH), 66.6 (CH), 61.8 (CH$_2$), 20.5 (CH$_3$), 16.6 ppm (CH$_3$); GPC (CHCl$_3$): M_{n} = 4100 g mol^{-1}, M_{w} = 4500 g mol^{-1}, $Đ_{\text{M}}$ = 1.20.

PLLA-SH: 2.0 g of the prepared protected poly(L-lactide) were dissolved in a solution of 11.9 mL (0.156 mol, 216 eq.) of 1-propanethiol in 15 mL of trichloromethane. Triethylamine was added until pH 8 was reached and the reaction mixture was stirred for 18 h at room temperature. After aqueous hydrochloric acid (1.0 mol L^{-1}) was added until pH 7 was reached, the crude product was precipitated from hexane, isolated, and washed with hexane. The product was dried under reduced pressure at 50 °C for 4 d to give PLLA-SH in quantitative yield.

^{1}H NMR (300 MHz, CDCl$_3$, 25 °C) = 5.15 (q, ^3J(H,H) = 7 Hz, 32 H; CH), 4.34 (q, ^3J(H,H) = 7 Hz, 1 H; CH), 4.24 (dt, ^3J(H,H) = 7 Hz, ^2J(C,H) = 1 Hz, 2 H; CH$_2$), 3.07 (br s, 1 H; OH), 2.73 (dt, ^3J(H,H) = 9 Hz, ^3J(H,H) = 7 Hz, 2 H; CH$_2$), 1.70–1.41 ppm (m, 106 H; CH$_3$, SH). $M_{\text{n,NMR}}$ = 2400 g mol^{-1}; ^{13}C NMR (75 MHz, CDCl$_3$, 25 °C) = 175.1 (OC=O), 169.6 (OC=O), 69.0 (CH), 66.6 (CH$_2$), 66.5 (CH), 23.0 (CH$_2$), 22.5 (CH$_3$), 16.6 ppm (CH$_3$); FTIR (ATR): ν = 2999 (w), 2949 (w), 1752 (s), 1452 (m), 1384 (m), 1358 (m), 1300 (w), 1265 (w), 1210 (s), 1182 (s), 1130 (s), 1086 (s), 1043 (s), 956 (w), 918 (w), 872 (w), 758 (m), 691 cm^{-1} (m); UV-vis (tetrahydrofuran): λ_{max} = 325 nm; differential scanning calorimetry (DSC): glass transition temperature T_{g} = 51 °C, crystallization temperature T_{c} = 89 °C, melting temperature T_{m} = 152 °C; GPC (CHCl$_3$): M_{n} = 4400 g mol^{-1}, M_{w} = 5500 g mol^{-1}, $Đ_{\text{M}}$ = 1.25.

PLLA@Au: A mixture of 3.0 g of PLLA-SH and 0.788 g (2.3 mmol) of chloroauric acid in 35 mL of dry tetrahydrofuran was stirred for 40 min, followed by the addition of lithium triethylborohydride (1 mol L^{-1} in tetrahydrofuran) upon completion of gas formation. The resulting product was precipitated from 500 mL of methanol, isolated, and washed first with methanol and then water. After drying the deep purple solid, 2.39 g (70 %) of the PLLA@Au nanoparticles were obtained.

FTIR (ATR): ν = 2999 (w), 2949 (w), 1752 (s), 1452 (m), 1384 (m), 1358 (m), 1300 (w), 1265 (w), 1210 (s), 1182 (s), 1130 (s), 1086 (s), 1043 (s), 956 (w), 918 (w), 872 (w), 758 (m), 691 cm^{-1} (m); UV-vis (CHCl$_3$): λ_{max} = 522, 356 nm; X-ray powder diffraction: 2Θ = 17.0 (PLLA), 19.4 (PLLA), 38.5 (Au(111)), 44.6 (Au(200)), 65.0 (Au(220)), 78.0 (Au(320)), 81.9° (Au(222)); TEM: 9.5 ± 2.8 nm average core diameter; TGA: 20 wt% Au; elemental analysis: 18 wt% Au, 0.7 wt% S; DSC: T_g = 45 °C, T_c = 100 °C, T_m = 147 °C.
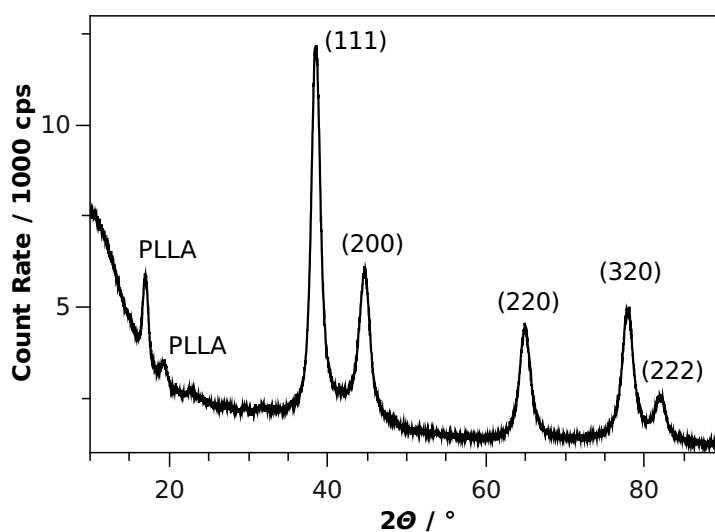

Figure 6.4. X-ray powder diffraction pattern of PLLA@Au. Aside from the characteristic pattern of the semicrystalline PLLA, the corresponding pattern of gold showed a distinct line broadening, characteristic for nano-sized crystallites.
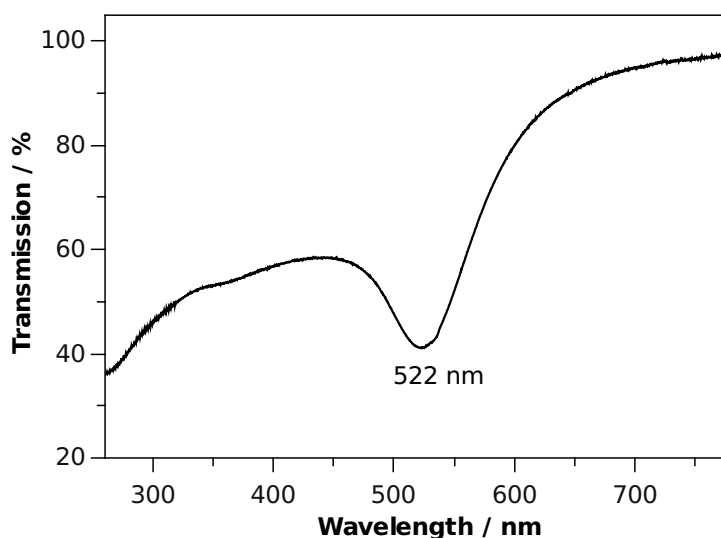
Figure 6.5. Due to the surface plasmon resonance of nanoparticulate gold, the UV-visible spectrum of PLLA@Au showed a pronounced, characteristic absorption at 522 nm.

Electrospinning of Composite Nanofibers: A solution of 0.5 wt% poly(L-lactide) ($M_{\mathrm{n}} = 313,000\,\mathrm{g\,mol^{-1}}$), 10 wt% PLLA@Au, and 0.25 wt% tetraoctylammonium bromide in dichloromethane was prepared and filled in a syringe equipped with a cannula (outer diameter 0.9 mm). Both the cannula and an aluminum foil covered collector electrode (15 cm gap) were connected to a high voltage power supply and a voltage of 17 kV was applied. The flow rate was set just fast enough to produce a steady jet. The resulting composite nanofibers had a gold content of 19 wt%, as determined by TGA.

Chemical Vapor Deposition of PPX: The composite nanofibers were coated using a Labcoater® 1 (Parylene Deposition System Model 2010, Specialty Coating Systems). 500 mg [2.2]paracyclophane were vaporized at 7 kPa and 150 °C, whereas the pyrolysis furnace was set to 650 °C. Deposition of PPX occurred below 30 °C and resulted in a uniform coating.

Thermal Degradation of the Template Material: In order to remove the PLLA template material, the PPX coated composite nanofibers were annealed at 280 °C and 10 Pa for 8 h. FTIR (ATR) spectra confirmed the absence of the template

polymer (see below, Figure 6.6). TGA: 9 wt% gold.

Butoxydimethylphenylsilane: A mixture of 4 g *n*-butanol, 32 mg dimethylphenyl-silane, and 34 mg of the gold-containing PPX tubes (3.06 mg gold) was stirred for 26 h at room temperature. Under gas formation, the reaction formed the adduct butoxydimethylphenylsilane in quantitative yield, as determined by gas chromatography (GC) and gas chromatography-mass spectroscopy (GC-MS) measurements. No product was formed without the presence of gold nanoparticles. The reaction was repeated 18 times using the same piece of catalyst nanotubes. After each cycle, the catalyst was washed with acetone. At 100 °C, the use of 5 mg of the gold-containing PPX tubes (0.45 mg gold), 623 mg of the silane, and 339 mg *n*-butanol resulted in 100 % of the siloxane product after 5 h.

GC: 13.10 min, 100 %; GC-MS: $m/z = 193$ (100) $[\text{M-(CH}_3)]^+$, 137 (98) $[\text{C}_6\text{H}_5\text{Si-(CH}_3)(\text{OH})]^+$, 135 (46) $[\text{C}_6\text{H}_5\text{Si(CH}_3)_2]^+$, 121 (25) $[\text{C}_6\text{H}_5\text{SiO}]^+$, 105 (13) $[\text{C}_6\text{H}_5\text{Si}]^+$, 91 (14) $[\text{C}_6\text{H}_5\text{CH}_3]^+$.

Dimethylphenylsilanol: A piece of 15 mg gold-containing PPX tubes (1.35 mg gold) was added to a solution of 107 mg dimethylphenylsilane in 1.18 g acetone. After the addition of 79 mg of deionized water, evolution of gas was observed. After 3.5 h, no more gas was formed and the adduct dimethylphenylsilanol was formed in quantitative yield, as determined by GC and GC-MS measurements. No product was formed without the presence of gold nanoparticles. The reaction was repeated at 80 °C using 5 mg of gold-containing PPX tubes, 37 mg of the silane, 824 mg deionized water, and 1.2 g dioxane. Quantitative yield was reached after 1.5 h.

GC: 10.13 min, 100 %; GC-MS: $m/z = 152$ (11) $[\text{M}]^+$, 137 (100) $[\text{M-(CH}_3)]^+$, 91 (6) $[\text{C}_6\text{H}_5\text{CH}_3]^+$, 77 (4) $[\text{C}_6\text{H}_5]^+$, 45 (8) $[\text{SiOH}]^+$, 28 (4) $[\text{Si}]^+$.
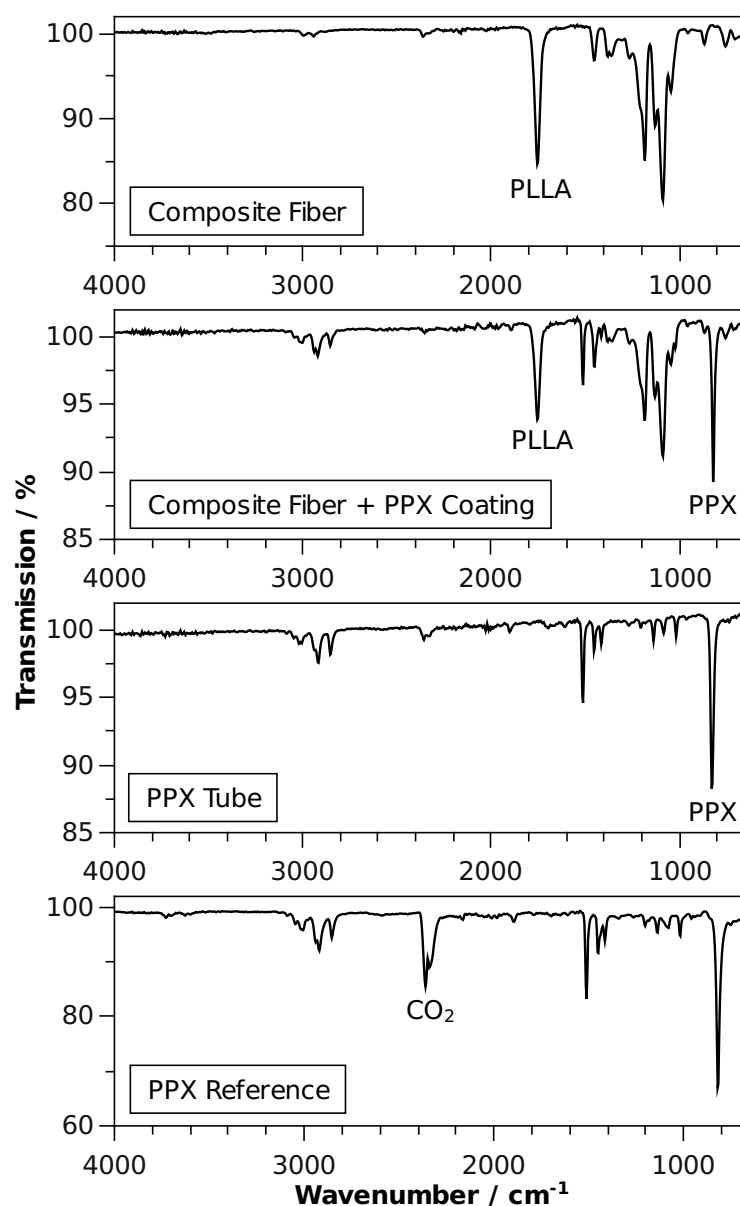
TUFT Process IR Studies:

Figure 6.6. FTIR spectra of the different samples during the TUFT process. After the template removal, there was no PLLA left inside the PPX tubes and the spectrum matched the PPX reference spectrum.

Leaching Studies: After introducing $100\,\mathrm{mg}$ of the gold-containing PPX tubes into $2\,\mathrm{mL}$ of either di- or trichloromethane while stirring, UV-vis spectra of the solvents were recorded both immediately and after $5\,\mathrm{h}$ (Figure 6.7).
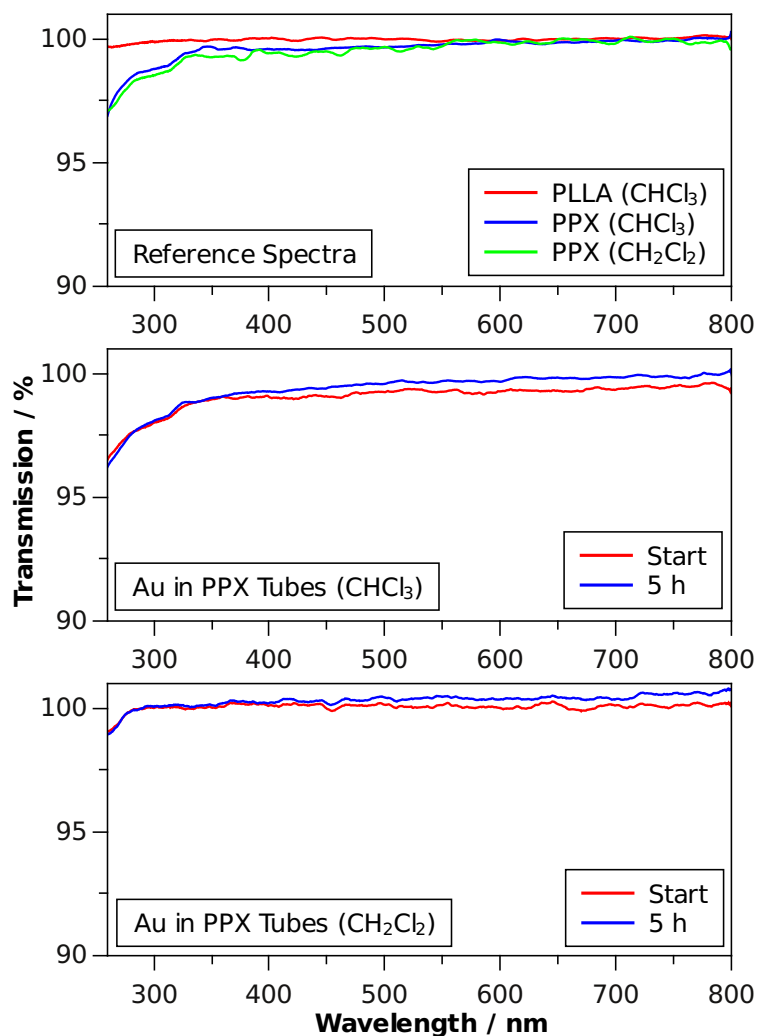
Figure 6.7. UV-vis spectra of the PPX tubes with incorporated gold nanoparticles as well as reference spectra of PLLA and PPX. The different spectra were recorded in either dichloromethane or trichloromethane. To study the leaching behavior, spectra were recorded immediately and after 5 h. In no case, the characteristic plasmon resonance absorption of gold nanoparticles at 522 nm was observed, hence the particles were immobilized inside the PPX tubes.

6.8 References (Supporting Information)

[1]   S. Aryal, K. C. R. Bahadur, N. Bhattarai, B. M. Lee, H. Y. Kim, *Mater. Chem. Phys.* **2006**, *98*, 463.

# 7 Conductive Gold Nanofibers Based on Gold-Filled Polymer Tubes

Fabian Mitschang,[a] Markus Langner,[a] Henning Vieker,[b] Armin Gölzhäuser,[b] Andreas Greiner[a,]*

[a]Makromolekulare Chemie II, Universität Bayreuth, Universitätsstraße 30, 95440 Bayreuth, Germany.

[b]Fakultät für Physik, Universität Bielefeld, Universitätsstr. 25, 33615 Bielefeld, Germany.

*Corresponding Author: E-mail: greiner@uni-bayreuth.de; Fax: +49-921-553393.

7.1 Abstract
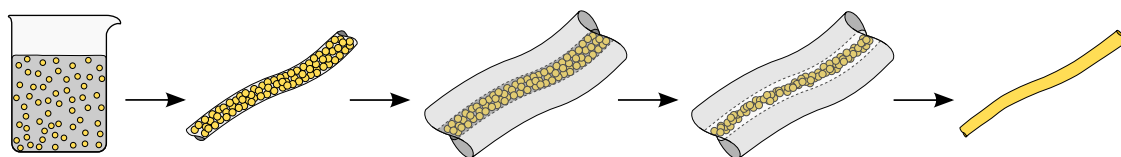
Continuous conductive gold nanofibers are prepared via the "tubes by fiber templates" process. First, the combination of poly(L-lactide)-stabilized gold nanoparticles with over 60 wt% gold, the electrospinning of composite nanofibers, and the chemical vapor deposition of poly(*p*-xylylene) leads to gold-filled core-shell fibers. Subsequent thermal treatment results in gold nanowires. The corresponding transition is studied by scanning helium ion microscopy.

7.2 Introduction

There are manifold applications for conductive metal nanowires ranging from microelectronics and sensorics[1,2] to electrodes and catalysts featuring a very large surface area.[3] Further, nanowires can be used for the production of LEDs[4] and photovoltaic cells.[5] Despite the various potential applications, the preparation of

continuous conductive metal nanowires remains a great challenge. Very few top-down methods are capable of producing conductive metal nanofibers, such as electron beam lithography or mechanical reduction.[2,6] In contrast, most bottom-up processes are based on templates[7] or self-assembly effects.[8] Major drawbacks of most methods are the limited nanowire length, the suitability for only selected materials, and the lack of upscalability.

A highly versatile method for the preparation of continuous composite polymer nanofibers is the electrospinning process.[9] Electrospun polymer nanofibers have successfully been used as a precursor for conductive nanowires. For instance, polymer nanofibers containing a gold salt could be introduced into a reducing solution and were subsequently treated using an oxygen plasma in order to quantitatively degrade the present polymer and fuse together the gold particles.[10] Alternatively, thermal treatment up to 500 °C of gold nanoparticle-polymer composite fibers also led to gold nanowires.[11] However, the surface of the resulting gold fibers showed pronounced roughness. In addition, distinct defects concerning the conductivity were observed.

Herein, we report on the preparation of continuous gold nanowires using the tubes by fiber templates (TUFT) process,[12,13] combining the electrospinning process with the chemical vapor deposition (CVD) of poly(*p*-xylylene) (PPX): Continuous electrospun composite nanofibers containing gold nanoparticles were homogeneously coated with PPX from the gas phase resulting in core-shell fibers. Due to the high thermal stability of PPX,[14,15] the inner template polymer could be quantitatively removed, leading to PPX tubes filled with gold aggregates. Eventually, thermal treatment resulted in degradation of the polymer shell and simultaneously fused the gold particles together. Combining transmission electron microscopy and scanning helium ion microscopy (featuring both the detection of secondary electrons and Rutherford backscattered ions), the transition towards continuous conductive gold nanowires was studied. It was found that temperatures exceeding 1000 °C led to gold wires featuring a smooth surface. The preparation of gold-filled PPX tubes was based on the TUFT process, as illustrated in Figure 7.1. The template polymer for both the core fiber and the stabilization of the gold nanoparticles was poly(L-lactide) (PLLA) since it can be quantitatively removed at 280 °C under reduced
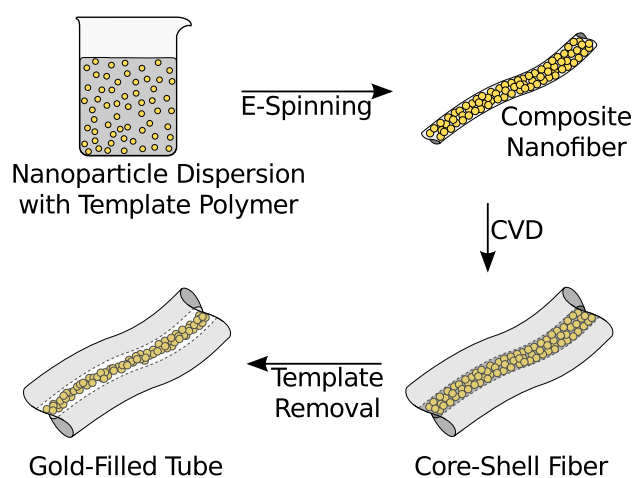
Figure 7.1. Overview of the used TUFT process leading to gold-filled PPX tubes: Electrospun composite nanofibers were coated with PPX using the chemical vapor deposition process. Subsequently, the inner template polymer was removed, resulting in PPX encapsulated gold aggregates.

pressure.[12,16] In order to prepare PLLA-stabilized gold nanoparticles, a thiol-end-functionalized PLLA (PLLA-SH) was synthesized (Supporting Information, Scheme 7.1). First, L-lactide was polymerized using a protected thiol for initiation and an aluminum catalyst. As calculated from the NMR spectrum, the molecular weight M_n of the protected polymer was $2800\,\mathrm{g\,mol^{-1}}$. In addition, gel permeation chromatography (GPC, poly(methyl methacrylate) calibration) showed a dispersity ($Đ_M$) of 1.20. Subsequent deprotection of the prepared polymer resulted in PLLA-SH in quantitative yield. NMR spectroscopy showed a M_n of $2600\,\mathrm{g\,mol^{-1}}$ and GPC analysis still resulted in a unimodal distribution with a dispersity $Đ_M$ of 1.25.

Next, the PLLA-stabilized gold nanoparticles (PLLA@Au) were prepared based on PLLA-SH and chloroauric acid (Supporting Information, Scheme 7.1). The corresponding solvent was THF and the reducing agent was sodium borohydride. Precipitation from methanol resulted in $70\,\%$ PLLA@Au as a deep purple solid. According to thermogravimetric analysis of the nanoparticles, the gold content was $61\,\mathrm{wt\%}$. The particles were redispersible in chloroform and tetrahydrofuran and did not show agglomeration throughout characterization. A transmission electron micrograph of the well dispersed particles is shown in Figure 7.2, as well as the result of GPC coupled with a diode array detector. The average diameter of the spherical parti-
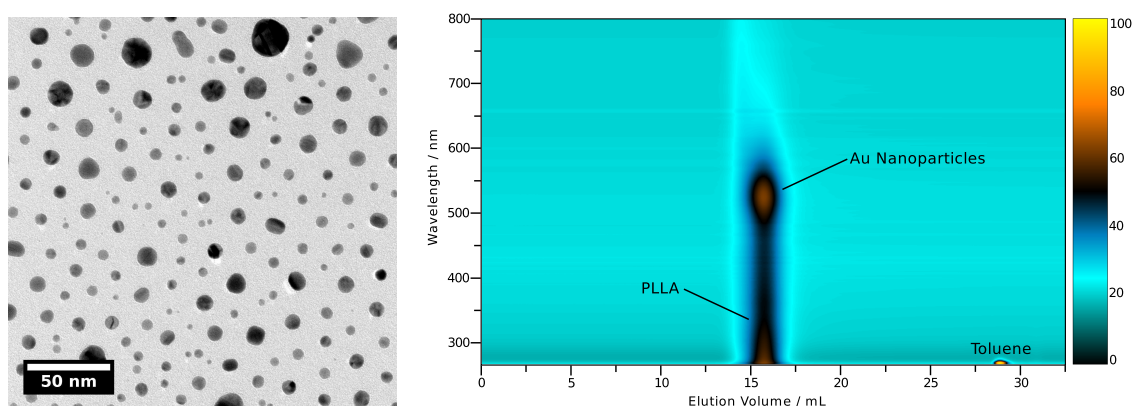
Figure 7.2. Analysis of PLLA@Au using transmission electron microscopy (left) and GPC coupled with a diode array detector (right).

cles was 8.5 ± 3.5 nm. The UV-visible spectrum at the retention time of 15.8 min combined the characteristic plasmon resonance absorption of gold nanoparticles at 525 nm[17] and the absorption of the free PLLA-SH polymer below 400 nm, proving that the polymer was connected to the gold particles. The signal of the added toluene reference can be found at 28.8 min. (For comparison, UV-visible spectra of PLLA-SH and PLLA@Au are given in the Supporting Information, Figure 7.7 and 7.8.)

For the electrospinning process of composite nanofibers, a homogeneous dispersion of 20 wt% PLLA@Au and 1 wt% template PLLA was prepared in dichloromethane. To prevent the formation of beads, 0.5 wt% of tetraoctylammonium bromide (TOAB) was added. The corresponding voltage was 15 kV. The resulting composite nanofibers were analyzed using both scanning electron microscopy (SEM) and transmission electron microscopy (TEM), as shown in Figure 7.3 (top). The fibers were uniform and free of beads. No pores were observed, and the average fiber diameter was 118 ± 38 nm. Moreover, the gold nanoparticles were homogeneously distributed throughout the PLLA matrix. Based on the processed electrospinning formulation, the gold content of the fibers was 57 wt%.

Using the chemical vapor deposition process, the nanofibers were coated with PPX.[18] The corresponding precursor [2.2]paracyclophane was evaporated at a reduced pressure at 150 °C, followed by pyrolysis at 650 °C. Subsequently, the resulting reactive monomer[19] polymerized at 25 °C from the gas phase onto the nanofibers
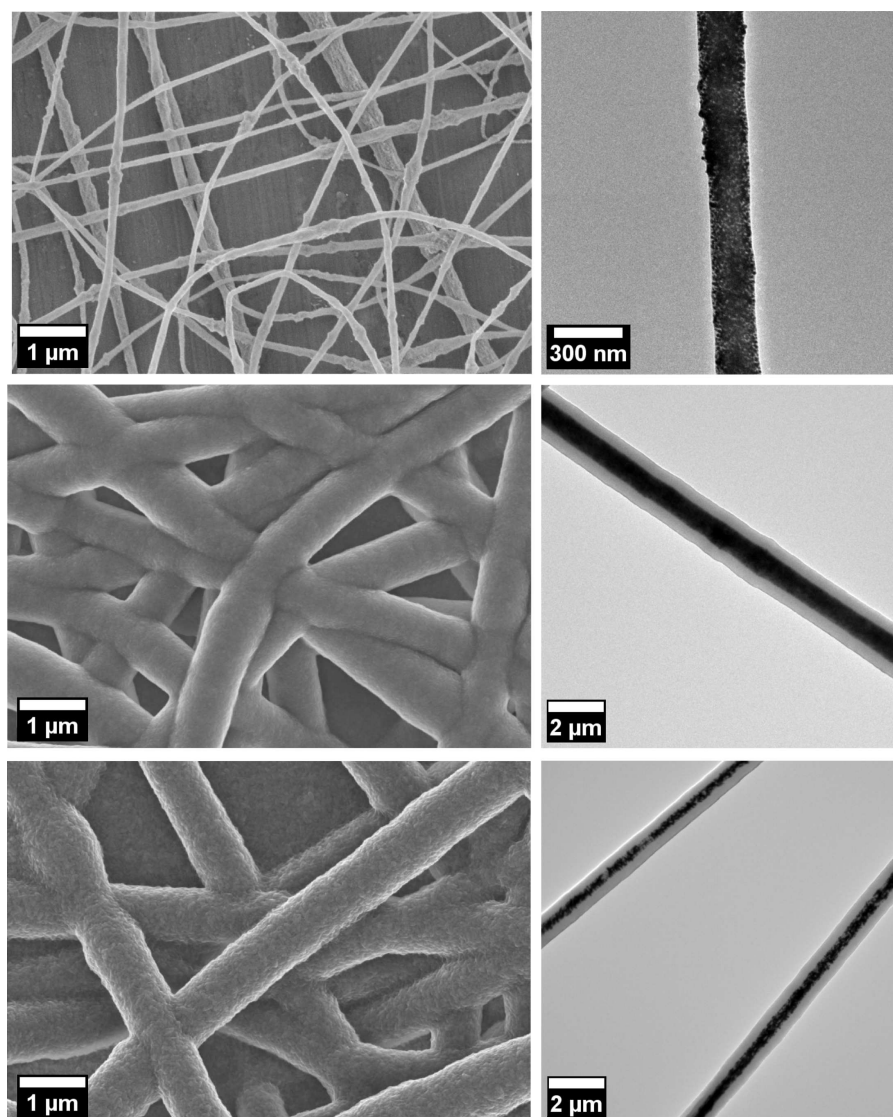
Figure 7.3. Electron micrographs of electrospun composite nanofibers (top row), corresponding core-shell fibers after the CVD process (middle row), and PPX tubes with encapsulated gold nanoparticles (bottom row). Left: Scanning electron micrographs. Right: Transmission electron micrographs.

(Supporting Information, Scheme 7.2). Both scanning and transmission electron micrographs of the resulting core-shell fibers are shown in Figure 7.3 (middle). The deposited PPX layer was homogeneous and free of visible cracks and pores. The average layer thickness was 345 ± 36 nm, as determined by SEM measurements.

In order to quantitatively remove the inner PLLA template polymer, the core-shell fibers were annealed at 280 °C and 70 Pa for 5 h. Micrographs of the gold-filled PPX tubes are shown in Figure 7.3 (bottom). In addition, corresponding IR spectra were recorded throughout the TUFT process to study the composition after each step, proving the quantitative degradation of PLLA (Figure 7.4).
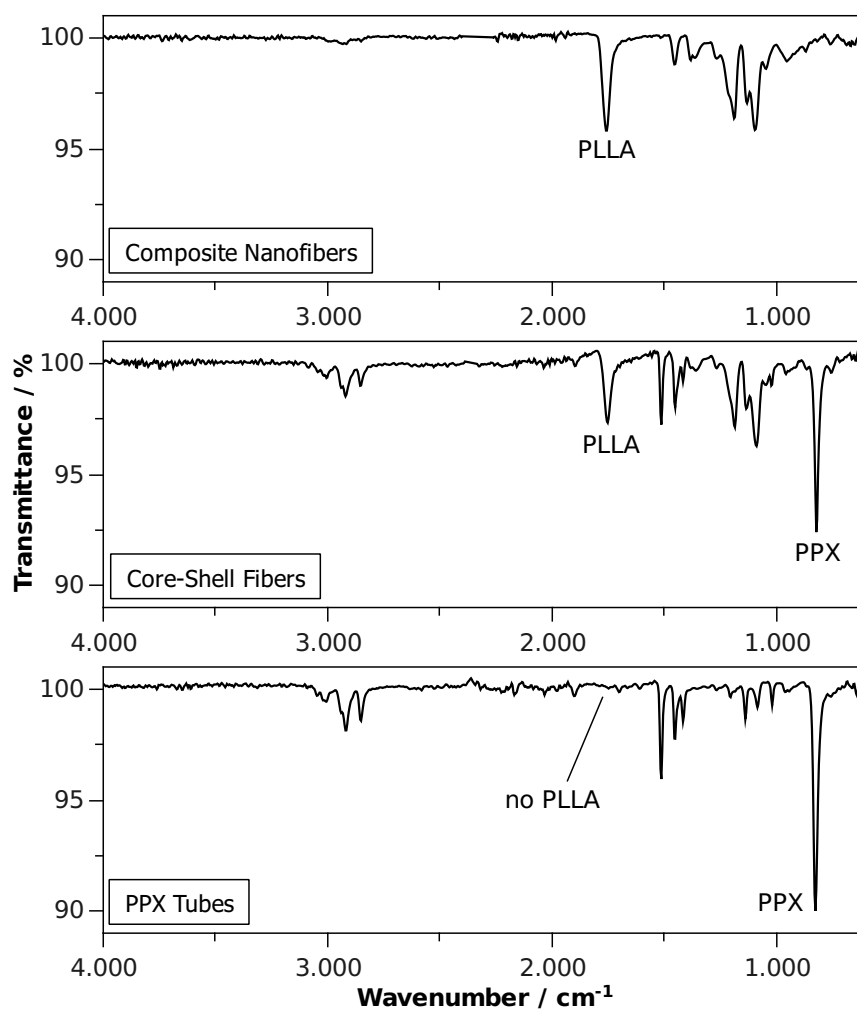

Figure 7.4. Recorded IR spectra of the electrospun composite nanofibers (top), the PPX coated core-shell fibers (middle), and the gold nanoparticle-filled PPX tubes (bottom).

Subsequently, the gold-filled PPX tubes were annealed using a Bunsen burner resulting in a temperature gradient from below 200 °C up to 1050 °C (see Experimental Section). Corresponding micrographs depicting the effect of different temperature ranges are shown in Figure 7.5. Further, in addition to the TEM measurements, scanning helium ion microscopy was used to characterize the transition of the gold-filled PPX tubes to gold nanowires. Whereas the detection of secondary electrons showed the topology of the sample, Rutherford backscattered ions highlighted areas of high conductivity.[20] As shown in Figure 7.5 (top to bottom), the PPX coating of the tubes degraded as the temperature increased, resulting in a very rough and inhomogeneous surface. At this point, the obtained system was visually similar to the wires prepared by Gries et al. at 500 °C.[11] However, at higher temperatures reaching up to 1050 °C, the remaining gold aggregates fused together and eventually led to continuous nanowires featuring a smooth surface. Throughout the transition, the average fiber diameter decreased significantly, whereas the conductivity increased from isolated areas to continuous nanowires. Using TEM, transmission high energy electron diffraction patterns of single nanowires were recorded. As a result, the presence of polycrystalline gold was confirmed (Supporting Information, Figure 7.6).
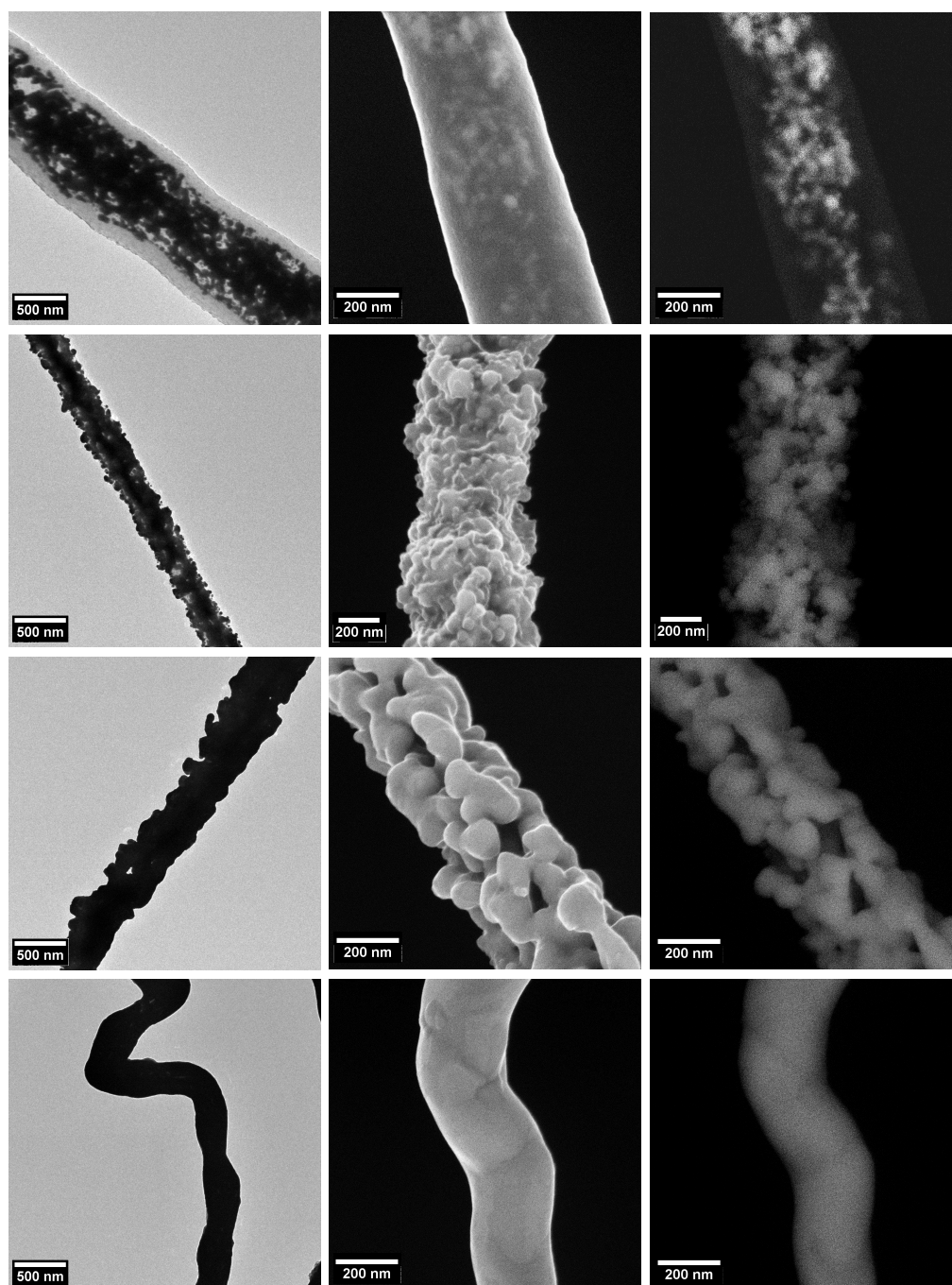
Figure 7.5. Micrographs depicting the temperature-induced transition to gold-nanowires (top to bottom). Left: TEM pictures; middle: Helium ion micrographs based on secondary electrons showing the surface; right: Scanning helium ion micrographs based on Rutherford backscattered ions highlighting areas of high conductivity.

7.3 Conclusion

In conclusion, poly(L-lactide)-stabilized gold nanoparticles containing 61 wt% gold were prepared based on thiol-functionalized poly(L-lactide) and chloroauric acid. Using the electrospinning process, uniform composite nanofibers with 57 wt% gold were prepared. Subsequent coating with PPX via the chemical vapor deposition process resulted in core-shell fibers with a shell thickness of 345 ± 36 nm. Thermal treatment up to 1050 °C led to the degradation of the polymer material while fusing the gold aggregates together. As a result, continuous gold nanowires featuring a smooth surface were obtained. Scanning helium ion microscopy was used to study the influence of a temperature gradient on the gold-filled PPX tubes. The detection of secondary electrons showed the heat-induced degradation of the polymer surface, whereas Rutherford backscattered ions were used to depict the increasing conductivity resulting in homogeneous, conducting gold nanofibers. The suitability of the presented concept for different metals and applications is as yet unexplored and the topic of current research.

7.4 Experimental Section

Materials and analytical methods

For detailed information on the materials used as well as on the analytical methods please see the Supporting Information.

Synthesis of 2-((2,4-dinitrophenyl)thio)ethanol[21]

A mixture of 1.41 mL 2-mercaptoethanol (20 mmol) in 16 mL trichloromethane was slowly added to a solution of 2.54 mL (20 mmol) 1-fluoro-2,4-dinitrobenzene and 5.6 mL (40 mmol) triethylamine in 24 mL of trichloromethane. The reaction mixture was stirred at 22 °C for 16 h, followed by addition of aqueous hydrochloric acid (1.0 mol L^{-1}) until pH 7. After washing the mixture twice with water, yellow needle-shaped crystals were collected from the organic phase and subsequently recrystallized from trichloromethane. After drying under reduced pressure at 50 °C the yield was 2.45 g (10 mmol, 50 %). ^{1}H NMR (300 MHz, CDCl$_3$, δ): 9.08 (d, $J =$

2.5 Hz, 1H, Ar H), 8.38 (dd, $J = 6.5$ Hz, $J = 2.5$ Hz, 1H, Ar H), 7.69 (d, $J = 9.0$ Hz, 1H, Ar H), 4.04 (q, $J = 5.7$ Hz, 2H, CH$_2$), 3.31 (t, $J = 6.0$ Hz, 2H, CH$_2$), 1.93 ppm (t, $J = 5.5$ Hz, 1H, OH); ^{13}C NMR (75 MHz, CDCl$_3$, δ): 158.0 (C-NO^2), 147.5 (Ar CS), 128.6 (Ar CH), 128.4 (Ar CH), 123.1 (Ar CH), 61.6 (CH$_2$OH), 36.7 ppm (CH$_2$S); FTIR (attenuated total reflectance (ATR)): $\nu = 3294$ (m, broad), 3095 (m), 3062 (m), 2971 (w), 2936 (w), 2856 (w), 1587 (s), 1527 (s), 1509 (s), 1467 (m), 1412 (m), 1392 (m), 1335 (s), 1289 (s), 1246 (s), 1151 (m), 1129 (m), 1097 (m), 1052 (s), 1017 (m), 992 (m), 955 (w), 915 (s), 857 (m), 828 (s), 749 (m), 729 (s), 694 (w), 666 (m), 603 cm^{-1} (m); UV-visible (tetrahydrofuran): $\delta_{max} = 337$, 269 nm.

Bulk polymerization of (*S,S*)-lactide

A suspension of 489 mg (2.0 mmol, 3 eq.) of the prepared initiator 2-((2,4-dinitro-phenyl)thio)ethanol in 10 mL of dry toluene was added to a mixture of 136 mg (0.67 mmol) of aluminum isopropoxide and 5 mL of dry toluene and stirred at 100 °C for 1 h. In order to remove the byproduct propan-2-ol, the mixture was distilled at 130 °C. 10 mL of dry toluene were added to the reaction and subsequently distilled off at 130 °C. This step was repeated once, followed by addition of 10 g (*S,S*)-lactide in 10 mL of dry toluene. The solvent was removed under reduced pressure, and the polymerization was carried out under an argon atmosphere in bulk. After 120 h at 130 °C, the formed crude white product was dissolved in 50 mL tetrahydrofuran and subsequently precipitated from heptane. The polymer was dried for 18 h at 50 °C under reduced pressure resulting in 7.70 g (77 %) of the protected poly(L-lactide). ^{1}H NMR (300 MHz, CDCl$_3$, δ): 9.06 (d, $J = 2.5$ Hz, 1H, Ar H), 8.40 (dd, $J = 9.0$ Hz, $J = 2.5$ Hz, 1H, Ar H), 7.71 (d, $J = 9.0$ Hz, 1H, Ar H), 5.14 (q, $J = 7.0$ Hz, 35H, CH), 4.49–4.25 (m, 3H), 3.32 (t, $J = 6.9$ Hz, 2H, CH$_2$), 2.74 (br s, 1H, OH), 1.64–1.42 ppm (m, 108H, CH$_3$), $M_{n,NMR} = 2800$ g mol^{-1}; ^{13}C NMR (75 MHz, CDCl$_3$, δ): 175.1 (OC=O), 169.6 (OC=O), 145.2 (Ar C), 144.9 (Ar C), 144.2 (Ar C), 127.4 (Ar C), 126.8 (Ar C), 121.9 (Ar C), 68.9 (CH), 66.6 (CH), 61.8 (CH$_2$), 20.5 (CH$_3$), 16.6 ppm (CH$_3$); GPC (CHCl$_3$): $M_n = 4100$ g mol^{-1}, $M_w = 5000$ g mol^{-1}, $Đ_M = 1.20$.

Deprotection of the protected PLLA

To a mixture of 11.88 mL (0.156 mol, 216 eq.) of 1-propanethiol in 15 mL of tri-chloromethane, 2.0 g of the protected PLLA were added, followed by triethylamine until pH 8. After 18 h at room temperature, the mixture was neutralized using aqueous hydrochloric acid (1.0 mol L^{-1}). The crude product was precipitated from hexane and subsequently isolated and washed with hexane. The white polymer was dried for 4 d at 50 °C under reduced pressure resulting in PLLA-SH in quantitative yield. ^{1}H NMR (300 MHz, CDCl$_3$, δ): 5.15 (q, J = 7.1 Hz, 32H, CH), 4.34 (q, J = 6.9 Hz, 1H, CH), 4.24 (dt, J = 6.5 Hz, J = 1.4 Hz, 2H, CH$_2$), 3.07 (br s, 1H, OH), 2.73 (dt, J = 8.5 Hz, J = 6.6 Hz, 2H, CH$_2$), 1.70–1.41 ppm (m, 106H, CH$_3$, SH). $M_{n,NMR}$ = 2400 g mol^{-1}; ^{13}C NMR (75 MHz, CDCl$_3$, δ): 175.1 (OC=O), 169.6 (OC=O), 69.0 (CH), 66.6 (CH$_2$), 66.5 (CH), 23.0 (CH$_2$), 22.5 (CH$_3$), 16.6 ppm (CH$_3$); FTIR (ATR): ν = 2999 (w), 2949 (w), 1752 (s), 1452 (m), 1384 (m), 1358 (m), 1300 (w), 1265 (w), 1210 (s), 1182 (s), 1130 (s), 1086 (s), 1043 (s), 956 (w), 918 (w), 872 (w), 758 (m), 691 cm^{-1} (m); UV-visible (CHCl$_3$): δ_{max} = 325 nm; differential scanning calorimetry (DSC): glass transition temperature T_g = 51 °C, crystallization temperature T_c = 89 °C, melting temperature T_m = 152 °C; GPC (CHCl$_3$): M_n = 4400 g mol^{-1}, M_w = 5500 g mol^{-1}, $Đ_M$ = 1.25.

Preparation of PLLA@Au

To a solution of 119.7 mg of PLLA-SH in 6.7 mL of dry tetrahydrofuran, 340.7 mg (0.87 mmol) of chloroauric acid were added. Under an argon atmosphere, a mixture of 73.2 mg (1.93 mmol, 2.2 eq.) of sodium borohydride in 1 mL of dry methanol was added dropwise, instantly changing the color of the reaction mixture to black. The crude product was precipitated from 50 mL of methanol and subsequently isolated using a centrifuge. After washing with methanol and drying under reduced pressure at 50 °C, 267 mg (92 %) of the dark red PLLA-stabilized gold nanoparticles were obtained. TGA: 61 wt% Au. FTIR (ATR): ν = 2999 (w), 2948 (w), 1754 (s), 1454 (m), 1385 (m), 1361 (m), 1300 (w), 1269 (w), 1211 (s), 1183 (s), 1132 (s), 1085 (s), 1044 (s), 955 (w), 918 (w), 870 (m), 756 (m), 693 cm^{-1} (m); UV-visible (CHCl$_3$): δ_{max} = 522 nm; TEM: 9.5 nm±3.5 nm average core diameter; X-ray powder diffraction:

$2\Theta = 16.8$ (PLLA), 38.4 (Au(111)), 44.6 (Au(200)), 64.8 (Au(220)), 77.6 (Au(311)); elemental analysis: 59 wt% Au, 21 wt% C.

Electrospinning

In order to prepare the composite nanofibers, a custom made electrospinning setup was used.[14] A homogeneous dispersion of 20 wt% PLLA@Au, 1 wt% PLLA, and 0.5 wt% tetraoctylammonium bromide in dichloromethane was prepared and subsequently electrospun at 24 ℃. The corresponding voltage was 15 kV, and the outer needle diameter was 0.9 mm. The flow rate of the formulation was set to 0.25 mL h^{-1}, and the electrode gap was 14 cm. The collector electrode was covered with aluminum foil or copper grids (Old400, Plano).

Chemical Vapor Deposition

Using a Labcoater® 1 (PSD 2010, Specialty Coating Systems), the prepared composite nanofibers were coated with PPX. The CVD process was carried out at a reduced pressure of 70 Pa. A precursor amount of 430 mg [2.2]paracyclophane was evaporated at 150 ℃, followed by pyrolysis at 650 ℃. The fiber mats were coated at 25 ℃.

Template Removal

The prepared core-shell fibers were annealed at 280 ℃ and 70 Pa for 5 h to quantitatively remove the PLLA material. Corresponding IR spectra are shown in Figure 7.4.

Preparation of Gold Nanowires

TEM grids (see Supporting Information) were used as a substrate for the preparation of gold-filled PPX nanotubes. The grids were held with flat tweezers, covering half of the sample with the other half being exposed to the outside. The air hole of a methane-fueled Bunsen burner was fully opened, resulting in a light blue flame of 5 cm. A digital thermometer (GTH 1200 A, Greisinger electronics) was used to determine the maximum temperature of 1050 ℃. Subsequently, the TEM grids

were brought into the hottest zone of the flame for 3 seconds. After removal of the tweezers from the flame, the samples were let to cool down to room temperature.

7.5 Acknowledgments

7.6 References

[1] a) Y. Wu, J. Xiang, C. Yang, W. Lu, C. M. Lieber, *Nature* **2004**, *430*, 61; b) Y. Engel, R. Elnathan, A. Pevzner, G. Davidi, E. Flaxer, F. Patolsky, *Angew. Chem. Int. Ed.* **2010**, *49*, 6830.

[2] P. Arora, A. Sindhu, N. Dilbaghi, A. Chaudhury, *Appl. Nanosci.* **2013**, *3*, 363.

[3] a) C. K. Chan, H. Peng, G. Liu, K. McIlwrath, X. F. Zhang, R. A. Huggins, Y. Cui, *Nat. Nanotechnol.* **2008**, *3*, 31; b) H.-H. Li, S. Zhao, M. Gong, C.-H. Cui, D. He, H.-W. Liang, L. Wu, S.-H. Yu, *Angew. Chem. Int. Ed.* **2013**, *52*, 7472.

[4] Z. Li, J. Kang, Z. Liu, C. Du, X. Lee, X. Li, L. Wang, X. Yi, H. Zhu, G. Wang, *AIP Adv.* **2013**, *3*, 042134.

[5] M. T. Borgström, J. Wallentin, M. Heurlin, S. Fält, P. Wickert, J. Leene, M. H. Magnusson, K. Deppert, L. Samuelson, *IEEE J. Sel. Top. Quant.* **2011**, *17*, 1050.

[6] a) A. M. Leach, M. McDowell, K. Gall, *Adv. Funct. Mater.* **2007**, *17*, 43; b) I. Park, Z. Li, A. P. Pisano, R. S. Williams, *Nanotechnology* **2010**, *21*, 015501.

[7] L. Dupré, T. Gorisse, A. L. Lebranchu, T. Bernardin, P. Gentile, H. Renevier, D. Buttard, *Nanoscale Res. Lett.* **2013**, *8*, 123.

[8] H. Feng, Y. Yang, Y. You, G. Li, J. Guo, T. Yu, Z. Shen, T. Wub, B. Xing, *Chem. Commun.* **2009**, *15*, 1984.

[9] a) S. Agarwal, A. Greiner, J. H. Wendorff, *Prog. Polym. Sci.* **2013**, *38*, 963; b) D. Li, Y. Xia, *Adv. Mater.* **2004**, *16*, 1151.

[10] S. Park, S. C. Moon, D. Chen, R. J. Farris, T. P. Russell, *J. Mater. Chem.* **2010**, *20*, 1198.

[11] K. Gries, H. Vieker, A. Gölzhäuser, S. Agarwal, A. Greiner, *Small* **2012**, *8*, 1436.

[12] M. Bognitzki, H. Hou, M. Ishaque, T. Frese, M. Hellwig, C. Schwarte, A. Schaper, J. H. Wendorff, A. Greiner, *Adv. Mater.* **2000**, *12*, 637.

[13] Z. Sun, J. Zeng, H. Hou, H. Wickel, J. H. Wendorff, A. Greiner, *Prog. Colloid Polym. Sci.* **2005**, *130*, 15.

[14] J. R. Schaefgen, *J. Polym. Sci.* **1959**, *41*, 133.

[15] A. Greiner, S. Mang, O. Schäfer, P. Simon, *Acta Polym.* **1997**, *48*, 1.

[16] D. Garlotta, *J. Polym. Environ.* **2001**, *9*, 63.

[17] G. A. Rance, D. H. Marsh, A. N. Khlobystov, *Chem. Phys. Lett.* **2008**, *460*, 230.

[18] a) W. F. Gorham, *J. Polym. Sci. Pol. Chem.* **1966**, *4*, 3027; b) A. Greiner, S. Mang, O. Schäfer, P. Simon, *Acta Polym.* **1997**, *48*, 1.

[19] C. A. Coulson, D. P. Craig, A. Maccoll, A. Pullman, *Discuss. Faraday Soc.* **1947**, *2*, 36.

[20] a) J. Morgan, J. Notte, R. Hill, B. Ward, *Micros. Today* **2006**, *14*, 24; b) D. C. Bell, *Microsc. Microanal.* **2009**, *15*, 147.

[21] H. Qiu, J. Rieger, B. Gilbert, R. Jérôme, C. Jérôme, *Chem. Mater.* **2004**, *16*, 850.

7.7 Supporting Information

Materials

Aluminum isopropoxide: Merck, for synthesis. Argon: Air Liquide, 99.999 %. Chloro-auric acid: Sigma-Aldrich, p.a., ≥ 49 % Au basis. Dichloromethane: AnalaR Norma-

pur, VWR Chemicals. 1-Fluoro-2,4-dinitrobenzene: Acros Organics, 98 %. (*S,S*)-Lactide: Aldrich, 98 %. 2-Mercaptoethanol: Acros Organics, 99 %. Methanol: BASF, purified by distillation. [2.2]Paracyclophane: Specialty Coating Systems, Parylene N. Tetrahydrofuran: BASF, dried over Solvona® (Dr. Bilger Umweltconsulting GmbH), purified by distillation. Poly(L-lactide): Resomer L210S, Boehringer Ingelheim. Sodium borohydride: Aldrich, 98 %. Tetraoctylammonium bromide: Fluka. Toluene: BASF, dried over calcium hydride (ABCR, 92 %), purified by distillation. Trichloromethane: BASF, purified by distillation. Trichloromethane-d: Roth. Triethylamine: BASF, purified by distillation.

Attenuated Total Reflectance Fourier Transform IR Spectroscopy

A FTIR spectrometer (Digilab, Excalibur Series) equipped with an attenuated total reflectance (ATR) unit (Pike Technologies, MIRacle) was used. Software: WinIRPro (Digilab, version 3.3.1.014).

Differential Scanning Calorimetry

A DSC 821^e (Mettler Toledo) and corresponding 40 μL aluminum crucibles (Mettler Toledo) were used under a nitrogen atmosphere. The system was calibrated using indium, *n*-octane, and zinc standards. A sample amount of about 11 mg was used for each measurement. The rate of cooling and the heating rate were set to 10 K min^{-1}. In order to determine the glass transition temperature T_g, the crystallization temperature T_c, and the melting temperature T_m, the software Star^e (Mettler Toledo, version 9.20) was used.

Elemental Analysis

The amount of both S and Au was determined by the analytical service facility of BayCEER (Bayreuth, Germany). Au was first dissolved in aqua regia and then analyzed by inductively coupled plasma optical emission spectroscopy (ICP-OES). The amount of S was determined by atomic absorption spectroscopy.

Gel Permeation Chromatography

The measurements were carried out at 30 °C. One drop of toluene was used as the internal standard. Polymers were characterized using the eluent trichloromethane (Fischer Scientific, HPLC grade) and a concentration of $1\,\mathrm{g\,L^{-1}}$. Further, three SDV columns (Polymer Standards Service, LinearXL 20 μ), a Smartline 1000 (Knauer, 10 mL pump head) pump (flow rate $1.0\,\mathrm{mL\,min^{-1}}$), and a refractive index detector (Knauer, RI 2300) were used. Software: WinGPC Unity (Polymer Standards Service, Build 5403). The system was calibrated using poly(methyl methacrylate) standards (Polymer Standards Service). The gold nanoparticles were measured using *N*,*N*-dimethylformamide (concentration $1.0\,\mathrm{g\ L^{-1}}$, flow rate $1.0\,\mathrm{mL\,min^{-1}}$) coupled with a diode array detector (Polymer Standards Service, SECcurity Diode Array Detector GPC1260 DAD). Three SDV columns (Polymer Standards Service, 10E4, 10E6, and 1000) were used. The system was calibrated using polystyrene standards (Polymer Standards Service). Software: WinGPC UniChrom with ChromPilot and 3D DAD module (Polymer Standards Service).

NMR Spectroscopy

^{1}H NMR (300 MHz) and ^{13}C NMR (75 MHz) spectra were recorded on a Bruker Ultrashield 300 spectrometer at room temperature in deuterated trichloromethane $(50\,\mathrm{g\,L^{-1}})$ using Icon-NMR (Bruker, version 4.2.4 build 10). To evaluate the spectra, TopSpin (Bruker BioSpin, version 3.0.b.7) was used. In order to calibrate the spectra, the trichloromethane signal at 7.26 ppm (^{1}H NMR) and 77.0 ppm (^{13}C NMR), respectively, was used.

Scanning Electron Microscopy

Micrographs were recorded on a LEO 1530 (Gemini) using the software Smart-SEM (Carl Zeiss SMT Ltd, version 5.4.5.0) and an InLens detector. The working distance was about 5.5 mm, and the accelerating voltage was 3 kV. Prior to the measurements, the samples were coated with 1.3 nm of platinum. In order to do so, a Cressington sputter coater (208HR, 50 mA, 0.1 mbar) equipped with a Cressington thickness controller (mtm20) was used. The micrographs were evaluated using

ImageJ (National Institute of Health, USA, version 1.44c), measuring at least 100 fibers and tubes, respectively.

Scanning Helium Ion Microscopy

An Orion Plus (Carl Zeiss) scanning helium ion microscope was used (research group Prof. Armin Gölzhäuser, Bielefeld University, Germany).

Thermogravimetric Analysis

A thermobalance TGA/SDTA 851^e (Mettler Toledo) was used in combination with 70 μm corundum crucibles and about 11 mg of each sample. The heating rate was set to 10 K min^{-1}. The measurements were carried out under a nitrogen atmosphere from 20 °C up to 800 °C. Software: Star^e (Mettler Toledo, version 9.20).

Transmission Electron Microscopy and Transmission High Energy Electron Diffraction

Transmission electron micrographs were recorded using an EM922Omega (LEO). A LaB$_6$ single crystal cathode (voltage: 200 kV) was used for both the nanoparticles (on carbon coated copper grids (Quantifoil Micro Tools, Quantifoil$^®$ Cu 300 mesh)) and the fibers/tubes (on uncoated copper grids (Ted Pella, Athene Grids, 400 mesh, 3.05 mm)). The corresponding software was DigitalMicrograph (Gatan). The diameter of the particles was evaluated using ImageJ (National Institute of Health, USA, version 1.44c), measuring 100 particles. Using the same microscope, the transmission high energy electron diffraction pattern of a gold nanowire was recorded (Figure 7.6).
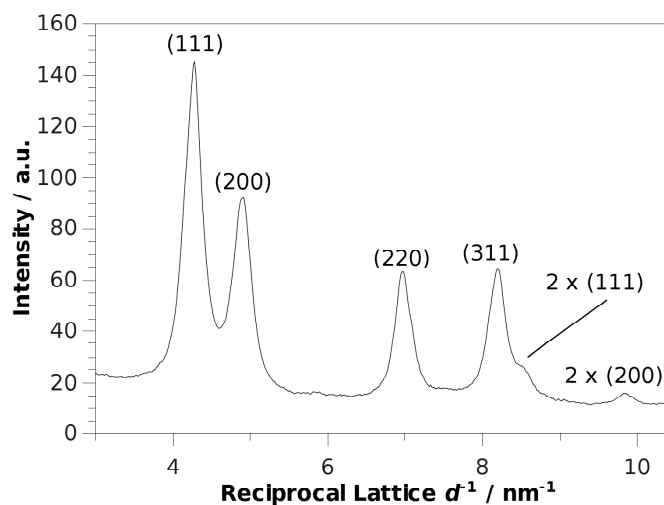
Figure 7.6. Recorded transmission high energy electron diffraction pattern of the prepared gold nanowires. The resulting pattern matched the specific pattern of polycrystalline face-centered cubic gold.[1]

UV-Visible Spectroscopy

Quartz glass cuvettes ($1\,cm \times 1\,cm \times 3.5\,cm$) were used in combination with a spectrometer V-670 (Jasco) at $25\,°C$ from $300\,nm$ up to $800\,nm$. The samples were dissolved/dispersed in tetrahydrofuran (about $0.08\,g\,L^{-1}$). Software: SpectraManager (Jasco, version 2.10.01).
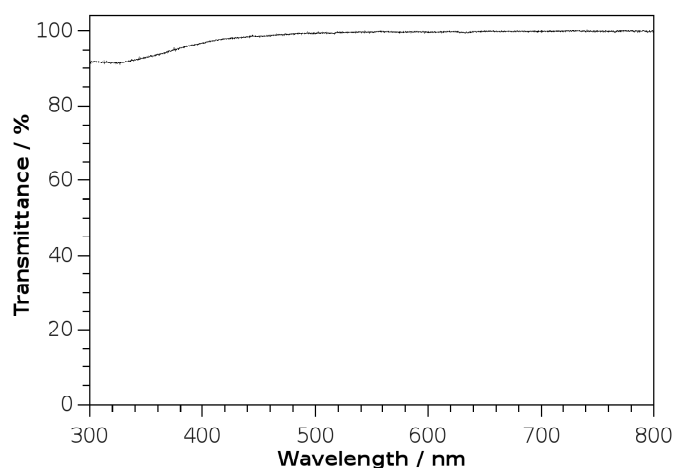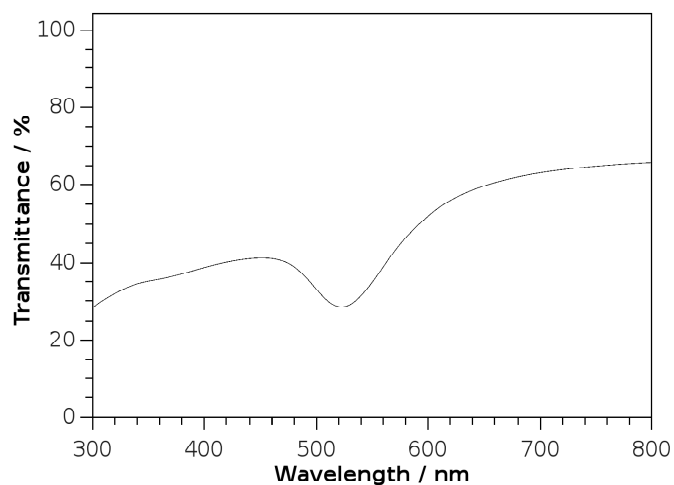

Figure 7.7. UV-visible spectrum of PLLA-SH.

Figure 7.8. UV-visible spectrum of PLLA@Au. At around 522 nm, the characteristic surface plasmon resonance absorption of gold nanoparticles was observed.

X-Ray Powder Diffraction

Measurements were carried out on an X-ray powder diffractometer X'Pert MPD Pro (PANalytical, Cu-K$_\alpha$, Ni filter, reflection electron diffraction) at room temperature using a voltage of 40 kV and a current of 40 mA, respectively.
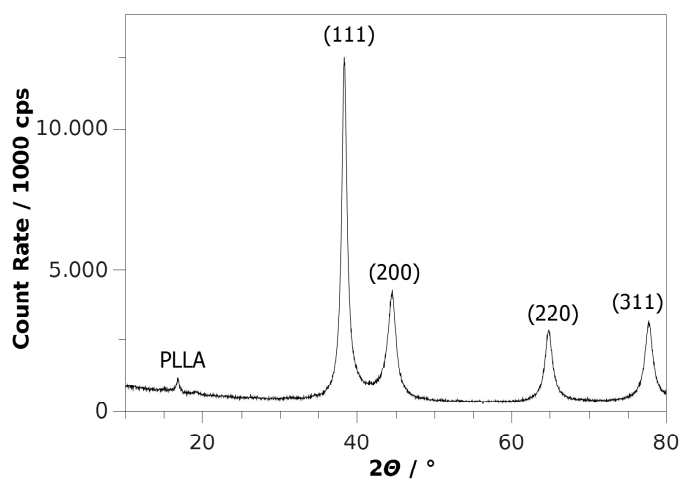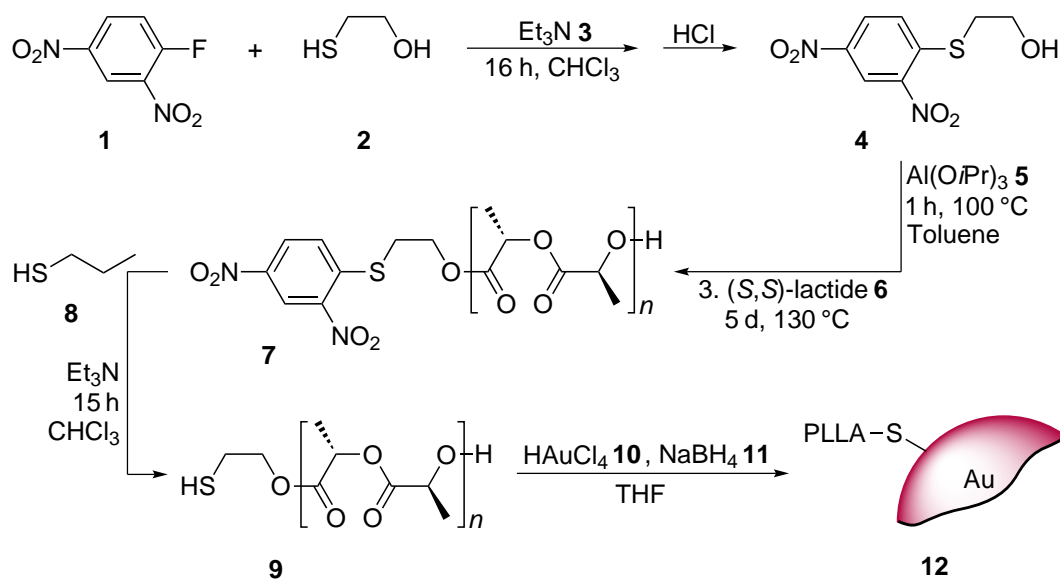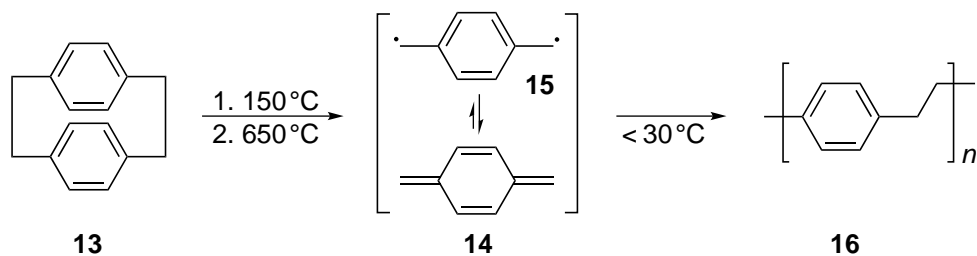

Figure 7.9. Diffraction pattern of PLLA@Au. The corresponding reflexes for both gold and PLLA were in accordance with the literature.[1,2]

Schemes

Scheme 7.1. Preparation of PLLA-stabilized gold nanoparticles **12** based on thiol functionalized PLLA **9** and chloroauric acid **10**.

Scheme 7.2. Corresponding reactions throughout the chemical vapor deposition of PPX **16** based on precursor [2.2]paracyclophane **13**.

7.8 References (Supporting Information)

[1] H. M. Chen, H. C. Lai, R. S. Liu, L.-J. Jang, *Chem. Phys. Lett.* **2006**, *428*, 93.

[2] N. Ogata, S. Yamaguchi, N. Shimada, G. Lu, T. Iwata, K. Nakane, T. Ogihara, *J. Appl. Polym. Sci.* **2007**, *104*, 1640.

8 List of Publications

[1]   Q. Jin, F. Mitschang, S. Agarwal, *Biomacromolecules* **2011**, *12*, 3684.

[2]   S. Maji, F. Mitschang, L. Chen, Q. Jin, Y. Wang, S. Agarwal, *Macromol. Chem. Phys.* **2012**, *213*, 1643.

[3]   F. Mitschang, B. K. Dettlaff, A. Studer, A. Greiner, *Abstr. Pap. Am. Chem. Soc.* **2013**, *246*, 1.

[4]   J. A. M. Hepperle, F. Mitschang, A. K. Bier, B. K. Dettlaff, A. Greiner, A. Studer, *RSC Adv.* **2013**, *3*, 25976.

[5]   F. Mitschang, B. K. Dettlaff, J.-P. Lindner, A. Studer, A. Greiner, *Macromolecules* **2013**, *46*, 8784.

[6]   H. Pletsch, L. Peng, F. Mitschang, A. Schaper, M. Hellwig, D. Nette, A. Seubert, A. Greiner, S. Agarwal, *Small* **2014**, *10*, 201.

[7]   F. Mitschang, H. Schmalz, S. Agarwal, A. Greiner, *Angew. Chem. Int. Ed.* **2014**, *in press.*

[8]   F. Mitschang, M. Langner, H. Vieker, A. Gölzhäuser, A. Greiner, *Small* **2014**, *submitted.*

9 List of Abbreviations and Symbols

δ	chemical shift
AFM	atomic force microscopy
aq.	aqueous
ATR	attenuated total reflection
br s	broad singlet
cps	counts per second
CTAB	cetyltrimethylammonium bromide
CuAAC	azide-alkyne Huisgen cycloaddition
CVD	chemical vapor deposition
$Đ$	dispersity $M_\mathrm{w} \times M_\mathrm{n}^{-1}$

d	day(s); doublet (NMR)
DAD	diode array detector
DLS	dynamic light scattering
DMF	*N*,*N*-dimethylformamide
DSC	differential scanning calorimetry
eq.	equivalent(s)
Et	ethyl group
FT	Fourier transform
G4	generation four (dendrimer)
G5	generation five (dendrimer)
GC	gas chromatography
Gew.	*see* wt
GPC	gel permeation chromatography
h	hour(s)
Hz	Hertz
HR-TEM	high-resolution TEM
*i*Bu	isobutyl group
ICP	inductively coupled plasma
*i*Pr	isopropyl group
IR	infrared
IUPAC	International Union of Pure and Applied Chemistry
J	coupling constant
m	mass; degree of polymerization
m	multiplet (NMR); medium absorption (IR)
Me	methyl group
min	minute(s)
M_n	number average molar mass
MS	mass spectrometry
M_w	mass average molar mass
n	degree of polymerization
NMR	nuclear magnetic resonance
TUFT	tubes by fiber templates

p.a.	pro analysis
PAMAM	poly(amido amine)
PLA	poly(lactic acid)
PLLA	poly(L-lactide)
PLLA@Au	poly(L-lactide)-stabilized gold nanoparticles
PLLA@SH	thiol-functionalized poly(L-lactide)
ppm	parts per million
PPX	poly(p-xylylene)
Pr	propyl group
q	quartet
quan.	quantitative
rpm	revolutions per minute
RT	room temperature
s	singlet (NMR); strong absorption (IR)
sat.	saturated
sBu	*sec*-butyl group
SEM	scanning electron microscope
T	temperature
t	triplet
TEM	transmission electron microscope
TEMPO	(2,2,6,6-tetramethyl-piperidin-1-yl)oxyl
TGA	thermogravimetric analysis
TOAB	tetraoctylammonium bromide
UV-vis	ultraviolet–visible
w	weak absorption
wt	weight

10 Acknowledgments

with the support of the University of Bayreuth Graduate School, for the opportunity to attend many interesting fairs and conferences, such as the ACS National Meeting in Indianapolis, which I very much appreciate.

Prof. Seema Agarwal was a great help and continually provided support and scientific feedback. Thanks also go to my colleagues who supported me with productive discussions and useful briefings for scientific equipment and methods. In particular, I would like to thank my former laboratory colleagues Stefan Bokern, Ph.D., and Ilka Paulus, Ph.D., for the many tips regarding nanoparticles and, respectively, the chemical vapor deposition process. Acknowledgments also go to Markus Langner for the very productive scientific discussions. Moreover, I thank Barbara K. Dettlaff (and Prof. Armido Studer, University of Münster) and Henning Vieker (Prof. Armin Gölzhäuser, Bielefeld University) for their contribution concerning the dendrimer-based catalysis and the scanning helium ion microscopy. The two secretaries, Edith Schmidt and Gaby Rösner-Oliver, always were very patient and helpful which I highly appreciate.

In addition, I am thankful for the support of my parents, Martina and Theo Mitschang, and my brother, Jonas Mitschang, who always knew a solution for computer-related issues. My deepest acknowledgments go to Sabrina Sebens, not only for proofreading many of the publications and this thesis, but also for her understanding and kindness.

11 (Eidesstattliche) Versicherungen und Erklärungen

(§5 Nr. 4 PromO)

Hiermit erkläre ich, dass keine Tatsachen vorliegen, die mich nach den gesetzlichen Bestimmungen über die Führung akademischer Grade zur Führung eines Doktorgrades unwürdig erscheinen lassen.

(§8 S. 2 Nr. 5 PromO)

Hiermit erkläre ich mich damit einverstanden, dass die elektronische Fassung meiner Dissertation unter Wahrung meiner Urheberrechte und des Datenschutzes einer gesonderten Überprüfung hinsichtlich der eigenständigen Anfertigung der Dissertation unterzogen werden kann.

(§8 S. 2 Nr. 7 PromO)

Hiermit erkläre ich eidesstattlich, dass ich die Dissertation selbständig verfasst und keine anderen als die von mir angegebenen Quellen und Hilfsmittel benutzt habe. Ich habe die Dissertation nicht bereits zur Erlangung eines akademischen Grades anderwertig eingereicht und habe auch nicht bereits diese oder eine gleichartige Doktorprüfung endgültig nicht bestanden.

(§8 S. 2 Nr. 9 PromO)

Hiermit erkläre ich, dass ich keine Hilfe von gewerblichen Promotionsberatern bzw. -vermittlern in Anspruch genommen habe und auch künftig nicht nehmen werde.

Bayreuth, 23. April 2014 ....

Fabian Mitschang